DOMINANT PATTERNS OF INTERANNUAL VARIABILITY IN THE NORTH ATLANTIC

FARHANA NAHED

Your file Votre référence
ISBN: 978-0-494-57483-6
Our file Notre référence
ISBN: 978-0-494-57483-6

Dominant patterns of interannual variability in the North Atlantic

by

Farhana Nahed

A thesis submitted to the
School of Graduate Studies
in partial fulfillment of the
requirements for the degree of
Master of Science

Computational Science Program
Memorial University of Newfoundland

August 2007

St. John's Newfoundland

Abstract

The low frequency variability of surface climate over the North Atlantic is described using 55 years of observations from the Comprehensive Ocean-Atmospheric Data set and NCEP reanalysis. Results are based on empirical orthogonal function analysis of sea surface temperature (SST), air temperature, wind, heat flux, and precipitation. The dominant spatial patterns of these parameters and sea level pressure are identified by using canonical correlation analysis. It is shown that the zonal wind and air temperature in the Labrador Sea are strongly correlated with the dominant modes of variability in the atmospheric circulation. The SST anomalies in the Labrador Sea are weakly correlated to the Sea Level Pressure (SLP) dominant modes of variability especially during the decadal periods of warming in the 1950s and the 1990s. It is suggested that the long term variability in the ocean circulation and sea ice at decadal time scale play a major role for the SST in the Labrador Sea during these periods.

Acknowledgements

First I would like to thank my supervisor Dr. Entcho Demirov for his continuous guidance and suggestions. He has been encouraging and always helpful. Without his guidance and support this thesis would not have taken this final form.

I would also like to thank all the faculty and staff of Computational Science program and Physics and Physical Oceanography Department for their assistance and support throughout my program. I would also like to thank Chris Stevenson for being so helpful with all of my computer problem.

Finally, I would like to thank Monowar and my friends, my Mom, Dad and others who have contributed to my research and thesis.

Table of Contents

Abstract i

Acknowledgements ii

Table of Contents iii

List of Figures v

1 Introduction

1.1 Scales of variability of Climatic System: causes, scales and implications..... 1

1.2 Implication of Climate Changes..... 5

1.3 The North Atlantic Oscillation..... 6

1.4 Relations between atmospheric and the North Atlantic ocean Variability..... 14

1.5 Problem description..... 16

2 Methods of Data Analysis

2.1 Statistical Methods of Description and Understanding of Atmospheric and Ocean data..... 18

2.2 Empirical Orthogonal Functions..... 22

2.3 Canonical Correlation Analysis (CCA)..... 25

2.3.1 Canonical Correlation Patterns..... 26

2.4 Computation of the Covariance Matrix..... 30

2.4.1 Eigenvalues and Eigenvectors of a Square Matrix..... 31

2.4.2 Data Structure..... 33

2.4.3 Algorithm of EOF Analysis..... 33

2.4.4 EOF Analysis Algorithm with Matlab..... 35

2.5 Computation CC patterns after a transformation to EOF Coordinates..... 36

3 Seasonal, Interannual and Interdecadal Variability of Atmospheric Characteristics and Sea Surface Temperature in the North Atlantic

3.1 Seasonal Variability..... 41

3.2 Inter-Annual and Inter-Decadal Variability..... 50

4 Empirical Orthogonal Function Analysis of SST and Atmospheric Data

4.1 Dominant modes of variability of the North Atlantic atmospheric circulation and NAO from 1948 to 2005..... 60

4.2 EOF analysis of near surface atmospheric parameters and SST..... 65

5 Canonical Correlation Analysis

5.1 Correlation Patterns of Variability in the North Atlantic..... 81

5.2 Correlation Patterns of Variability in the Labrador Sea..... 90

6 Conclusion and Future Works 102

Abbreviations.....104

Bibliography 106

List of Figures

1.1 Idealized, schematic spectrum of Atmospheric Temperature 4

1.2 Satellite image of sea ice 5

1.3 North Atlantic oscillation index.....8

1.4 Positive and negative NAO 10

3.1 Seasonal mean air temperature.....42

3.2 Seasonal mean zonal wind.....44

3.3 Seasonal mean sea surface temperature 47

3.4 Seasonal mean Total Heat Flux.....49

3.5 Inter-annual and inter-decadal Variability of Air Temperature.....51

3.6 Inter-annual and inter-decadal Variability of wind.....54

3.7 Inter-annual and inter-decadal Variability of SST.....56

3.8 Inter-annual and inter-decadal Variability of heat flux.....58

4.1 Dominant EOFs of SLP and their time series of NA.....64

4.2 Dominant EOFs of air temperature and time series of NA.....66

4.3 Dominant EOFs of air SST and time series of NA.....68

4.4 EOF analysis of SST (Deser & Blackmon).....70

4.5 Time series of winter sea ice (Deser & Blackmon).....71

4.6 Dominant EOFs of wind and time series of NA.....72

4.7 Dominant EOFs of precipitation and time series of NA.....74

4.8 Dominant EOFs of heat flux and time series of NA.....75

4.9 Difference of average heat flux winter month of NA SLP EOF.....77

4.10 Difference of average $\Delta SST' / \Delta t$ of NA SLP EOF (Cayan).....78

5.1 Canonical correlation of SST in the North Atlantic.....85

5.2 Canonical correlation of air temperature in the North Atlantic.....86

5.3 Canonical correlation of zonal wind in the North Atlantic.....87

5.4 Canonical correlation of turbulent heat flux in the North Atlantic.....88

5.5 Canonical correlation of precipitation rate in the North Atlantic.....89

5.6 Canonical correlation of SST in the Labrador Sea 94

5.7 Water Transport Index.....95

5.8 Canonical correlation of air temperature in the in the Labrador Sea.....98

5.9 Canonical correlation of zonal wind in the in the Labrador Sea.....99

5.10 Canonical correlation of turbulent heat flux in the Labrador Sea.....100

5.11 Canonical correlation of precipitation rate in the Labrador Sea.....101

1. INTRODUCTION

1.1 Scales of variability of Climate System: Causes, Scales and implications

The climate has varied significantly and continuously on time scales ranging from years to glacial periods and to the age of the earth. The variability of climate can be expressed in terms of two basic modes: the forced variations, which are the response of the climatic system to changes in the external forcing and the free variations due to internal instabilities and feedbacks, leading to nonlinear interactions among the various components of the climatic system.

The changes in the purely external factors that affect the climatic system, but are not influenced by the climatic variables themselves, constitute what may be called the external causes of climatic changes, whereas those changes that are related to nonlinear interactions among the various physical processes in the internal system are called internal causes. The distinction between the two classes of causes is not always very clear.

The external causes comprise variations in both astronomical and terrestrial forcing. The astronomical factors would include changes (a) in the intensity of solar irradiance; (b) in the orbital parameters of the earth (eccentricity of the orbit, axial precession and obliquity of the ecliptic); and (c) in the rate of rotation of the earth.

Among the terrestrial forcing we must consider (a) variations in atmospheric composition (mixing ratios of carbon dioxide and ozone, aerosol loading, etc.) due to volcanic eruptions and human activity; (b) variations of the land surface due to land use (deforestation, desertification, etc.); (c) long-term changes of tectonic factors such as

continental drift, mountain-building processes, polar wandering, etc. Some other possible terrestrial and astronomical forcing mechanisms are changes in solar output, the collision of the earth with interplanetary matter, changes in volcanic activity, and changes in the geothermal flux.

The internal causes are associated with many positive and negative feedback mechanisms and other strong interactions between the atmosphere, oceans, and cryosphere. These processes can lead to instabilities or oscillations of the system, which can either operate independently or introduce strong modifications on the external forcing. Let us show by some examples what we mean by the difference between an externally forced variation and an internally free change. The seasonal or diurnal variations of the climate are clearly related to the external astronomical forcing. But there are day-to-day weather variations that take place independently of any changes in external forcing. These irregular fluctuations with time scales of several days to a week may be connected with the passage of migratory atmospheric perturbations (highs and lows on the weather map) or with the passage of a frontal system. They are to be considered free, because they result from the internal baroclinic instability of the zonal current which depends only on the critical value of the latitudinal gradient of the temperature.

Figure 1.1 shows an idealized variance spectrum of the atmospheric temperature during its past history as evaluated by Mitchell (1976). The analysis of the spectrum shows several spikes and broader peaks. The spikes are astronomically dictated, strictly periodic components of climate variation, such as the diurnal and annual variations and their harmonics, whereas the broad peaks represent variations that are, according to Mitchell (1976), either quasiperiodic or aperiodic however, with a preferred time scale of

energization. Many of these broad peaks cannot be directly explained by the known external forcings. They indicate the existence of a strong free variability within the system.

The peak at three to seven days is associated with the synoptic disturbances mainly at mid-latitudes. The slightly raised region of the spectrum at 100-400 years is associated with the "little ice age" that began near the early 17th Century with rapid expansion of the mountain glaciers in Europe. The peak near 2500 years is perhaps due to the cooling observed after the "climatic optimum," about 5000 years ago, which predominated during the great ancient civilizations. The next three peaks are perhaps related to deterministic astronomical variations of the orbital parameters of the earth, which are supposed to be responsible for the ice ages (Milankovitch, 1941): (a) the eccentricity of the orbit of the earth with a cycle of about 100 000 years, (b) the axial precession with a cycle of around 22000 years, and (c) the change in the obliquity of the ecliptic or the axial tilt with a period of about 41000 years. Finally, the peaks near 45 and 350 million years may, according to Mitchell (1976), be related to glaciations due to orogenic and tectonic effects and to continental drift.

For a linear system the externally forced variations would lead to a simple relationship of cause and effect: if the forcing is an oscillatory process the response of the system would have exactly the same frequency. As we have seen, this is however, not always the case, since the internal climatic system is inherently unstable and never reaches the equilibrium state.

Climate variability results from complex interactions of forced and free variations because the climate system is a dissipative, highly nonlinear system with many sources of

instabilities. The interactive and often nonlinear nature of the instabilities and the feedback mechanisms of the climate system make it very difficult to obtain a straightforward interpretation of cause and effect.

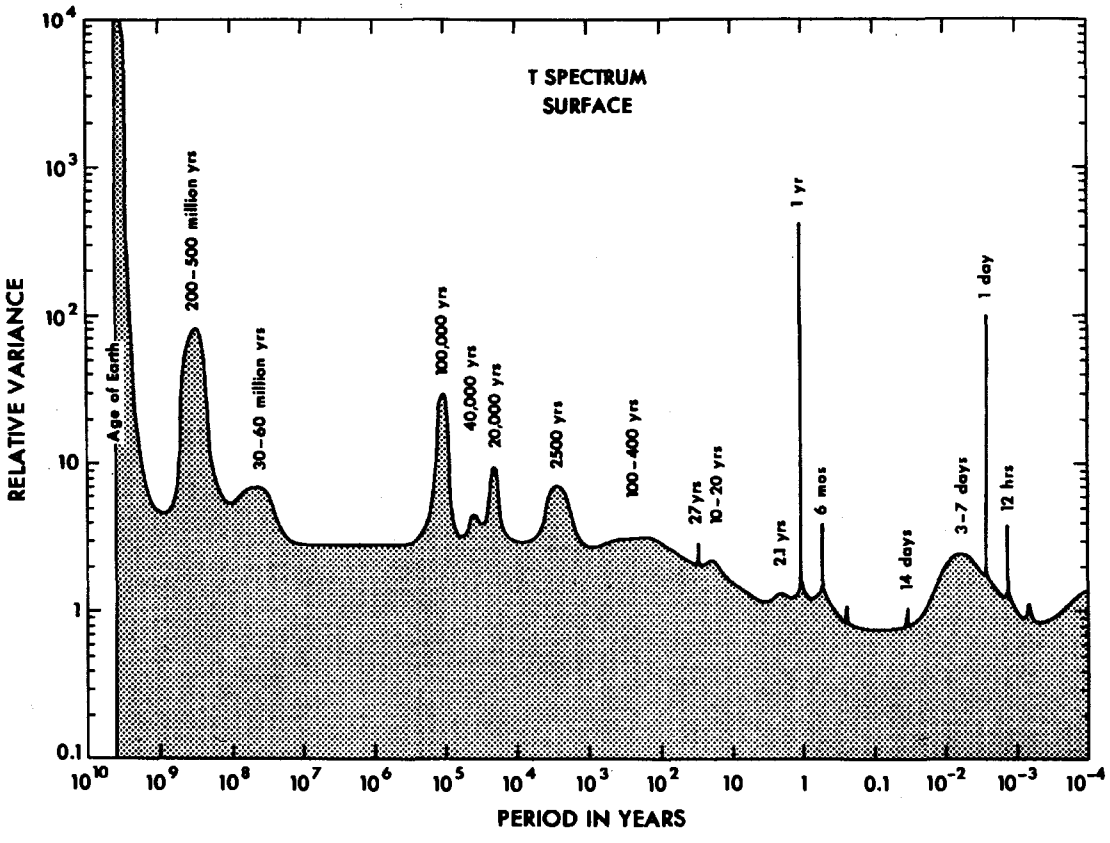

***Fig1.1**: Idealized, schematic spectrum of atmospheric temperature between 10^{-4} and 10^{10}yr adapted from Mitchell (1976)*

1.2 Implication of Climate Changes

During the recent two-three decades the climate change became a critical issue for the atmospheric and geophysical sciences. An important aspect of global changes is multi and quasi-decadal, inter-annual climate variability. The North Atlantic is the only place in the Northern Hemisphere where the atmosphere communicates deep oceanic water masses through convective over-turning (Talley 1984). Today we know that warmer temperatures have been causing more and more ice to melt during summer in the Northern Hemisphere. This change is linked directly to global warming. In 2005 and 2006, the extent of winter ice was about 6% smaller than the average amount over the past 26 years. The retreat is also significantly larger than the long-term decrease of 1.5% to 2% in winter ice cover observed per decade over the same time period.

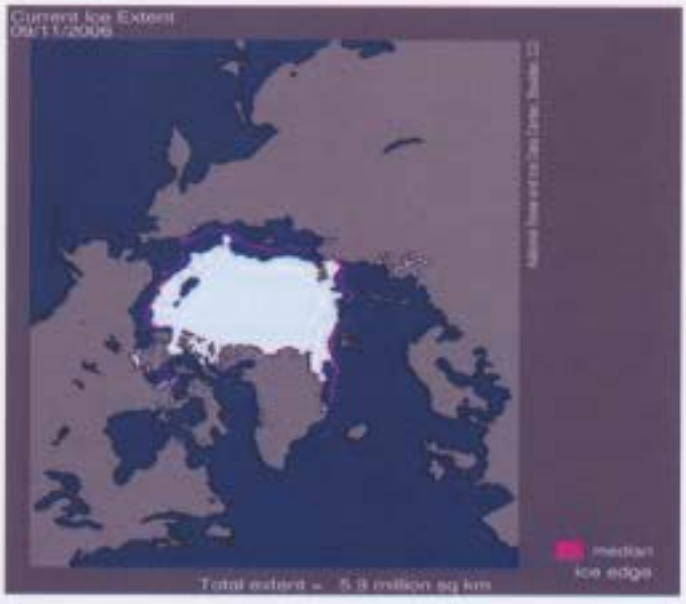

Fig 1.2: *This satellite image shows sea ice extent on 11 September 2006. The pink line shows the average ice extent for September, averaged between 1979 and 2000 (Image: NSIDC)*

If sea surface temperature (SST) variations in the North Atlantic at the climatic timescale are predicted it may be possible to improve the forecast of the global climate system. Climate variability on decadal and longer time scales is a subject of increasing interest of relevance. El Nino is perhaps the best-known example of the impact that changing sea surface temperature has on our climate. Every three to seven years, this warming of surface ocean waters in the eastern tropical Pacific brings winter droughts and deadly forest fires in Central America, Indonesia, Australia, and southeastern Africa, and lashing rainstorms in Ecuador and Peru. El Nino affects thousands of people worldwide, and billions of dollars in economic impact. But changing SST patterns have broader implications than just the El Nino and La Nina cycle.

In the Northern Hemisphere especially over the middle and high latitude during cold month, the most prominent and recurrent pattern of atmospheric variability is the North Atlantic oscillation (NAO). NAO refers to a redistribution of atmospheric mass between the arctic and the subtropical Atlantic. NAO produces large changes in the mean wind speed and direction over the Atlantic, the heat and moisture transport between the Atlantic and the neighboring continents, and the intensity and number of storms, their paths, and their weather. NAO has direct affect on agricultural harvests, water management, and energy supply and demand.

1.3 The North Atlantic Oscillation

The **North Atlantic Oscillation (NAO)** is a climatic phenomenon in the North Atlantic Ocean of fluctuations in the difference of sea-level pressure between the Icelandic Low and the Azores high. Through east-west rocking motions of the Icelandic Low and the

Azores high, it controls the strength and direction of westerly winds and storm tracks across the North Atlantic. It is related to and highly correlated with the so called Arctic Oscillation.

The NAO is the dominant mode of winter climate variability in the North Atlantic region ranging from central North America to Europe and much into Northern Asia. It is a large scale seesaw in atmospheric mass between the subtropical high and the polar low. The corresponding index (Fig 1.3) varies from year to year, but also exhibits a tendency to remain in one phase for intervals lasting several years.

The NAO has a strong implication on the track of storms and depressions across the North Atlantic Ocean and into Europe. The storm track exhibits variations from winter to winter in its strength and position, but a particularly recurrent variation is for the storm track to be either strong with a north-eastward orientation taking depressions into NW Europe or weaker with an east-west orientation taking depressions into Mediterranean Europe. Since the Atlantic storms that travel into Europe control the rainfall, there is a strong influence on European precipitation patterns.

The year-to-year variability in storm tracks is associated with a change in the mean atmospheric circulation averaged over the winter season. This variability is usually seen in the anomalous sea level pressure (SLP) patterns associated with high or low NAO winters. When the Iceland Low pressure centre is deeper than usual, the Azores High is stronger than usual, and vice versa. The change in the mean atmospheric circulation drives patterns of warming and cooling over much of the northern hemisphere. For example, when the NAO index is high, the SLP gradient between Iceland and the Azores/Iberia is enhanced, driving stronger westerly and southwesterly flow that carries

warm maritime air over the cold winter Eurasian land mass, bringing anomalously warm winter temperatures.

Westerly winds blowing across the Atlantic, bring moist air into Europe. In years when westerlies are strong, summers are cool, winters are mild and rain is frequent. If westerlies are suppressed, the temperature is more extreme in summer and winter leading to heat waves, deep freezes and reduced rainfall.

The permanent low-pressure system over Iceland (the Icelandic Low) and the permanent high-pressure system over the Azores (the Azores High) control the direction and strength of westerly winds into Europe. A large difference in the pressure at the two stations (a high index year, denoted NAO+) leads to

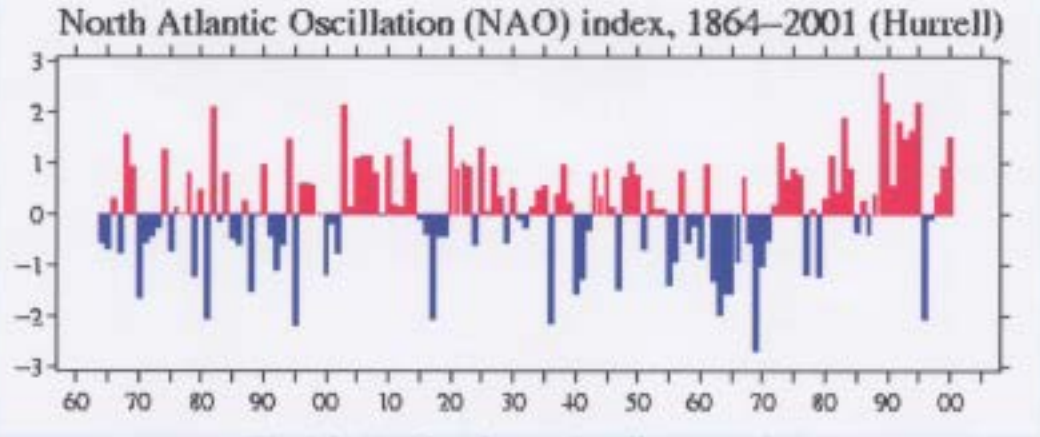

Fig 1.3: *North Atlantic Oscillation Index*

increased westerlies and, consequently, cool summers and mild and wet winters in Central Europe and its Atlantic façade. In contrast, if the index is low (NAO-), westerlies are suppressed, these areas suffer cold winters and storms track southerly toward the Mediterranean Sea. This brings increased storm activity and rainfall to southern Europe and North Africa.

Especially during the months of November to April, the NAO is responsible for much of the variability of weather in the North Atlantic region, affecting wind speed and wind direction changes, changes in temperature and moisture distribution and the intensity, number and track of storms.

Although having a less direct influence than for Western Europe, the NAO is also believed to have an impact on the weather over much of eastern North America. During the winter, when the index is high (NAO+), the Icelandic low draws a stronger southwesterly circulation over the eastern half of the North American continent which prevents Arctic air from plunging southward. In combination with the El Nino, this effect can produce significantly warmer winters over much of the United States and southern Canada.

The sea level pressure averaged over the winter is easier to measure than the storms themselves, so the variability of the NAO can be measured by the difference between the mean winter SLP at Gibraltar and the mean winter SLP over Iceland. Some people use Lisbon or the Azores instead of Gibraltar, but it makes little difference.

The Positive NAO index phase shows a stronger than usual subtropical high pressure center and a deeper than normal Icelandic low. The increased pressure difference results in more and stronger winter storms crossing the Atlantic Ocean on a more northerly track. This results in warm and wet winters in Europe and in cold and dry winters in northern Canada and Greenland. The eastern US experiences mild and wet winter conditions

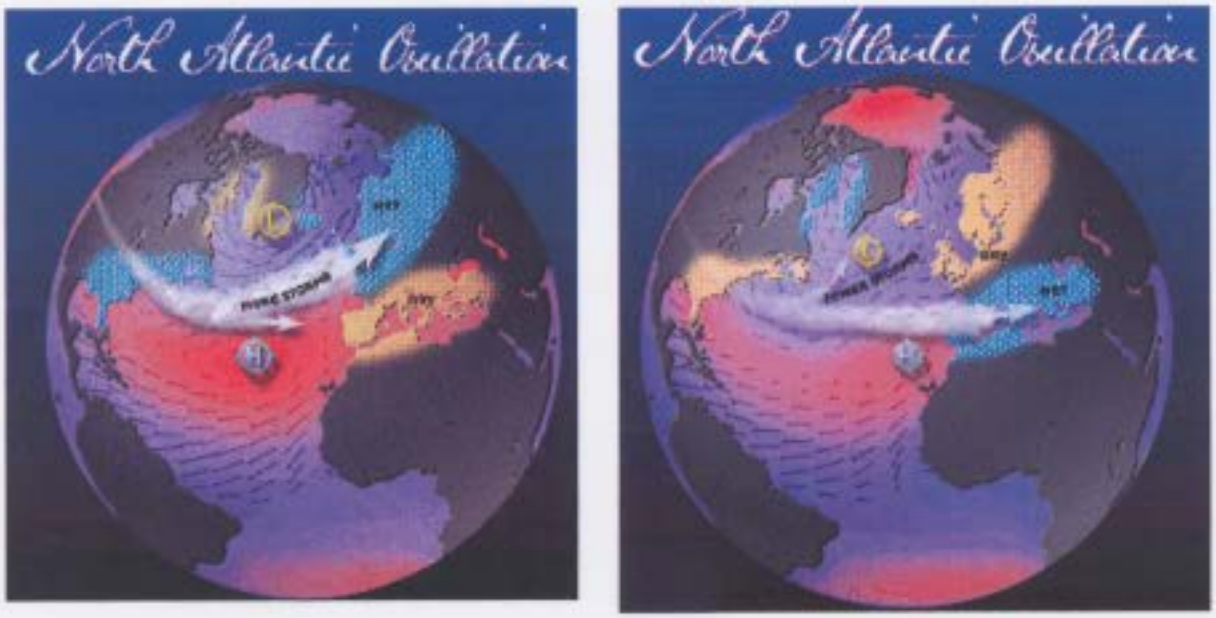

***Fig 1.4**:Left Panel Positive North Atlantic Oscillation, Right Panel Negative North Atlantic Oscillation.*

The negative NAO index phase shows a weak subtropical high and a weak Icelandic low. The reduced pressure gradient results in fewer and weaker winter storms crossing on a more west-east pathway. They bring moist air into the Mediterranean and cold air to northern Europe. The US east coast experiences more cold air outbreaks and hence snowy weather conditions. Greenland, however, will have milder winter temperatures.

The NAO and its time dependence for instance appear central to the global change debate. Surface temperatures over the Northern Hemisphere are likely warmer now than at any other time over the past millennium (Mann et al.,1999; Jones et al., 2001) and the rate of warming has been specially high over the past 40 years (Folland et al., 2001; Hansen et al., 2002). A substantial fraction of this most recent warming is linked to the behavior of the NAO (Hurrell, 1996), in particular a trend in its index from large

amplitude anomalies of one phase in the 1960s to large amplitude anomalies of the opposite phase since the early 1980s. This change in the atmospheric circulation of the North Atlantic accounts for several other remarkable alterations in weather and climate over the extratropical Northern Hemisphere as well, and it has added considerably to the debate over our ability to detect and distinguish between natural anthropogenic climate changes. While it has long been recognized that the North Atlantic Ocean varies appreciably with the overlying atmosphere (Bjerknes, 1964), another reason invigorated interest in the NAO is that the richly complex and differential responses of the surface layer, intermediate and deep layers of the ocean to NAO forcing are becoming better documented and under stood (Visbeck et al, 1998). The intensity of winter time convective renewal of intermediate and deep waters in the Labrador Sea and Greenland-Iceland-Norwegian Seas for instance, is not only characterized by large interannual variability, but also by interdecadal variations that appear to be synchronized with fluctuations in the NAO (Dickson et al., 1996). These changes in turn affect the strength and character of the Atlantic thermohaline circulation and the horizontal flow of the upper ocean, thereby altering the oceanic poleward heat transport and the distribution of sea surface temperature.

On seasonal time scales, the upper North Atlantic Ocean varies primarily in response to changes in the surface winds, air-sea heat exchanges and freshwater fluxes associated with NAO variations (*Cayan,* 1992a,b). This does not mean, however, that the extratropical interaction is only one-way. The dominant influence of the ocean on the overlying atmosphere is to reduce the thermal damping of atmospheric variations, and this influence becomes greater on longer time scales. The extent to which the influence of

the ocean extends beyond this local thermodynamic coupling to affect the evolution and dynamical properties of the atmospheric flow is probably small, but the effect is non-zero (*Robinson,* 2000; *Kushnir et al.*, 2002).

New statistical analyses have revealed patterns in North Atlantic SSTs that precede specific phases of the NAO by up to 9 months, a link that likely involves the remarkable tendency of the extratropical ocean to preserve its thermal state throughout the year (Kushnir et al., 2002.) On longer time scales, recent modeling evidence suggests that the NAO responds to slow changes in global ocean temperatures, with changes in the equatorial regions playing central role. (Hoerling et al., 2001). A second pathway that offers hope for improved predictability of the NAO involves links through which changes in stratospheric wind patterns might exert some downward control on surface climate (Thompson et al, 2000). The NAO has a demonstrated influence on the physics, hydrology, chemistry and biology of freshwater ecosystem across Northern Hemisphere (NH) (Straile et al., 2003).

The spatial pattern related to NAO can be identified from the eigenvectors of the cross-covariance matrix,computed from the time variations of the grid point values of SLP or some other climate variable. The eigenvectors, each constrained to be specially and temporally orthogonal to the others, are then scaled according to the amount of total data variance they explain. This linear approach assumes preferred atmospheric circulation states come in pairs, in which anomalies of opposite polarity have the same spatial structure. The largest amplitude anomalies in SLP usually occur during the boreal winter months; however, throughout the year the leading pattern of variability is characterized by a surface pressure dipole, and thus may be viewed as the NAO,although the spatial

pattern is not stationary (*Barnston and Livezey*, 1987; *Hurrell and van Loon*, 1997; *Portis et al.*, 2001). Since the eigenvectors are, by definition, structured to explain maximum variance, it is expected that the "centers of action" of the leading EOFs will coincide with the regions of strongest variability.

Most studies of the NAO focus on the NH winter months, when the atmosphere is most active dynamically perturbations grow to their largest amplitudes. As a result, the influence of the NAO on surface temperature and precipitation as well as on ecosystems is also greatest at this time of the year.

In conclusion the North Atlantic Oscillation has a large climatic influence on the North Atlantic Ocean and surrounding land masses. It is a major controlling factor in basic meteorological variables such as surface wind, temperature and precipitation which have large socio-economic impacts on energy, agriculture, industry, traffic and human health throughout the whole of Europe and eastern North America.

Early in this century, scientists aware of the NAO also became interested in its socio-economic impacts (Meinardus, 1905). When more recently the NAO came into the focus of scientific work again, a number of studies considered the influence of this large scale variability pattern on local meteorological quantities such as seasonal mean precipitation, temperature and wind velocity (e.g. Wallace and Gutzler, 1981; Deser and Blackmon, 1993; Hurrell, 1995; Rogers, 1990; Malberg and Bökens, 1997; Ulbrich and Christof, 1999).

1.4 Relations between atmospheric and the North Atlantic Ocean variability

There has been an intensification of efforts toward describing and understanding climate variability in the North Atlantic Ocean, in the past decade. A significant fraction of that variability is associated with the NAO. While the NAO state may be characterized by an index of that pressure difference (e.g., Hurrell 1995), the NAO is so strong mode that alternative indices based on surface air temperature differences (van Loon and Rogers 1978), storms (Rogers 1997), sea ice (Deser et al. 2000), sea surface temperature (SST) patterns (Deser and Blackmon 1993; Kushnir 1994; Sutton and Allen 1997), or SST gradients (Czaja and Marshall 2001), when regressed on SLP, yield much the same dipole SLP anomaly patterns.

When averaged for the winter months, the SLP-based index (Hurrell 1995) exhibits interannual to decadal and interdecadal fluctuations. High and low states of the NAO index reflect enhanced and diminished midlatitude westerlies, with related shifts in wind patterns and intensities of air–sea exchanges of heat (Cayan 1992a,b), freshwater (Hurrell 1996), and momentum (Visbeck et al. 1998). Since the general oceanic circulation, including upper ocean gyres and thermohaline overturning, is wind and buoyancy forced, there is little surprise in finding oceanic patterns in the observational record that are coordinated with the low frequency components of atmospheric variability. Notable are SST anomalies that develop directly as a time-integrated response to persistent NAO air–sea heat flux anomalies (Bjerknes 1964; van Loon and Rogers 1978; Deser and Blackmon 1993; Kushnir 1994). If the NAO SLP–SST–heat content fluctuations were the only signals of coordinated atmosphere–ocean variability, then that association would be

amenable to a null hypothesis explanation: that the ocean integrates atmospheric forcing to redden the spectral response relative to the forcing spectrum (Hasselmann 1976; Frankignoul and Hasselmann 1977). Battisti et al. (1995), for example, hindcast winter SST for the North Atlantic using observed atmospheric circulation anomalies and an ocean simulated as a field of one-dimensional mixed layers on the top a diffusive deep ocean (no advection). The relative success of this and similar SST hindcasts for large areas of the North Atlantic has given considerable weight to the idea of mixed layer integration of surface heat flux as the leading mode of extratropical ocean–atmosphere interactions.

The upper ocean's mean advective–diffusive heat balance involves a large annual surface heat flux from the midlatitude ocean into the overlying atmosphere, supported by oceanic heat transport convergence into the region. Thus SST anomalies are more than merely one-dimensional mixed layer responses to local atmospheric forcing; they reflect departures of the heat balance from the climatological annual mean and seasonal cycles. These departures can lead to interannual persistence of winter SST anomalies through a reemergence mechanism (Alexander and Deser 1995) whereby a winter mixed layer anomaly is seasonally sequestered beneath a summer thermocline and then reappears in the subsequent winter.

The observations indicate that this mechanism acts both locally (viewing as an Eulerian field) and in a Lagrangian framework. Underlying the decadal evolution of the observed oceanic heat content patterns are not only the thermal inertia of winter mixed layer dynamics but also modulations of the ocean gyre circulation.

1.4 Problem Description

The objective of this thesis is to evaluate the impact of the variability of the atmospheric circulation on the Labrador Sea. This evaluation is done through analysis of available data from observations and atmospheric reanalysis. One major goal of this work is to assess if the variability of atmospheric near surface parameters and SST of the Labrador Sea is predictable by using information about the SLP only. The later provides information about the major modes of atmospheric circulation and their change in time. The thesis includes analysis of the relation between SLP modes and variability of the Labrador Sea based on the traditional methods of Empirical Orthogonal Function (EOF) and Canonical Correlation Analysis (Chapter2).

The interannual variability of the North Atlantic is discussed in Chapter 3. Chapter 4 presents results from EOF analysis of the studied prameters. The discussion in Chapter 4 defines the major characteristics and events of the North Atlantic variability during the recent 50 years.

Chapter 5 discusses the connection between the variability of the atmospheric circulation and the interannual change of the near surface atmospheric parameters and SST in the Labrador Sea.

Chapter 2

2. Methods of Data Analysis

This chapter describes the methods used in the analysis of long term variability in the North Atlantic SST and atmospheric characteristics. The approach is based on the use of statistical methods for analysis of simultaneous multivariate data. The aim of the study is to describe the dominant patterns of spatial variability about the long term mean. This can be accomplished through use of Empirical Orthogonal Functions (EOF) and Canonical Correlation Patterns (CCA) analysis.

2.1 Statistical Methods of Description and Understanding of Atmospheric and Ocean Data

The climate is a complex dynamical system and its variability is influenced by a great number of external factors. In climate studies only small portion of these factors can be considered, while the rest are usually considered as background noise. Correspondingly we consider every climate characteristics $\boldsymbol{X}$ as a sum of two components

$$\mathbf{X} = \mathbf{X}_d + \mathbf{X}'$$

Here $\boldsymbol{X}_d$ is a deterministic part of $\boldsymbol{X}$ which is the subject of our study. $\boldsymbol{X}'$ is non-deterministic, stochastic component of $\boldsymbol{X}'$ which is not correlated to $\boldsymbol{X}_d$.

The statistical approach has certain drawbacks due to the fact that small variations in ocean and atmospheric characteristics which usually are considered as noise some times can have significant impact on the large-scale variability. Ocean vertical mixing, for instance, which has spatial scales of centimeters or millimeters, may have significant impact on the large scale circulation. This feedback between the large and small scales is due to the nonlinear dynamics of the climate system. Nonlinear components of the hydrodynamic equations include important advective terms. The thermodynamic part also contains various nonlinear processes. The nonlinearities make the climate system unpredictable beyond certain characteristic times. These characteristic time scales are different for the climate subsystems such as the ocean, atmosphere, lithosphere and cryosphere. The climate subsystems also can interact in a complex way influencing each other on different time scales. The interactions often have the character of positive and negative feedbacks. One important feedback, which is a main interest of this study is the feedback between SST and atmospheric circulation. The surface momentum and buoyancy fluxes drive the ocean circulation. The ocean currents transport heat and salt polewards. This transport heats the poles and makes the ocean surface in the polar and subpolar areas warmer. At the same time the ocean surface temperature influences back the atmospheric circulation. The feedback between the atmosphere and ocean processes is observed at different scales in variability of the characteristics of the two sub-systems at different scales. One example is ElNino and Southern Oscillation (ENSO) which is observed in the results simultaneous variability in ocean and atmospheric characteristics in the tropical Pacific Ocean at interannual time scale.

Another example is the North Atlantic Oscillation (NAO) which dominates atmospheric circulation variability over the North Atlantic at a decadal time scale. While there is strong evidence that NAO dominates the variability of atmosphere over the North Atlantic and therefore the atmospheric forcing of ocean circulations, the importance of SST to the atmosphere is not widely accepted

In this study, we assume that the long term sea surface temperature and atmospheric characteristics over the North Atlantic Ocean consist of two components, one which is related to the interaction between atmosphere and ocean over the North Atlantic and second, which is stochastic. The latter is due to error in observations or calculation of the ocean and atmospheric parameters, or is related to processes not observable in the available data. EOF and CCA techniques are used in this study to identify patterns of simultaneous variability in the atmosphere and surface layer of the North Atlantic Ocean.

Let $\vec{X}_t$ represents certain atmospheric or oceanic characteristics at some vertical level. $\vec{X}_t$ is a vector of dimension $N=m*n$ which contains values of the 2-dimensional characteristics with dimension n in latitude and m in longitude. The mean state expectation of X_t is $\vec{\mu} = E(\vec{X})$. Statistical parameters have considerable complexity in the climatological context. In particular, the computed mean is not entirely reliable as an estimate of the climate system's true long term mean state. The computed mean usually contain errors caused by taking observations over a limited observing period, at a discrete times and a finite number of locations. It may also be affected by the presence of instrumental, recording, and transmission errors. The climatological mean should be understood also to be a moving target because today's climate is different from that which prevailed thousands years ago.

The time mean of the characteristics X_t is denoted by $\hat{\vec{\mu}}$. Then the variability of $\vec{X}_t$ is described in terms of anomalies $\vec{X}' = \vec{X}_t - \hat{\vec{\mu}}$. The anomalies at two different points often have a tendency to vary jointly. This 'co-variability' may be quantitavely described by the covariance matrix $\sum_{XX} = \boldsymbol{E}\left(\vec{X}'_t \vec{X}'^{\mathrm{T}}_t\right)$where $\boldsymbol{E}$ is the expectation operator. In statistics covariance indicates the strength and direction of a linear statistical relationship between two random variables. When the linear relationship is stronger, then the covariance also becomes higher. The time mean $(\vec{\mu})$ and covariance matrix $\sum$only describe statistical properties of important class of random processes. A random variable, or a random process, is said to be stationary if all the statistical parameters are independent of time. As a result, parameters such as the mean and variance, also do not change over time or position. Most statistical techniques assume that the observed process is stationary.

Most climate parameters that are sampled more frequently that one per year are not stationary but cyclo-stationary, simply because of the seasonal forcing of the climate system. Long-term averages of monthly mean sea-level pressure exhibit a marked annual cycle. The mean annual cycle is computed as monthly mean$\left(\hat{\vec{\mu}}(m), m = 1,....12\right)$. The anomalies remaining after subtracting the monthly mean are:

$$\boldsymbol{X}'_t = \boldsymbol{X}_t - \hat{\vec{\mu}}(m)$$

In the following, the studied atmospheric and ocean characteristics will be assumed that they are cyclo stationary. Two methods are used in this study to identify the major modes of interannual variability. First EOF analysis is used to identify the dominant pattern in

anomaly fields of atmospheric and ocean characteristics. The canonical correlation analysis is then applied in a study of the interrelation between basic modes of variability.

2.2 Empirical Orthogonal Functions

Lets consider a stochastic characteristic $\vec{X}$ with mean $\hat{\vec{\mu}}$. Assume that the anomalies $\vec{X}'_t$ can be expanded in to a finite series $\vec{X}'_t = \sum_i^K \hat{\alpha}_{i,t} \hat{\vec{e}}^i$ with time dependent coefficient $\hat{\alpha}_{i,t}$ and fixed patterns $\hat{\vec{e}}^i$ (Empirical Orthogonal Functions) and $K = m * n$. The variance of the time coefficients $\hat{\alpha}_{i,t}$ usually decreases quickly with increasing index i, so that good approximations $\vec{X}'_t \approx \sum_{i=1}^{K'} \hat{\alpha}_i \vec{e}^i$ are usually possible for $K' << n * m$. The patterns are chosen to be orthogonal so that optimal coefficients $\hat{\alpha}_{i,t}$ are obtained by simply projecting the anomalies $\vec{X}'_t$ onto the patterns $\hat{\vec{e}}^i$. The coefficients $\hat{\alpha}_i$ are the EOFs coefficients. The first step of the EOF analysis is to find one pattern $\vec{e}^1$, such that $\in_1 = \boldsymbol{E}(\left\| \vec{X} - \left\langle \vec{X}, \vec{e}^1 \right\rangle \vec{e}^1 \right\|^2)$ is minimized. Here the scalar product is defined as $\left\langle \vec{a}, \vec{b} \right\rangle = \sum_{i=1}^K a_i b_i *$,

where * denotes complex conjugate, and the norm is $\|a\| = \sqrt{\langle \vec{a}, \vec{a} \rangle}$. This first step finds the projection of the random vector $\vec{\mathbf{X}}$ onto one-dimensional subspace spanned by the fixed vector $\vec{e}^1$. The variance of $\vec{\mathbf{X}}$ which is contained in this subspace is:

$$E_1 = \mathbf{E}\left(\left\|\vec{X}\right\|^2 - 2\left\langle \vec{X}, \vec{e}^1 \right\rangle * \vec{X}^T \vec{e}^1 + \left\langle \vec{X}, \vec{e}_1 \right\rangle * \left\langle \vec{X}, \vec{e}^1 \right\rangle\right)$$

$$= \mathbf{E}\left(\left\|\vec{X}\right\|^2 - \left\langle \vec{X}, \vec{e}^1 \right\rangle * \left\langle \vec{X}, \vec{e}^1 \right\rangle\right)$$

$$= \mathrm{var}(\vec{X}) - \mathrm{var}\left(\left\langle \vec{X}, \vec{e}^1 \right\rangle\right) \qquad (1)$$

where the variance of the random vector $\vec{\mathbf{X}}$ is defined to be the sum of variances of the elements of $\vec{\mathbf{X}}$ and T denotes matrix or vector transpose. It can be shown that $Var\left(\left\langle \vec{X}, \vec{e}^1 \right\rangle\right) = \vec{e}^{1T} \Sigma_{XX} \vec{e}^1$ where Σ is the covariance matrix of $\vec{\mathbf{X}}$. The solution for the first EOF vector $\vec{e}^1$, which minimizes $E_1 =. \left(\left\|\vec{X} - \left\langle \vec{X}, \vec{e}^1 \right\rangle \vec{e}^1\right\|^2\right)$ under the constraint $\left\|\vec{e}^1\right\| = 1$ can be found by using method of the Lagrange multipliers with the constrain $\left\|\vec{e}^1\right\| = 1$. The minimization of equation (1) leads to:

$$\frac{d}{d\vec{e}^1}\left[-\vec{e}^{1T} \Sigma_{XX} \vec{e}^1 + \lambda\left(\vec{e}^{1t} \vec{e}^1 - 1\right)\right] \qquad (2)$$

$$= 2\Sigma_{xx} \vec{e}^1 + 2\lambda \vec{e}^1 = 0$$

where t denotes complex conjugate of transposed vector. This equation means that the first EOF is the eigen vector $\vec{e}^1$ of the covariance matrix Σ_{XX} eigen value λ.

To find the second EOF we have repeated the same procedure by minimizing $\in_2 =. \left(\left\|\vec{X} - \left\langle \vec{X}, \vec{e}^1 \right\rangle \vec{e}^1 - \left\langle \vec{X}, \vec{e}^2 \right\rangle \vec{e}^2\right\|^2\right)$ with $\left\|\vec{e}^2\right\| = 1$.

The result is that $\vec{e}^2$ is the eigen vector of Σ_{XX} that corresponds to its second largest eigenvalue λ_2. This second pattern is orthogonal to the first because the eigenvectors of a Hermitian matrix Σ_{XX} are orthogonal to one another.

We can continue in this way to define the following EOFs. The result of this process may be formulated in the following way:

Let $\vec{X}$ *be an m-dimentional random vector with mean* $\vec{\mu}$ *and covariance matrix* $\sum_{xx}$. *Let* $\lambda_1 \geq \lambda_2 \geq ... \geq \lambda_m$ *be the eigen values of* $\sum_{xx}$ *and let* $\vec{e}^1,...,\vec{e}^m$ *be the corresponding eigenvectors of unit length. Since* $\sum_{xx}$ *is the Hermitian, the eigenvalues are non-negative and the eigenvectors are orthogonal.*

(i) The *k* eigenvectors that correspond to $\lambda_1,...,\lambda_k$ minimize

$$\epsilon_k = . \left(\left\|(\vec{X} - \mu) - \sum_{i=1}^{k} \left\langle \vec{X} - \vec{\mu}, \vec{e}^i \right\rangle \vec{e}^i \right\|^2\right)$$

(ii) $$\epsilon_k = Var(\vec{X}) - \sum_{i=1}^{k} \lambda_i$$

(iii) $$Var(\vec{X}) = \sum_{i=1}^{m} \lambda_i$$

The EOF coefficients or principal components $\alpha_i = \left\langle \vec{X}, \vec{e}^i \right\rangle = \vec{X}^T \vec{e}^{i*} = \vec{e}^{iT} \vec{X}$ are uncorrelated and hence independent. The covariance of α_i and α_j satisfies the relation:

$$Cov(\alpha_i, \alpha_j) = \mathbf{E}\left(\left\langle \left(\vec{X} - \vec{\mu}\right), \vec{e}^i \right\rangle \left\langle \left(\vec{X} - \vec{\mu}\right), \vec{e}^j \right\rangle^* \right)$$

$$= \vec{e}^{iT} \mathbf{E}\left(\left(\vec{X} - \vec{\mu}\right)\left(\vec{X} - \vec{\mu}\right)^T \right) \vec{e}^j = \vec{e}^{iT} \sum \vec{e}^j = \lambda_j \vec{e}^{iT} \vec{e}^j = 0$$

Usually major part of the variance of $\vec{X}$ can be represented by the first few EOFs. If the original variable has m components the approximation of $\vec{X}$ by $\vec{\alpha} = (\alpha_1,...,\alpha_k)$ with $k' << K$. Using only limited number of EOFs leads to a significant reduction of amount

of analyzed data while retaining most of the variance. It is possible to clearly associate the first EOF with a known physical process but this is much more difficult to do with the second EOF because it is constrained to be orthogonal to the first EOF. Additional analysis is needed in order to connect the computed EOFs with the underlying dynamics. This analysis is usually based on the existing knowledge about the process and/or applications of statistical methods like CCA.

The basic hypothesis of the EOF analysis is that studied characteristics $\boldsymbol{X}$ may be split into two parts – deterministic $\boldsymbol{X}_d$ and stochastic noise $\boldsymbol{X}'$. In the EOF analysis we need to distinguish between the EOFs which correspond to $\boldsymbol{X}_d$ and to $\boldsymbol{X}'$. The former are the ones, which are going to be used in pattern analysis.

After computing the EOF analysis, one needs to select the number of dominant EOFs, which spawn the space of X_d. The most popular procedure to separate physically relevant and noise related EOFs is based on so called Rule *N*. The latter is based on the assumption that the phase space (spanned by all EOFs) can be splitted into two subspaces one which contains only noise, and second, which contains dynamic variability. It is assumed that the dynamical sub-space is spanned by the EOFs with large and well separated eigen values. Another approach is suggested by North et al., (1982) which is based on estimation of typical errors for $\hat{\lambda}_i$ and eigen vectors $\hat{\vec{\mathbf{e}}}^i$

$$\Delta\lambda_i \approx \sqrt{\frac{2}{n}}\lambda_i \text{ and } \Delta\hat{\vec{e}}^i \approx \frac{C'\Delta\lambda_i}{\lambda_j - \lambda_i}\vec{e}^i$$

The North's "Rule-of-Thumb' states that

If the sampling error of a particular eigenvalue $\Delta\lambda$ is comparable to or larger than the spacing between λ and a neighboring eigenvalue, then the sampling error $\Delta\vec{e}$ of the EOF will be comparable to the size of the neighboring EOF.

2.3 Canonical Correlation Analysis (CCA)

Canonical Correlation Analysis is used to study the joint variability of random vectors $\vec{X}$ and $\vec{Y}$. The objective of CCA is to find a pair of patterns $\vec{f}_X{}^1$ and $\vec{f}_Y{}^1$ so that the correlation between linear combinations $\vec{X}^T\vec{f}_X{}^1$ and $\vec{Y}^T\vec{f}_Y{}^1$ is maximized. A second pair of patterns $\vec{f}_X{}^2$ and $\vec{f}_Y{}^2$ is found so that $\vec{X}^T\vec{f}_X{}^2$ and $\vec{Y}^T\vec{f}_Y{}^2$ are the most strongly correlated linear combinations of $\vec{X}$ and $\vec{Y}$ that are not correlated with $\vec{X}^T\vec{f}_X{}^1$ and $\vec{Y}^T\vec{f}_Y{}^1$, and so on.

2.3.1 Canonical Correlation Patterns

Let us consider a m_X dimensional random vector $\vec{X}$ and a m_Y dimensional random vector $\vec{Y}$. It is required to find a m_X dimensional vector $\vec{f}_X$ and a m_Y dimensional vector $\vec{f}_Y$ such that the inner products $\beta^X = \langle \vec{X}, \vec{f}_X \rangle$ and $\beta^Y = \langle \vec{Y}, \vec{f}_Y \rangle$ have maximum correlation. i.e.:

$$\rho = \frac{Cov(\beta^X, \beta^Y)}{\sqrt{Var(\beta^X)Var(\beta^Y)}} = \frac{\vec{f}_X{}^T Cov(\vec{X}, \vec{Y}) \vec{f}_Y}{\sqrt{Var(\langle \vec{X}, \vec{f}_X \rangle) Var(\langle \vec{Y}, \vec{f}_Y \rangle)}} \quad (1)$$

where β^X and β^Y are called **canonical variates**. If a pair of vectors $\vec{f}_X$ and $\vec{f}_Y$ maximizes the above equation then all vectors $\alpha_X \vec{f}_X$ and $\alpha_Y \vec{f}_Y$ do the same for any nonzero α_X and α_Y. Thus $\vec{f}_X$ and $\vec{f}_Y$ can be arbitrary normalized. We can choose the patterns such that

$$Var(\langle \vec{X}, \vec{f}_X \rangle) = \vec{\mathbf{f}}_X^T \Sigma_{XX} \vec{f}_X = 1$$

$$Var(\langle \vec{Y}, \vec{f}_Y \rangle) = \vec{\mathbf{f}}_Y^T \Sigma_{YY} \vec{f}_Y = 1$$

where Σ_{XX} and Σ_{YY} are the covariance matrices of $\vec{X}$ and $\vec{Y}$. The above equation can be rewritten as $\rho = \vec{f}_X^T \sum_{XY} \vec{f}_Y$ (4) where Σ_{XY} is the cross covariance matrix $\Sigma_{xx} = \mathbf{E}((\vec{\mathbf{X}} - \vec{\mu}_X)(\vec{\mathbf{Y}} - \vec{\mu}_Y))$. Similarly to the approach used in previous section

vectors $\vec{f}_X$ and $\vec{f}_Y$ are found by maximizing

$$\in = \vec{f}_X{}^T \sum_{XY} \vec{f}_Y + \zeta\left(\vec{f}_X{}^T \sum_{XX} \vec{f}_X - 1\right) + \eta\left(\vec{f}_Y{}^T \sum_{YY} \vec{f}_Y - 1\right) \quad (5)$$

where ζ and η are Lagrange multipliers that are used to account for constraints (2) and (3). Setting the partial derivatives of $\in$ to zero, we get

$$\frac{\partial \in}{\partial \vec{f}_X} = \sum_{XY} \vec{f}_Y + 2\zeta \sum_{XX} \vec{f}_X = 0 \quad (6)$$

so that $\sum_{XX}^{-1} \sum_{XY} \vec{f}_Y = -2\zeta \vec{f}_X$ (7)

and

$$\frac{\partial \in}{\partial \vec{f}_Y} = \sum_{XX}^{T} \vec{f}_X + 2\eta \sum_{YY} \vec{f}_Y = 0 \quad (8)$$

which is equivalent to

$$\sum_{YY}^{-1} \sum_{XY}^{T} \vec{f}_X = -2\eta \vec{f}_Y \quad (9)$$

Then (9) is substituted into (7) to obtain a pair of eigen-equations for $\vec{f}_X$ and $\vec{f}_Y$

$$\sum_{XX}^{-1} \sum_{XY} \sum_{YY}^{-1} \sum_{XY}^{T} \vec{f}_X = 4\zeta\eta \vec{f}_X \quad (10)$$

$$\sum_{YY}^{-1} \sum_{XY}^{T} \sum_{XX}^{-1} \sum_{XY} \vec{f}_Y = 4\zeta\eta \vec{f}_Y \quad (11)$$

The eigenvectors of the two matrices are related to each other through a simple equation: if $\vec{f}_X$ is a solution of equation (10) then $\sum_{YY}^{-1} \sum_{XY}^{T} \vec{f}_X$ is a solution of equation (11) provided that their joint eigenvalue is nonzero. Finally equation (4) is maximized by letting $\vec{f}_X$ and $\vec{f}_Y$ be the solution of equations (10) and (11) that corresponds to the

largest eigenvalue $\lambda = 4\zeta\eta$. We have got the canonical random variables $\beta^X = \left\langle \vec{X}, \vec{f}_X \right\rangle$ and $\beta^Y = \left\langle \vec{Y}, \vec{f}_Y \right\rangle$ that are most strongly correlated, the natural next step is to find the value of ρ. Using equation (4), (6), (8) and (2), (3) in sequence we find:

$$\begin{aligned}\rho^2 &= \vec{f}_X^T \sum_{XY} \vec{f}_Y \vec{f}_Y^T \sum_{XY}^T \vec{f}_X \\ &= 4\eta\zeta \vec{f}_X{}^T \sum_{XX} \vec{f}_X \vec{f}_Y^T \sum_{YY} \vec{f}_Y \\ &= \lambda\end{aligned}$$

In this way we have found that the correlation is the square root of the eigenvalue that corresponding to eigenvectors $\vec{f}_X$ and $\vec{f}_Y$.

To obtain $m = \min(m_X, m_Y)$ pairs of patterns $\left(\vec{f}_X^i, \vec{f}_Y^i\right)$ and m corresponding pairs of canonical variates the derivation detailed above can be repeated.

$$\beta_i^X = \left\langle \vec{X}, \vec{f}_X^i \right\rangle \qquad (12)$$

$$\beta_i^Y = \left\langle \vec{Y}, \vec{f}_Y^i \right\rangle \qquad (13)$$

with correlation $\rho_i = Cov\left(\beta_i^X, \beta_i^Y\right) = \sqrt{\lambda_i}$, i-1,2,…,m.

The canonical variates and patterns are indexed in order of deceasing eigenvalue λ_i. Pairs of canonical variates are uncorrelated $(i \neq j)$.

$$Cov\left(\beta_i^X, \beta_j^X\right) = Cov(\beta_i^Y, \beta_j^Y) = Cov\left(\beta_i^X, \beta_j^Y\right) = 0$$

Assume $\vec{\mathbf{X}}$ and $\vec{\mathbf{Y}}$ are of the same dimension of *m.* Then the canonical variates $\vec{\beta}^X = \left(\beta_1^X, ..., \beta_m^X\right)^T$ and $\vec{\beta}^Y = \left(\beta_1^Y, ..., \beta_m^Y\right)^T$ can be viewed as the result of coordinate transforms that have been applied to $\vec{\mathbf{X}}$ and $\vec{\mathbf{Y}}$. The transformations relate $\vec{\beta}^X$ and $\vec{\beta}^Y$ to $\vec{\mathbf{X}}$ and $\vec{\mathbf{Y}}$ through unknown matrices $\mathbf{F_X}$ and $\mathbf{F_y}$: $\vec{\mathbf{X}} = \mathbf{F_X}\vec{\beta}^X$, $\vec{\mathbf{Y}} = \mathbf{F_Y}\vec{\beta}^Y$ (14)

To find $\mathbf{F_X}$ we need $\vec{\beta}^{\mathbf{X}} = \left(\left\langle \vec{\mathbf{X}}, \vec{\mathrm{f}}_{\mathrm{X}}^{1} \right\rangle, \ldots, \left\langle \vec{\mathbf{X}}, \vec{\mathrm{f}}_{\mathrm{X}}^{\mathrm{m}} \right\rangle\right)^{T} = \mathrm{f}_{\mathrm{X}}^{\mathrm{T}} \vec{\mathbf{X}}$ where $\mathrm{f_X}$ is the $m \times m$ matrix with eigenvector $\vec{\mathrm{f}}_{\mathrm{X}}^{\mathrm{i}}$ in its *i*th column. Thus

$$Cov\left(\vec{\mathbf{X}}, \vec{\beta}^{X}\right) = Cov\left(\vec{\mathbf{X}}, \mathrm{f}_{\mathrm{X}}^{\mathrm{T}} \vec{\mathbf{X}}\right) = Cov\left(\vec{\mathbf{X}}, \vec{\mathbf{X}}\right) f_X = \Sigma_{\mathbf{XX}} f_X$$

Substituting equation (14) for $\vec{X}$, we get

$Cov\left(\vec{\mathbf{X}}, \vec{\beta}^{X}\right) = Cov\left(\mathbf{F_X} \vec{\beta}^{X}, \vec{\beta}^{X}\right) = \mathbf{F_X} Cov\left(\vec{\beta}^{X}, \vec{\beta}^{X}\right) = \mathbf{F_X}$ since $Cov\left(\vec{\beta}^{X}, \vec{\beta}^{X}\right) = \mathrm{I}$. Thus

$\mathbf{F_X} = \Sigma_{\mathbf{XX}} \mathrm{f_X}$ and similarly $\mathbf{F_Y} = \Sigma_{\mathbf{YY}} \mathrm{f_Y}$.

The columns of $\mathbf{F_X}$ and $\mathbf{F_Y}$. $\vec{\mathbf{F}}_{\mathbf{X}}^{\mathbf{i}}$ and $\vec{\mathbf{F}}_{\mathbf{Y}}^{\mathbf{i}}$, are called the **canonical correlation patterns.** The canonical variates β_i^X and β_i^Y are called also **canonical correlation coordinates** are normalized to unit variance, the canonical correlation patterns are expressed in the units of the field they represent and they indicate the typical strength of the mode represent by the patterns.

2.4 Computation of the Covariance Matrix

The correlation matrix [R] is introduced as a device for compactly representing the mutual correlations among K variables. The computation begins with the $(n \times K)$ matrix [X] of data values whose correlations are to be computed. Each row of this matrix is a vector, consisting of one observation each of K variables. The number of these rows is the same as the sample size, n, since each of these row vectors is a sample point (in K dimensions). Thus, [X] is essentially just an ordinary data table. An individual data element $x_{i,k}$ is the *i*th observation of the *k*th variable.

Define the (n * n) matrix [1], whose elements are all equal to 1. The $(n \times K)$ matrix of anomalies (in the geophysical sense of variables with their means subtracted), or centered data [X'] is then

$$[X'] = [X] - \frac{1}{n}[1][X] \qquad (1)$$

The second term in Equation (1) is a $(n \times K)$ matrix containing the sample means. Its n rows are all the same, and each consists of the K sample means in the same order as the corresponding variables appear in each row of [X]. Multiplying [X'] by the transpose of itself, and dividing by n - 1, yields an estimation S of the covariance matrix Σ_{XX}

$$[\Sigma_{xx}] = \frac{1}{n-1}[X']^T[X']$$

The covariance matrix $[\Sigma_{xx}]$ is a symmetric $(K \times K)$ matrix whose diagonal elements are the sample variances of the K variables, and whose other elements are the covariances

among the K variables. For example, $s_{1,1}$ is the sample variance of the first variable, and $s_{1,2}$ is the sample covariance between the first and the second variables. Because variances are so often expressed in terms of covariance matrices, it is fairly common to see the notation $s_{i,i}$ for the sample variance, which is equivalent to the more common and familiar s_i^2.

2.4.1 Eigenvalues and Eigenvectors of a Square Matrix

The formal definition of an eigenvalue of a matrix **A** is that it is any value λ, which is a root of the characteristic equation of the matrix,

$$\det(A - \lambda * I) = 0$$

λ is an eigenvalue of **A** if and only if there is a nonzero vector **x**, known as an eigenvector (or sometimes a "right" eigenvector), with the property that

$$A * x = \lambda * x$$

Note that there must also be a "left" eigenvector **y**, with the property

$$y * A = A' * y = \lambda * y$$

The characteristic equation has exactly N roots, so a matrix has N eigenvalues. An important consideration is whether any eigenvalue is a repeated root, which determines how hard the eigenvector computation will be.

If a matrix has the maximum possible number of linearly independent eigenvectors (namely N, the order of the matrix), then the eigenvalues and eigenvectors can be used to diagonalize the matrix. This only happens when the matrix is normal.

A nonzero vector **x** is an eigenvector of the square matrix **A** if

$$A * x = \lambda * x$$

for some scalar value λ, called the associated eigenvalue.

Sometimes this eigenvector is more particularly described as a right eigenvector, so that we may also consider left eigenvectors, that is, vectors **y** for which it is true that

$y * A = A' * y = \mu * y$ for some scalar μ.

For every eigenvalue of a matrix, there is at least one eigenvector. Every nonzero multiple of this eigenvector is also an eigenvector. If, and only if, an eigenvalue is a repeated root, then there may be more than one linearly independent eigenvector associated with that eigenvalue. In particular, if an eigenvalue is repeated 3 times, then there will be 1, 2 or 3 linearly independent eigenvectors corresponding to that eigenvalue.

For many statistical applications, eigenvalues and eigenvectors are calculated for real (not containing complex or imaginary numbers), symmetric matrices. Eigenvalues and eigenvectors of such matrices have a number of important and remarkable properties, some of which also hold for the eigenvalues and eigenvectors of square matrices more generally. The first of these properties is that the eigenvectors of symmetric matrices are orthogonal. That is, their dot products with each other are zero. Furthermore, since each eigenvector is defined to have unit length, the dot product of any eigenvector with itself is one:

$$x_i^T x_j = \begin{cases} 1, i = j \\ 0, i \neq j \end{cases}$$

2.4.2 Data Structure

Let us assume that we have measurements of some variable at locations $(\lambda_1,\varphi_1),(\lambda_2,\varphi_2)...(\lambda_P,\varphi_P)$ taken at times $t_1,t_2,...t_n$ where λ_K is latitude and φ_K is longitude of *k*th points. For each times $t_j\,(j=1,...n)$ we can think of the p-dimensional vector $F_{ji}\,(i=1,...p)$ as one map of the field .We store this measurements in a matrix **F** as n maps each being p points long. So one row of matrix **F** is one map for time t_j. We arrange each map into row vector in **F** with size p. We can then interpret each of the p columns in **F** as a time series for a given location. The EOF analysis is performed using **F** as the data matrix.

2.4.3 Algorithm of EOF Analysis

Let us assume that we have removed the mean from each of the p time series in **F**, so that each column has zero mean. We form the covariance matrix of **F** by calculating $\mathbf{R}=\mathbf{F}^{\mathrm{T}}\mathbf{F}$, and then we solve the eigenvalue problem. $\mathbf{RC}=\mathbf{C}\Lambda$

Λ is a diagonal matrix containing the eigenvalues λ_i of R. The c_i column vector of **C** are the eigenvectors of R corresponding to eigenvalues λ_i. Both Λ and **C** are the size $p\times p$. For each eigenvalue λ_i chosen we find the corresponding eigenvector c_i. Each of this eigenvectors can be regarded as a map. These eigenvectors are the EOFs we are looking for. In what follows we always assume that the eigenvectors are ordered according to the size of the eigenvalues. Thus, EOF1 is the eigenvector associated with

the biggest eigenvalue, and the one associated with the second biggest eigenvalue is EOF2, etc. Each eigenvalue λ_i, gives a measure of the fraction of the total variance in R explained by the mode. The value in percentage is found by dividing the λ_i by the sum of all the other eigenvalues (the trace of Λ).

The eigenvector matrix **C** has the property that $\mathbf{C^TC=CC^T=I}$ or the EOFs are uncorrelated over space. Another way of stating this is to say that the eigenvectors are orthogonal to each other.

The pattern obtained when an EOF is plotted as a map, represents a standing oscillation. The time evolution of an EOF shows how this pattern oscillates in time. To see how the first EOF evolves in time we calculate:

$$\mathbf{a_1=Fc_1}$$

The n components of the vector $\vec{a_1}$ are the projections of the maps in F on EOF1, and the vector is a time series for the evolution of EOF1. In general, for each calculated EOFj, we can find a corresponding $\vec{a_j}$. These are the expansion coefficients of the EOFs. Just as the EOFs where uncorrelated in space, the expansion coefficients are uncorrelated in time.

A common use of EOF is to reconstruct a cleaner version of the data by truncating this sum at some $j = N << p$; that is, we only use the EOFs of the first (largest) few eigenvalues or the most significant EOFs. The rational is that the first N eigenvectors are capturing the dynamical behavior of the system and the other eigenvectors (corresponding to the smallest eigenvalues) are just due to random noise. This assumption does not always have to be true.

The algorithm for finding EOF is:

- First form matrix . from the observations, and remove the time mean of each time series.
- Then find the covariance matrix $\mathbf{R}=\mathbf{F}^{\mathrm{T}}\mathbf{F}$.
- Then find the eigenvalues and eigenvectors of R by solving $\mathbf{RC} = \mathbf{C\Lambda}$
- Afterwards find the biggest eigenvalues and their corresponding eigenvectors, the EOFs.
- Then find the expansion coefficients by calculating $\mathbf{a_j}=\mathbf{FC_j}$

2.4.4 EOF analysis Algorithm with Matlab

Matlab algorithm was developed for EOF analysis that includes the following steps.

- Define a matrix M, with each row as one map, and each column a time series for a given station. That means in matrix M, the data need to be put in such a way that row represents map and column represents time series.
- Remove the mean of the column.
- Form the covariance matrix by the command: **R=F'*F**;
- Calculate the eigenvalues and eigenvectors of the covariance matrix.
- Find the expansion coefficients corresponding to eigenvalue number i.
- Compute the vector giving the amount of variance explained for each eigenvalue.

2.5 Computation of CC patterns after a Transformation to EOF Coordinates

In the calculation of CCA, if the data are transformed into EOF space before the analysis the CCA algebra becomes considerably simpler. Suppose that only the first k_X and k_Y EOFs are retained, so that

$$\vec{X} \approx \sum_i^{kx} \alpha_i^{X+} \vec{e}_X^{i+}$$

$$\vec{Y} \approx \sum_i^{ky} \alpha_i^{Y} \vec{e}_X^{i+} \qquad (20)$$

We have used the renormalized versions of the EOFs and their coefficients $\alpha_i^+ = (\lambda_i)^{-1/2} \alpha_i$ and $\vec{\mathbf{e}}^{\mathbf{iT}} = (\lambda_i)^{1/2} \vec{e}^{\,i}$. The CCA is then applied to the random vector $\vec{X}' = \left(\alpha_1^{X+}, ..., \alpha_{k_X}^{X+}\right)^T$ and $\vec{Y}' = \left(\alpha_1^{Y+}, ..., \alpha_{k_Y}^{Y+}\right)^T$. An advantage of this approach is that it is often possible to use only the first few EOFs.

Another advantage is that the algebra of the problem is simplified since $\sum_{X'X'}$ and $\sum_{Y'Y'}$ are both identity matrices. Thus according to the equations (10, 11) $\vec{\mathbf{f}}_{X'}^{\,i}$ and $\vec{\mathbf{f}}_{Y'}^{\,i}$ are eigenvectors of $\sum_{X'Y'} \sum_{X'Y'}^T$ and $\sum_{X'Y'}^T \sum_{X'Y'}$ respectively. As these are non-negative definite symmetric matrices, the eigenvectors are orthogonal. Moreover, the canonical correlation patterns $\vec{\mathbf{F}}_{X'}^{\,i} = \vec{\mathbf{f}}_{X'}^{\,i}$ and $\vec{\mathbf{F}}_{Y'}^{\,i} = \vec{\mathbf{f}}_{Y'}^{\,i}$.

A minor disadvantage is that the patterns are given in the coordinates of the renormalized EOF space. To express the pattern in the original coordinate space it is necessary to reverse transformation (20) with (18) and (19):

$$\vec{\mathbf{f}}_X^{\,i} = \sum_{\mathbf{j=1}}^{\mathbf{k_X}} \left(\lambda_j^X\right)^{1/2} \left(\vec{\mathbf{f}}_{X'}^{\,i}\right)_j \vec{\mathbf{e}}_X^{\,j}$$

$$\vec{\mathbf{f}}_Y^{\,i} = \sum_{\mathbf{j=1}}^{\mathbf{k_Y}} \left(\lambda_j^Y\right)^{1/2} \left(\vec{\mathbf{f}}_{Y'}^{\,i}\right)_j \vec{\mathbf{e}}_Y^{\,j}$$

$$\vec{\mathbf{F}}_X^{\,i} = \sum_{\mathbf{j=1}}^{\mathbf{k_X}} \left(\lambda_j^X\right)^{1/2} \left(\vec{\mathbf{f}}_{X'}^{\,i}\right)_j \vec{\mathbf{e}}_X^{\,j}$$

$$\vec{\mathbf{F}}_Y^{\,i} = \sum_{\mathbf{j=1}}^{\mathbf{k_Y}} \left(\lambda_j^Y\right)^{1/2} \left(\vec{\mathbf{f}}_{Y'}^{\,i}\right)_j \vec{\mathbf{e}}_Y^{\,j}$$

The canonical correlation patterns are no longer orthogonal after the above back transformation and $\mathbf{f} \neq \mathbf{F}$.

Chapter 3

Seasonal, Interannual and Interdecadal Variability of Atmospheric Characteristics and Sea Surface Temperature in the North Atlantic

The physical processes in the ocean surface layer play an important role in formation of the atmosphere and ocean variability. The incident solar radiation absorbed by the ocean heats the surface layer. The ocean surface is in contact with the atmosphere and exchanges heat and water with the near surface air masses.

Seasonal and latitudinal variations in ocean sea surface temperature are driven primarily by variations of insolation. The amount of solar radiation incident on the ocean surface depends on the latitude, season and time of the day. The mean solar flux per unit area perpendicular to the solar beam at the mean position of Earth is equal to $S_0 = 1367$ w/m^2. The Earth is approximately spherical; and the planets surface is heated differentially. The solar heat flux at the ocean surface depends on the local solar zenith angle θ_S at each latitude. It is equal to zero at the equator and approaches 90^0 at high latitudes. Beyond the astronomical factors, the solar radiation incident to the ocean surface depends also on atmospheric characteristics. The solar heat enters the atmosphere is partly reflected back to the space and partly absorbed by the air molecules. The amount and spectrum of the solar radiation at the ocean surface depends therefore on the content of greenhouse gasses and clouds in the atmosphere.

The solar heat flux per unit area in the upper atmosphere is

$$Q = S_0 \left(\frac{\bar{d}}{d} \right)^2 \cos\theta_S$$

where $\bar{d}$ is the mean distance from which the flux density S_0 is measured, and d is the actual distance from the sun. The solar radiation Q_0 incident on the ocean surface is large in the equatorial areas and smaller in the polar ocean. The ocean reflects back part of the solar heat Q_0 incident to its surface. The amount of the reflected radiation depends on the roughness of the ocean surface. The strongest reflection is observed in the ocean areas covered by ice. The part of the radiation reflected by the ocean surface is called albedo α_S, which for the major part of the ocean has a value $\alpha_S \approx 0.3$. In the polar ocean α_S may have values higher than 0.3.

The ocean emits back to the atmosphere outgoing long wave radiation R_L. It is greatest over the tropical ocean, where cloud cover is relatively low. R_L is lowest in the polar regions and in regions of persistent high cloudiness in the equatorial areas.

The zonal averaged annual mean net radiation

$$R_{net} = Q_0(1-\alpha_s) - R_L$$

is positive equator-ward of 40^0 of latitude and negative pole-ward of that latitude. Assuming that the ocean and atmosphere are in steady state conditions, which means that long term annual mean ocean and atmospheric characteristics do not change, one can write the balance of the energy at the ocean surface as

$$R_{net} - LE - SH - \Delta Feo = 0$$

where LE is the latent heat, SH the sensible heat, ΔFeo is the horizontal flux out of the column of ocean below the ocean surface. We will often refer to ΔFeo also as the meridional heat flux. ΔFeo is due to the horizontal circulation and turbulent mixing in the ocean.

The meridional heat transport exists in both atmosphere and ocean. If this transport would not exist, the tropics would be much warmer and the poles much colder. The net turbulent heat flux.

$$H_T = LE + SH$$

is the heat exchange through the ocean surface due to processes of turbulent mixing in the boundary layers of atmosphere and upper ocean.

The near surface atmospheric and ocean characteristic depend in a complex way on the surface energy balance. At the same time some of them like SST, atmospheric temperature, humidity, wind speed influence the intensity of the heat exchange through the surface. In this way, the near surface atmospheric and ocean characteristics may be considered as important indicators for the long-term changes in state of the atmosphere and ocean. This section presents analysis of interannual variability in the near surface atmospheric characteristics and SST.

Following the previous studies of Kushnir (1994), Deser and Blackmon (1993) the winter SST and atmospheric parameters are studied here. During the winter the convective processes intensify the vertical turbulent mixing in the surface ocean layer. The depth to which the vertical transport of heat reaches during this season varies usually from about 100m in mid-latitudes up to about 2000m in the deep convection areas. During the rest of the year the vertical mixing is limited to a relatively thin surface layer.

In this chapter first the seasonal mean characteristics of SST, atmospheric temperature, zonal wind and net turbulent heat flux are described. The seasonal variability usually is much stronger than variability at interannual and interdecadal time scales. The later however is important because it shows the tendencies in the ocean and atmospheric variability at long time scales. The winter anomalies of SST and near surface atmospheric characteristics are discussed in section 2.

3.1 Seasonal Variability

This section describes the seasonal variability of atmospheric characteristics and SST. The seasonal mean parameters are calculated for winter December, January, February (DJF), spring March, April, May (MAM), summer June, July, August (JJA) and autumn September, October, November (SON) seasons. As described in the previous section the near surface atmospheric characteristics and SST distribution depends on the radiative fluxes, interaction between the atmosphere an ocean and atmospheric dynamics (see Fig 3.1). The dependence of the absorbed solar radiation on the latitude results in quasi-zonal structure of atmospheric parameters i.e. their variability in zonal direction is smaller than in meridional. The air temperature equatorward of 30^0N, where the net radiative balance is positive, is relatively high and remains between 20^0 and 30^0 during the whole year. In the subpolar areas the seasonal mean air temperatures change from –5 to +10 degrees C.

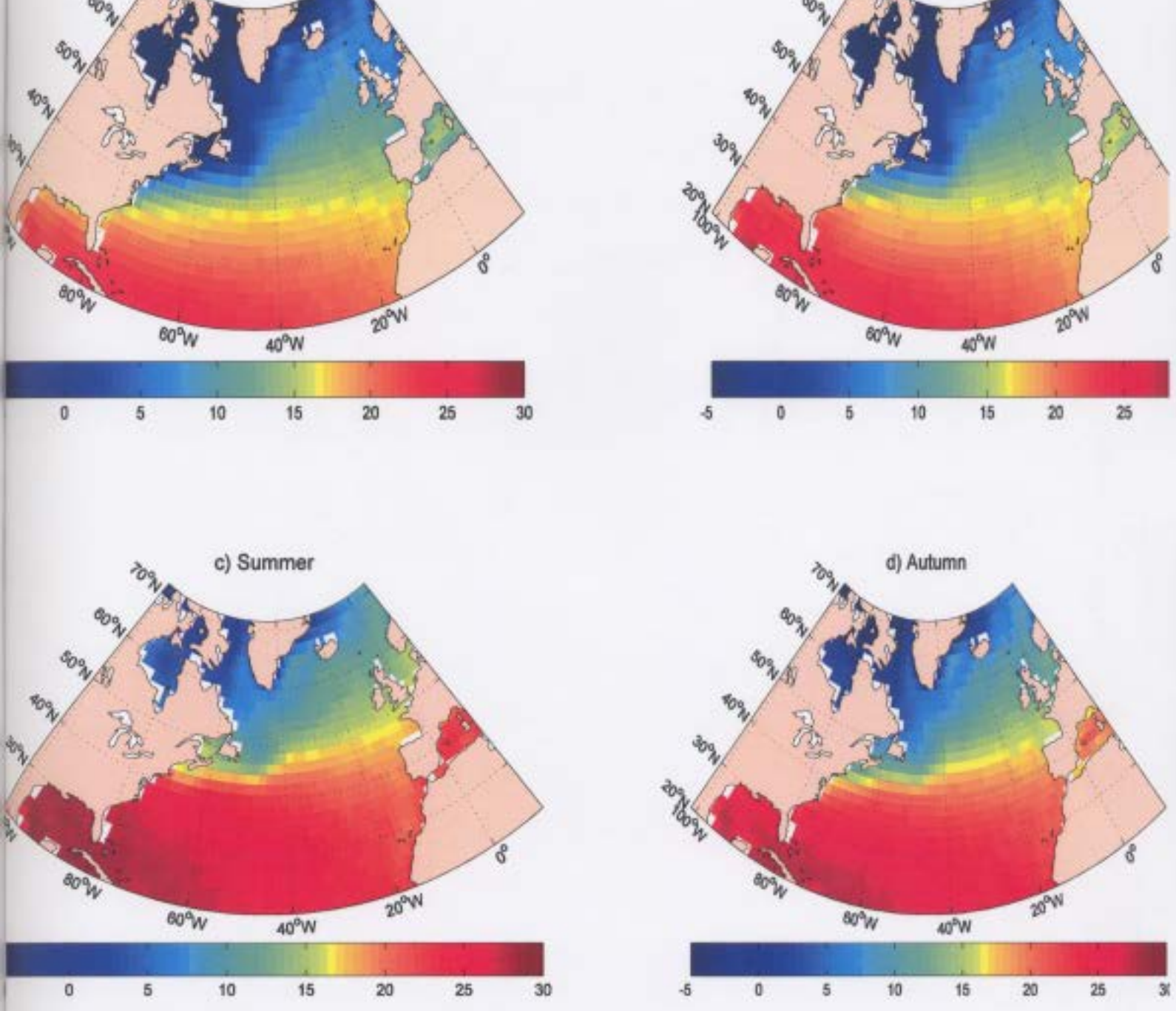

Fig 3.1:Seasonal Mean Air Temperature (^{0}C).(a)Winter,(b)Spring,(c)Summer,(d)Autumn

There is also a longitudinal change in the atmospheric temperatures during all seasons. In all seasons the maximum of air temperature is in the western part of the tropical ocean. This is the area of Gulf Stream, which transports warm waters along the North America Coast. The Gulf Stream heat transport is a major contributor to the meridional ocean heat transport in the subtropical North Atlantic. The atmospheric temperature in eastern subtropical North Atlantic is colder than in western and central part of the basin. This is an area of intensive upwelling, where cold waters are transported from the deep ocean to the surface. The relatively cold ocean waters in the upwelling areas near the eastern coast of the Sub-tropical North Atlantic cool the near surfaces air.

The atmospheric temperature differs also in the eastern and western part of the sub-polar North Atlantic. As in the sub-tropics, this difference is due to the transport in the ocean. The ocean current along the western coasts of the sub-polar North Atlantic transport cold waters from the polar areas towards the Labrador Sea. This currents transport also sea-ice which melts in spring in the Labrador Sea. The melting of the ice causes additional cooling and freshening of the surface waters. The temperature in the eastern sub-polar North Atlantic is influenced by the Gulf Stream, which transports warm waters, towards the polar areas. The seasonal atmospheric temperatures here are 10^0 to15^0 higher than in the western part of the sub-polar North Atlantic.

The atmospheric zonal wind (Fig 3.2) over the North Atlantic is influenced by two major elements of the atmospheric circulation. These are the passats in the tropical area

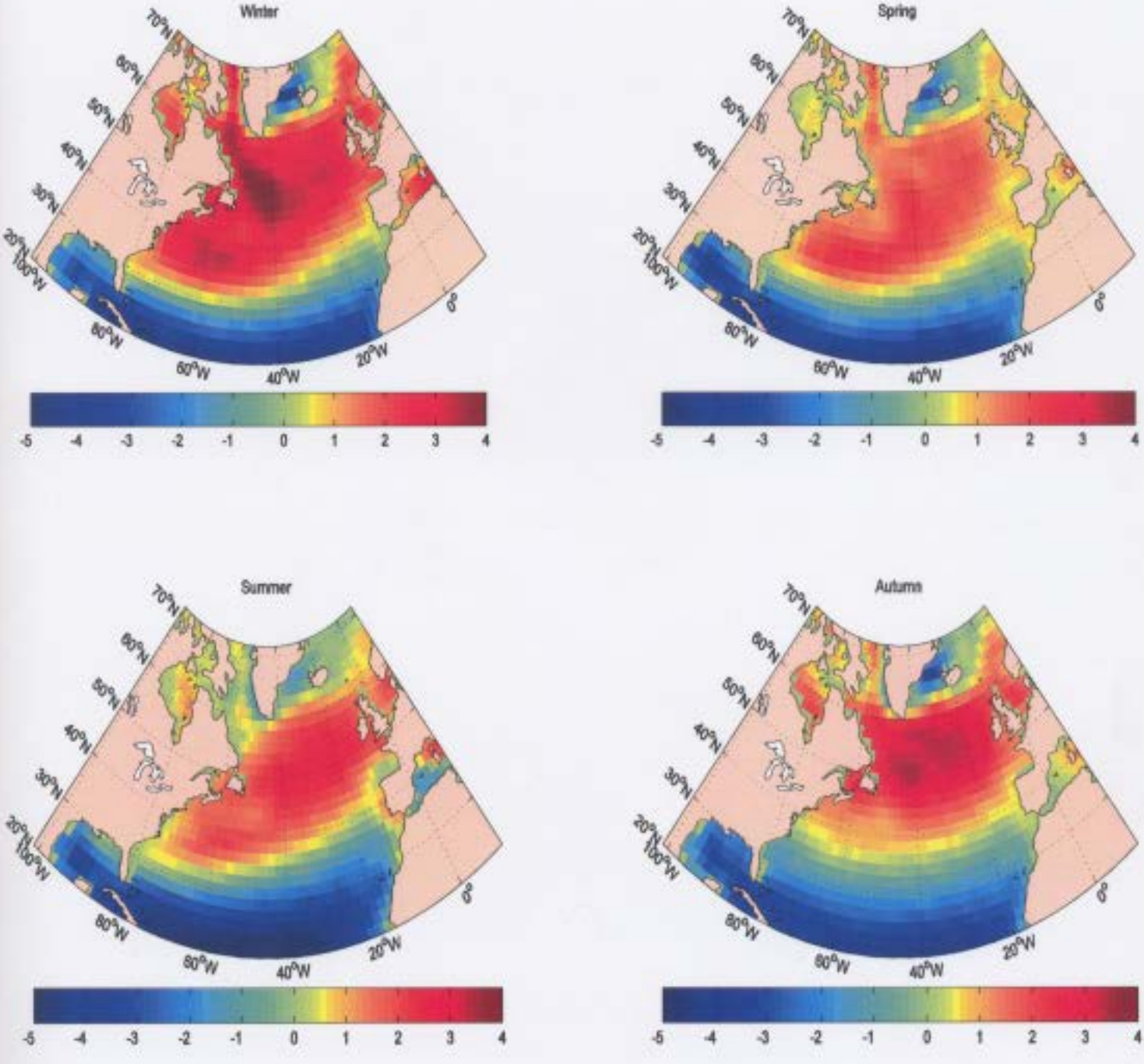

Fig 3.2: *Seasonal Mean Zonal Wind (m/s). a) Winter b) Spring c) Summer d) Autumn*

and westerlies in the mid-latitudes. The passat winds in the tropical area are predominantly easterlies. They persist with some seasonal variability during the whole year. The later is driven by the upward atmospheric flow in equatorial area. Here humid air masses warmed by the ocean surface move upward. At high altitudes the dominant flow is poleward, where the uplifted at the equator air masses, propagate towards the tropics. The passats form the lower branch of Hadley circulation, and they bring dry air masses towards the equator. Passats have a strong westward component, which is present at low latitudes during all seasons (Fig 3.2 a, b, c, d). In summer the Hadley cell intensifies in the Northern Hemisphere. Correspondingly the passats have their strongest seasonal mean zonal component during this season (Fig 3.2c).

The westerlies in the mid and sub-polar latitudes persist during all seasons. This is the area of polar jet stream. It forms between latitudes 30^0N and 70^0N. The strong eastward flow at high altitudes is formed due to the meridional gradient of atmospheric temperature and is a consequence of the thermal wind relation, which governs the large-scale geophysical flows. Additionally there is a tendency of developing cyclonic disturbances in mid-latitudes along the jet stream to form fronts. The frontogenesis processes related to the dynamics of cyclones, result in concentration of north-south temperature gradients into relatively narrow regions. This contributes to the sharpness of the jets. The area of positive zonal wind in mid-latitudes (Fig 3.2) is the zone where intensive cyclones and related frontal systems pass the North Atlantic. During the winter, the cyclones bring relatively cold and dry air masses over the North Atlantic. Additionally the cyclonic atmospheric eddies are related with strong near surface winds. As discussed in the beginning of this chapter, under these conditions the surface heat and

water fluxes intensify the areas where the contrast between atmospheric and ocean temperature is high. The process of cyclogenesis is stronger in winter and autumn. Correspondingly these are the seasons of strongest westerlies and related storms passing the mid latitudes of North Atlantic. Strong easterlies are present along the eastern coast of Greenland. They have strongest magnitude in winter and autumn.

The SST, as the atmospheric temperature has a well defined zonal distribution. The equatorial and tropical areas of the North Atlantic are warm during the whole year. The temperature here varies between 20^0 to 25^0C with maximum in summer when the absorbed solar radiation is higher. The minimum of the SST during all seasons is in the sub-polar areas. Deviation from the zonal structure of SST distribution is observed in the areas of western boundary currents- Gulf Stream, the Labrador Current and East Greenland Current.

The Gulf Stream and its extension, the North Atlantic current, transports warm waters towards the Northeastern part of the North Atlantic. The SST along the North American coast and the western coast of Europe is high due to this transport. The Labrador Current and the eastern Greenland current transport cold waters toward the coast of North East North Atlantic. This flow, which during the winter and spring transports also sea-ice, has the strongest impact on the SST during these seasons. Another area of deviation from the zonal distribution of SST is in the North Western Africa upwelling region.

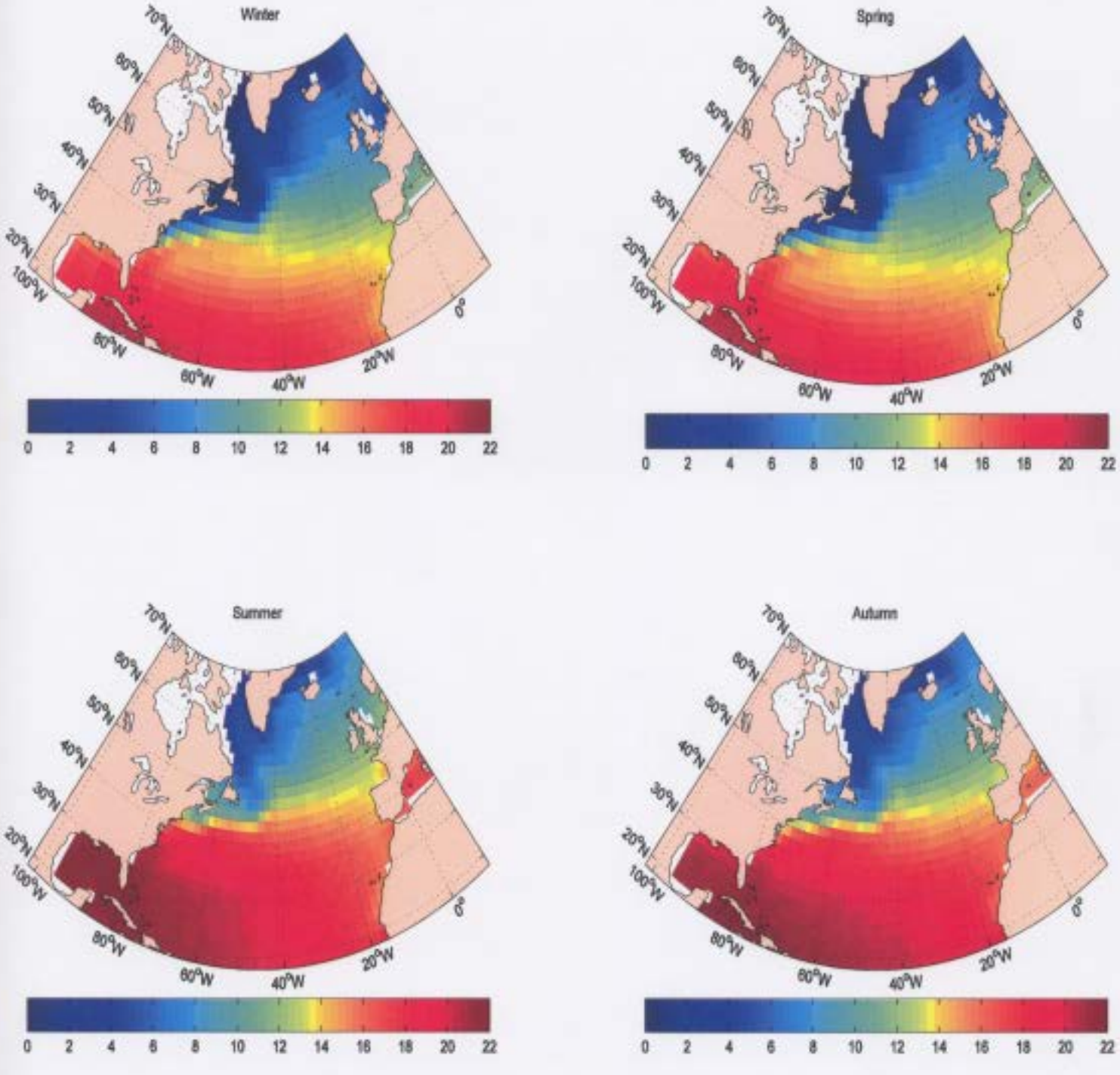

Fig 3.3: Seasonal Mean SST (^{0}C) . a) Winter, b) Spring, c) Summer, d) Autumn

The spatial and temporal variability of T_A and SST have similar patterns. One reason for this is the surface turbulent heat transport. The direction of the surface turbulent heat transport across the surface is always towards the cooler component of the system ocean atmosphere, which keeps T_A and SST close.

Net heat flux Q_{net} consists of two radiative flux components, which are the surface shortwave and longwave radiation and two components of the turbulent heat: sensible and latent heat fluxes. Q_{net} over the oceans is one of the key parameters governing the atmosphere-ocean interaction. It is required for weather prediction and climate studies related to the global energy balance and water cycle. Using suitable models, net heat flux can be used to reproduce and predict variations of the global ocean regime and its impact on atmospheric dynamics, as well as variations in regional hydrological processes and water resources and responses to such environmental changes as the increase in greenhouse gas forcing. Here we discuss the seasonal variability of turbulent net heat flux H_T. Its dominant component is the evaporative heat loss. The sensible heat exchange at the ocean surface is smaller, except over the warm Gulf Stream.

H_T is predominantly negative in the whole North Atlantic. In the tropics there is an area of strong heat loss by the ocean, which coincides, with the zonal belt of passats winds. This is the area of strong evaporation and negative latent heat flux. The turbulent heat flux in the Gulf Stream area is negative during all the seasons. The heat loss by the ocean here is strongest in winter when the contrast between the atmospheric and sea temperatures is relatively large. H_T has high seasonal variability also in the Labrador and Greenland seas.

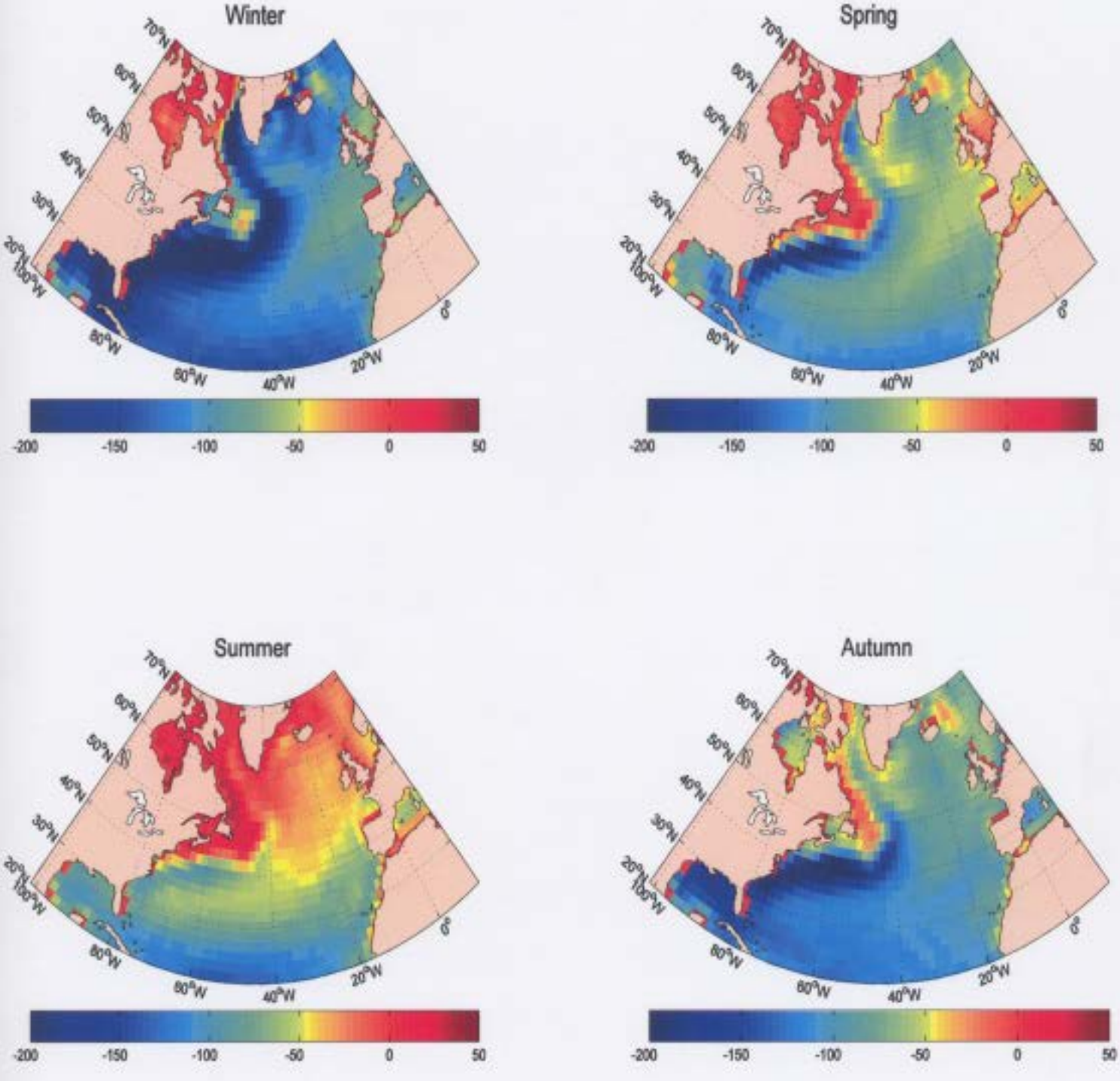

Fig 3.4: *Seasonal Mean Total Heat Flux (W/m^2) (a) Winter, (b)Spring, (c) Summer, (d) Autumn*

These are two areas of deep water formation, which are strongly cooled during the winter (Fig 3.4 a,b). In summer the heat loss through the turbulent exchange here is relatively weak.

3.2 Inter-Annual and Inter-Decadal Variability

In this section winter anomalies of atmospheric characteristics and SST are discussed. The anomalies are calculated for winter months only and then averaged for every year. The annual mean anomalies are then used to describe the interannual variability of the North Atlantic.

As mentioned in the previous section the SST and near surface atmospheric temperature are quasi-zonaly distributed. This fact was used in previous studies (see Kushnir,1994) of the North Atlantic interannual variability, where the anomalies were studied separately in several zonal belts of the basin. In the previous section it was shown that there are two major areas in the North Atlantic which have different characteristics and dynamics: 1) the subtropical North Atlantic is characterized by high SST, T_A and wind (passats) which have westward direction 2) the mid and high latitudes with colder atmosphere, ocean surface and winds with predominant eastward direction. Here we study SST and atmospheric characteristics averaged for these two regions.

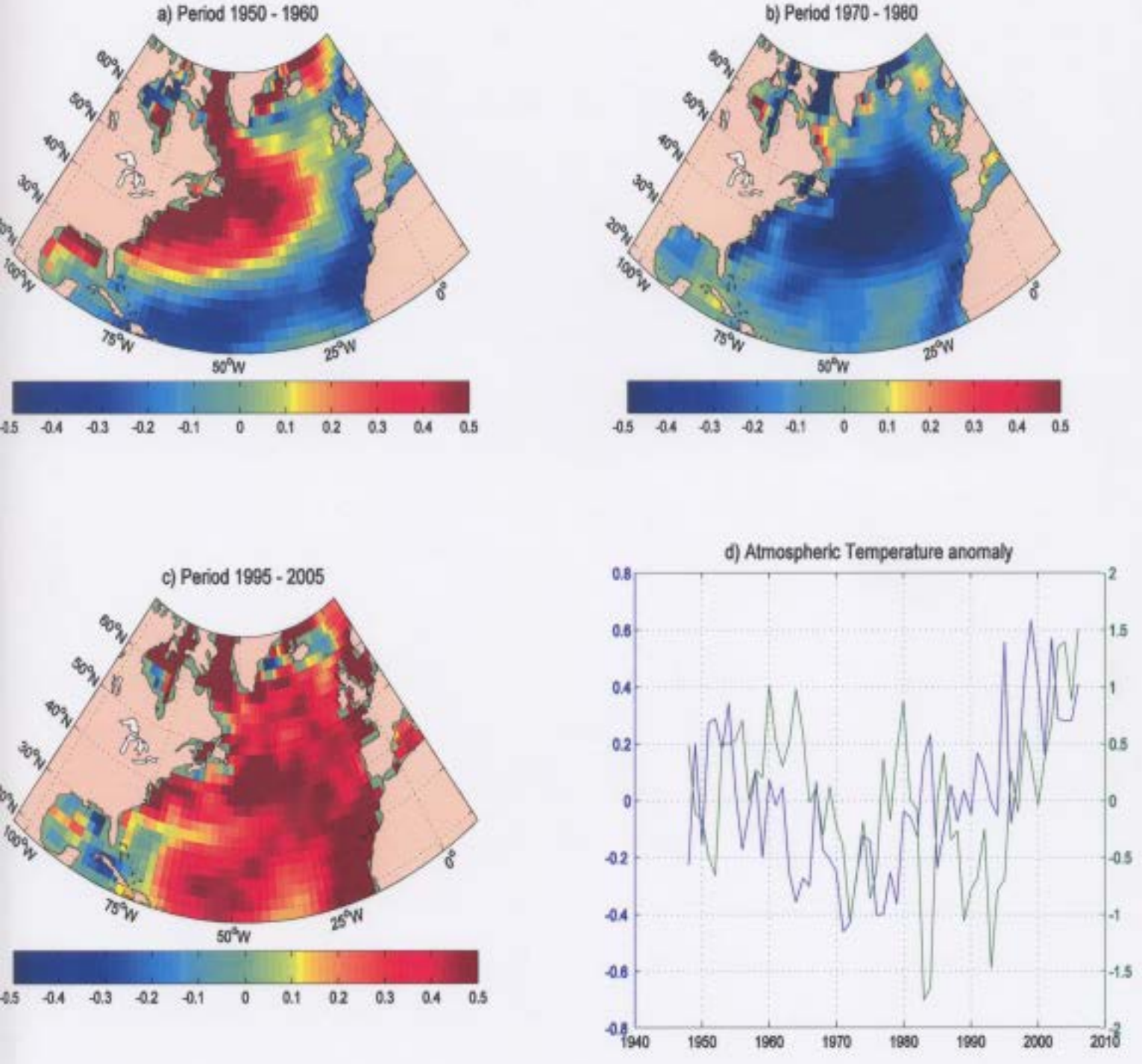

Fig 3.5: Inter-Annual and Inter-Decadal Variability of Air Temperature

Fig 3.5.d shows the air temperature anomaly averaged within two zonal belts, $20^0 \leq \varphi \leq 45^0$ and $45^0 \leq \varphi \leq 70^0$. Here after, the zonal belt $20^0 \leq \varphi \leq 45^0$ will be shortly referenced as the southern area, and the zonal belt $45^0 \leq \varphi \leq 70^0$ as the northern area. The surface atmospheric temperature anomaly distributions in the two areas (Fig 3.5 d) show some similarities. The decadal mean anomalies are predominantly positive in the both regions in early 1950s and negative in the 1970s. The temperature anomalies in the two areas (southern and northern) show a warming trend at the end of the study period from 1995 to 2005. In the southern region (blue line) this trend starts in the late 1980s while in the northern region (green line) it begins later- in the second half of the 1990s.

The spatial distribution of the atmospheric temperature anomaly averaged for three periods of time : (a) from 1950 to 1960, (b) from 1970 to 1980 and (c) from 1995 to 2005 are shown on Fig 3.5 a, b, c. The first period 1950-1960 (Fig 3.5 a) was relatively warm in the Western North Atlantic. The pattern of the highest atmospheric temperature extends along the Gulf Stream area, the Labrador Sea and off east coast of Greenland. Negative atmospheric temperature anomalies are observed in the zonal belt between 20^0N and 30^0N and along the Western North Africa and Western European coasts.

The cold atmospheric temperatures during the 1970s dominate in a zonal region of the North Atlantic between 30^0N and 55^0N, in the Northern Labrador Sea and along the Northwestern Africa coast. Slightly positive anomalies are observed in the rest of the North Atlantic. The comparison of Fig 3.5 with Fig 3.2 suggests that the mid-latitude areas of strongest warming in the 1950s and cooling in the 1970s approximately coincides with the mid-latitude area of westerlies. In the tropical areas where the

dominant winds are passats, the anomalies were negative in the 1950s and close to zero in the 1970s. In the late 1990s the atmospheric anomalies are positive almost in the whole North Atlantic with the exception of a small region in the Caribbean basin.

The wind anomalies in the northern and southern areas are clearly anticorrelated during the period from 1948 to 1995 (Fig 3.6 d). From 1950-1965 the zonal westerlies in the northern area tend to decrease, while the zonal wind anomaly increases in the southern sub-region. During the rest of the period until 2005, the wind interannual variability is opposite in the two regions. The reason for this anticorrelation between winds anomalies in the sub-regions, which is discussed in more details in the next chapter, are related to the variability of the North Atlantic Oscillation (NAO).

The zonal air mass transport is an important factor for the air-sea interaction over the North Atlantic. Intense zonal winds bring relatively dry air from the continent over the ocean. The weakening of the zonal winds off the coast of Newfoundland in the 1950s is related to weakening of storms and cold air masses transport in this area. Correspondingly the winter of 1950s were warmer than usual in this part of the North Atlantic. In opposite the westerlies were stronger than usual in 1970s (Fig.3.6.b). The winters of 1970s were correspondingly colder than usual at mid-latitudes (Fig.3.5.b). However, the comparison of (3.5c) and (3.6c) shows that this relation between the zonal wind and T_A anomalies is not always present.

In the 1990s the zonal wind anomalies in the whole North Atlantic show overall increase in the intensity of both system- westerlies in the mid and polar latitude, and easterlies in

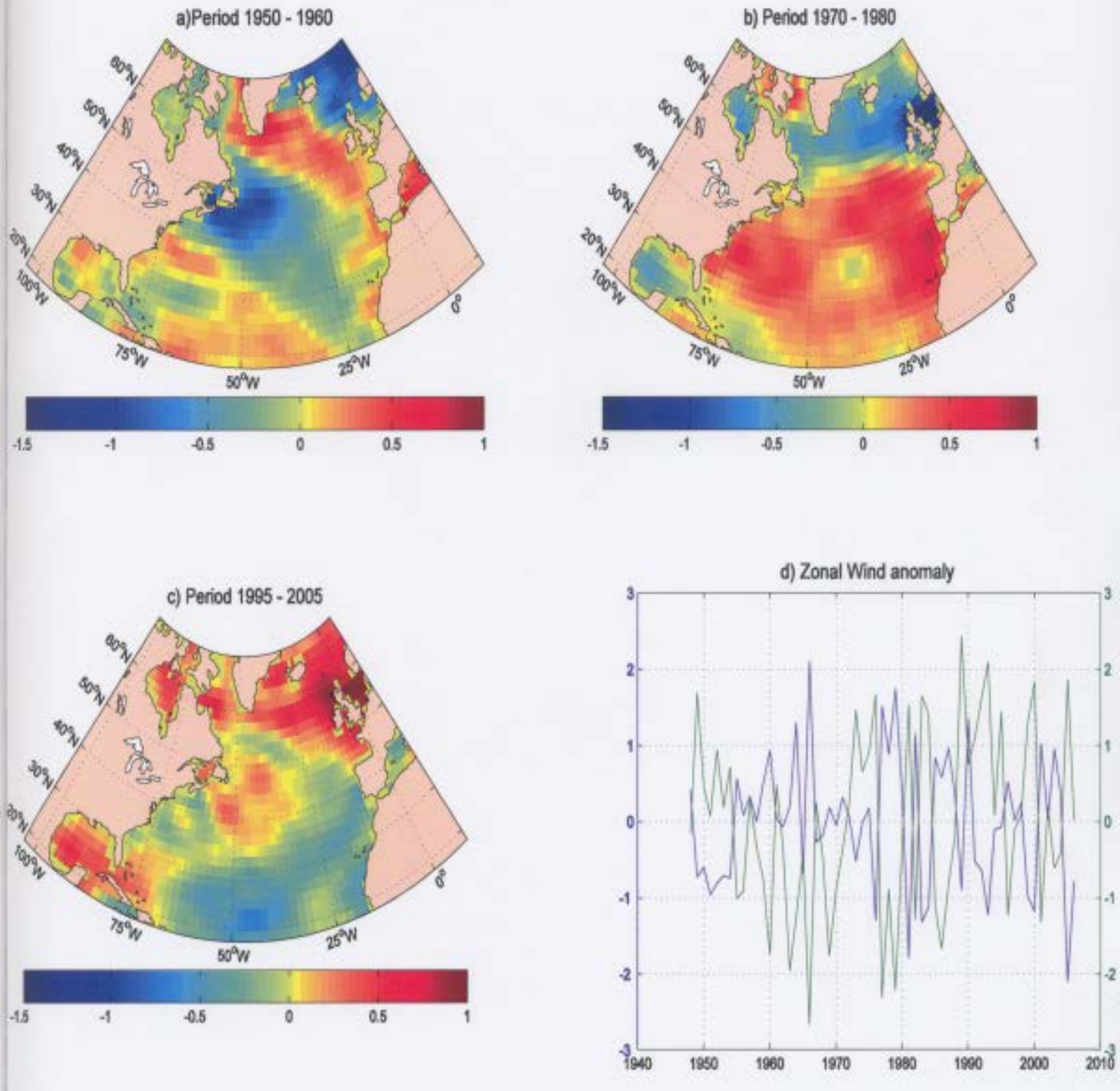

Fig 3.6: Inter-Annual and Inter-Decadal Variability of Wind

the tropics. One would expect that the intensified transport of continental cold and dry air would intensify the heat loss in the both areas. T_A (Fig 3.5) and SST anomalies (see below) however are both positive over the main part of the basin. This presumably may be explained by the fact that there are other factors beyond the zonal transport, which influence the surface atmospheric temperature distribution during this period. Two of the most important factors which remain beyond this study are radiative fluxes and meridional transport. They are the major 'candidates' which may be responsible for the overall warming of the North Atlantic.

Fig 3.7 of SST anomalies clearly show presence of three periods in the North Atlantic SST variability. The SST anomalies are in general positive in the 1950s and negative in the 1970s. After 1995, the SST anomaly increase until the end of the period which is 2005. The patterns of SST in the 1950s, 1970s and in the 1990s are very similar with the pattern of T_A, suggesting that the variability of these two parameters is strongly connected.

The net heat flux (Fig 3.8) exhibits more complex variability than the parameters discussed so far. The net heat flux depends in a complex way on T_A, SST and wind speed. The variability of all these parameters together with atmospheric humidity influences the net heat flux. In the 1950s the net heat flux is predominantly positive in the almost whole North Atlantic except the area of Gulf Stream and North Atlantic current.

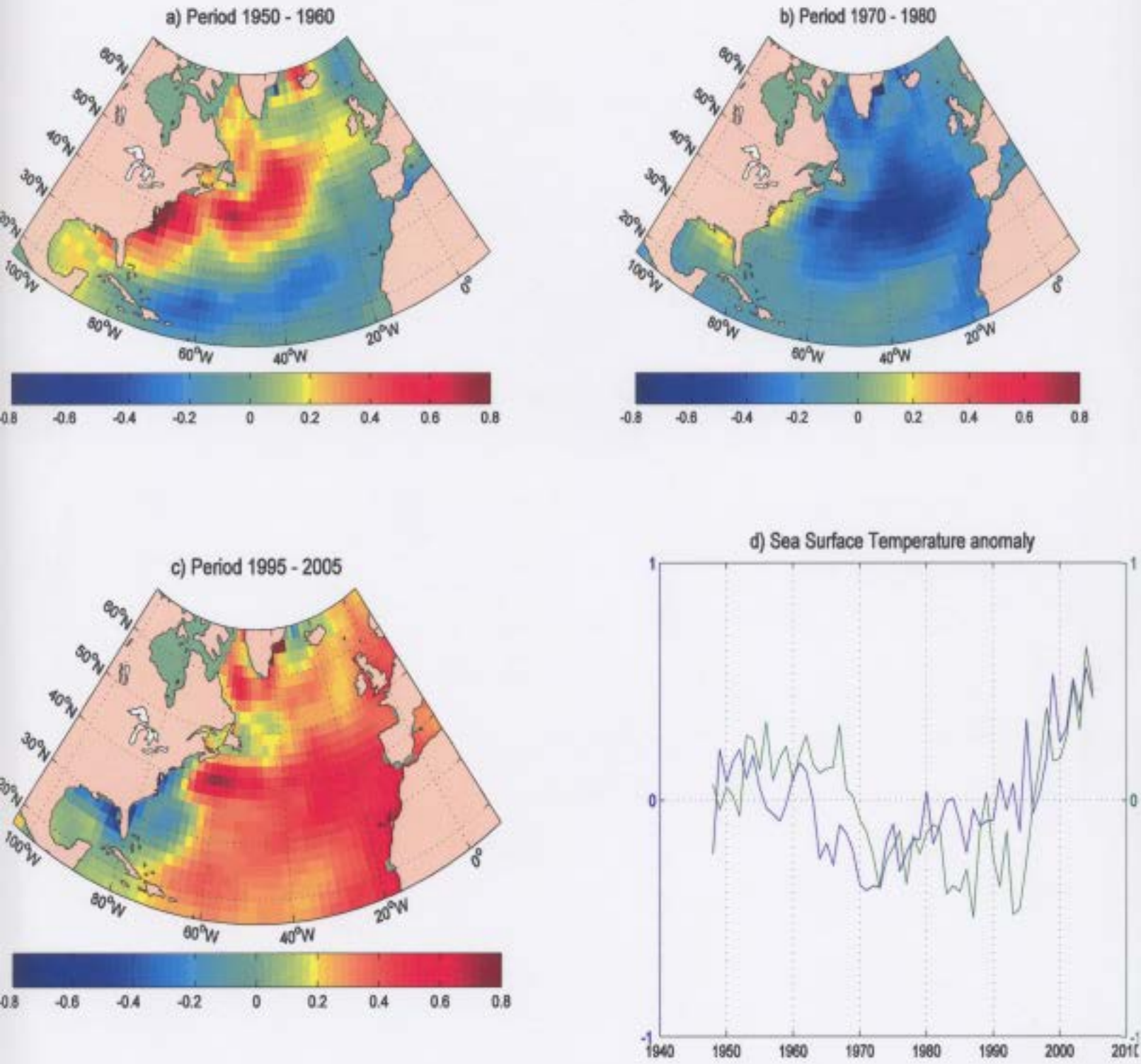

Fig 3.7: Inter-Annual and Inter-Decadal Variability of SST

In the 1970s the heat flux is predominantly negative with exception of the Gulf Stream area and a area off the coast of Western Europe. In the 1990s the heat flux anomaly in tropical and subtropical North Atlantic is positive. In the areas of deep-water formation in the Labrador and Greenland Sea the heat flux is negative. In the northern Labrador Sea, there is an area of positive heat flux anomaly, which however is relatively small. The spatial mean of the heat flux anomaly in the 2000 (Fig 3.8 a) is positive in the southern and negative in northern area.

The analysis of seasonal mean and anomalies of the surface atmospheric characteristics and SST suggest that there are distinct patterns of ocean-atmosphere relationship associated with interannual variability. The middle and high latitude SST and T_A display a long term fluctuations with positive anomalies in the 1950s and 1990s and negative anomalies in the 1970s. The zonal wind anomalies are negatively correlated in middle and low latitudes. The patterns in the zonal wind show some relation with the SST and T_A anomalies in the mid latitudes in the 1950s and in the 1970s. In the 1990s this relation is less evident. In this period the turbulent net heat flux is predominantly negative in the polar areas and positive in the low and middle latitudes.

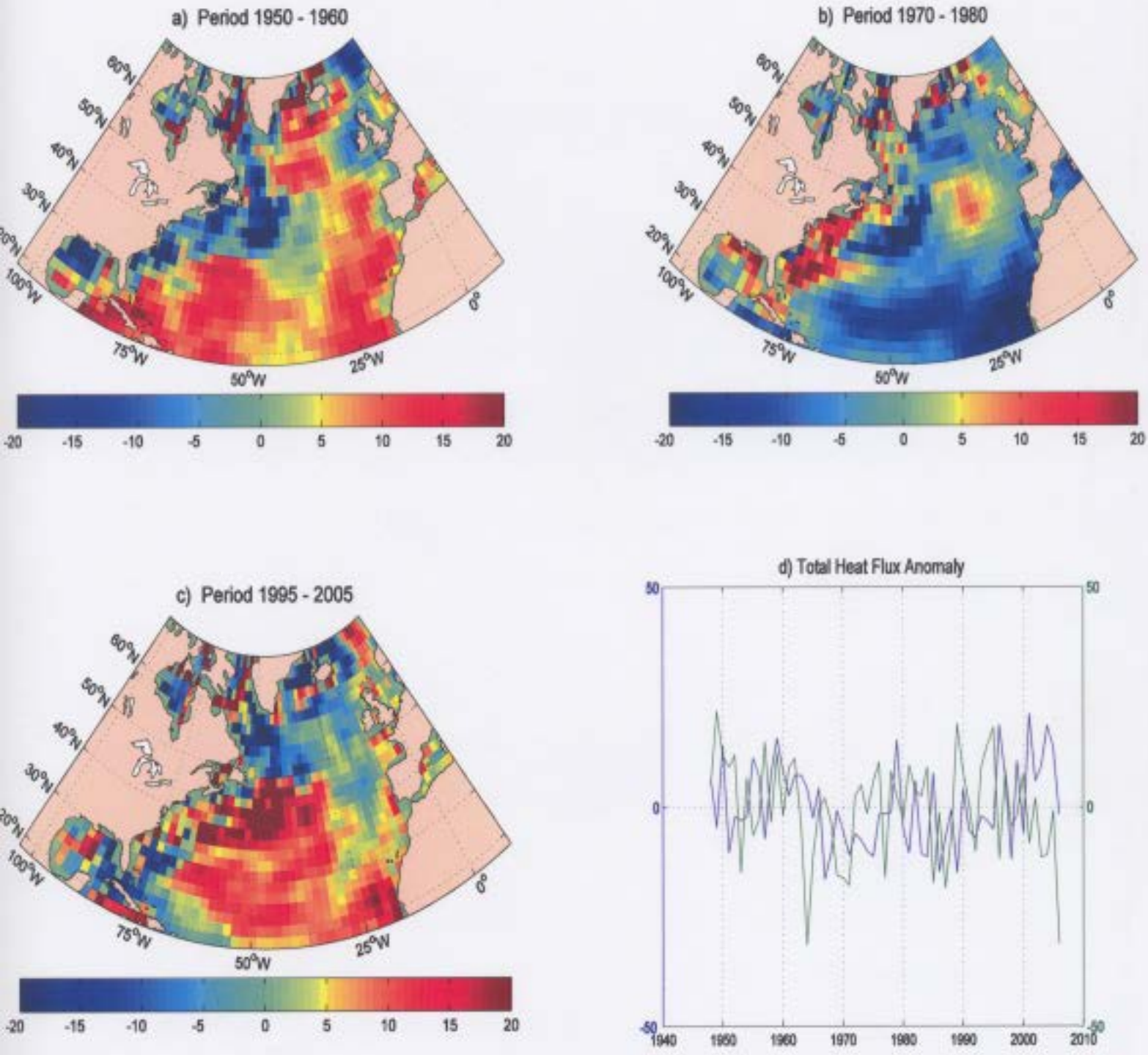

Fig 3.8: Inter-Annual and Inter-Decadal Variability of Total Heat Flux

Chapter 4

Empirical Orthogonal Function Analysis of SST and Atmospheric Data

The aim of Empirical Orthogonal Function (EOF) analysis is to determine the principal modes of variability of the studied data. Empirical Orthogonal Function analysis is a decomposition of a signal or dataset on to orthogonal basic is of functions, which are determined from the data. EOF method finds both time series and spatial patterns (see Chapter 2). Once the eigenvectors are found, it is important to separate those eigenvectors (or EOFs) which contain data that represent physically relevant patterns from those that represent only noisy variations. It has also been noticed that in analysis of this type, the eigenvalues fall exponentially and most of the variability is captured only by very few vectors.

The data used in this study are time series of monthly mean anomalies of SST and atmospheric data in the North Atlantic and Labrador Sea for winter months (DJF) of the period between 1948 and 2005. The SST fields are taken from COADS data set (Woodruff et al., 1987) and have a horizontal resolution of 2 degrees. The atmospheric parameters are from National Center for Environmental Predictions (NCEP). The analysis covers the North Atlantic sector north of 20^0N. At each grid point the anomalies have been calculated by subtracting the long term monthly mean.

4.1 Dominant modes of variability of the North Atlantic atmospheric circulation and NAO from 1948 to 2005

The first EOF of sea level pressure (SLP) of North Atlantic, explains 44% of the total variance present in the original data. The large positive values centered around latitude 45° N and the large negative values centered around 65° N are indicative of two regions whose mean sea level pressures are generally inversely related. This EOF defines a pattern which is a well-known low-frequency atmospheric circulation pattern called the North Atlantic Oscillation (NAO). The NAO is characterized by large-scale SLP variability associated with a subtropical high / polar low system over the Northern Atlantic. During a positive NAO, (positive values on Fig 4.1b) the subtropical high is stronger than usual and the polar low is deeper than usual. The increased pressure gradient causes stronger winter storms to cross over the Atlantic. During a negative NAO, the subtropical high and polar low are both weaker than usual, resulting in fewer / less severe storms crossing the Atlantic.

The intensity of the NAO is usually studied by using the so-called NAO index, which is the normalized difference of pressure anomalies over Iceland and Portugal. This characteristic can be calculated for the last 200 years, because SSP data for these two stations are available for this period of time. The SSP analysis data, which we use in these calculations, are available for not more than 50 years. Though such data do not allow analyzing a long enough sequence of temporal variability of SSP, they provide much better information about the spatial variability of SSP than the two point observations (Portugal, Iceland) only.

There is a wide range of atmospheric and ocean variability attributed to the changing NAO, which have the potential to cause change in the marine environment. In particular in many studies during the recent two decades, it was shown that processes of water mass formation in the North Atlantic are related to the NAO. The radical interannual and interdecadal changes in the production of the convectively formed mode waters of the West Atlantic, which Dickson et al.(1996) suggest to be a part of a coordinated pan-Atlantic pattern of convective activity, driven by the changing NAO. From the late 1950s to 1970, a regime of cold winter air temperatures and extreme snowcover greatly enhanced the land-sea temperature gradient at the US eastern seaboard, spinning up more storms than normal offshore (Dickson and Namias, 1976; Hayden, 1981). The local effect was to focus the center of maximum storm activity off the US eastern seaboard where the cold stormy conditions caused maximum cooling the ocean surface (see Fig 3.5b and 3.7b) and formation and ventilation of the Eighteen-Degree. The remote effect was to reduce storminess over the Labrador Sea, so that Labrador Sea convection became increasingly suppressed and fresh water built up at the surface (Lazier, 1980, 1988, 1995). Labrador Sea Water (LSW) production resumed abruptly in winter 1971-1972 with a rapid removal of the surface fresh water accumulation by the vertical spreading as the cold winter regime ended at the US east coast and intense, chill northwesterlies and storminess returned to the Labrador Sea. Later the tendency has been towards intensifying and deepening ventilation of the Labrador Sea, with a progressive cooling and freshening of LSW during the period of the 1990s. The LSW density increased as convection began to produce cold but saline sublayer of North Atlantic Deep Water (Dickson et al., 1996). This variability in the LSW formation is related to the changes in

the atmospheric characteristics driven by the NAO. From the 1950s the EOF1 coefficient (Fig 4.1b) has decreased from positive to its lowest (negative) value for the whole period 1948-2005, which occurred in the 1960s. This period was the period of low storm activity in the North Atlantic and was characterized by high Atmospheric and surface ocean temperatures (Fig 3.5, Fig 3.7).

The connection between the ocean variability and NAO was however different in the 1990s. It is known that the NAO had a tendency to be positive since the late 1980s. This is the period when NAO had its highest intensity (see Fig 4.1b) for the whole period 1948-2005. The SST during this period (see Fig 3.7a) showed a strong tendency towards increasing. This tendency started earlier (in 1990) in the southern region (southern of 45^0) and later (in 1995) in the northern region. The low correlation of NAO and SST suggests that beyond the direct air-sea interaction, there was probably another factor, which influenced the SST variability in the 1990s. As mentioned in introduction of Chapter 3 an important factor for the thermal regime of the North Atlantic is the ocean circulation. The long term variability of the ocean heat transport however remains a challenging problem due to the lack of data. The most important contributors to the meridional transport are Gulf Stream and North Atlantic Current.

As Curry and McCartney (2001) point out, the main North Atlantic Current is driven by the gradient of potential energy anomaly (*PE*) across the mutual boundary between the subtropical and subpolar gyre. Since *PE* reflects the vertical density structure and heat content of the upper ocean to well below the wind-driven layer, it follows that coordinated changes of opposite sign in the production and characteristics of the mode waters in each gyre will have the potential to drive deep-seated changes in the *PE*

gradient, and hence in the strength of Atlantic gyre circulation. If these changes in the density and heat content of mode waters are attributable to the NAO, then the amplification of the NAO to extreme values over the past three or four decades is likely to have been followed by a corresponding multidecadal spin-up of the Atlantic gyre circulation.

From the observed *PE* differences between the centers of the two gyres, Curry and McCartney calculated that the long term increase in the NAO index to the mid 1090s was accompanied by a 30% increase in the east going baroclinic mass transport along the gyre-gyre boundary. Both subpolar and subtropical gyres contributed equally to the changes in their transport index. Thus in response to the NAO, the North Atlantic gyre circulation during the early 1990s is likely to have been at its strongest for more than a century.

The second EOF of SLP over North Atlantic exhibits 27% variance, which is called the Eastern Atlantic (EA) pattern (Barnston and Livezey, 1987). The EA is related to an atmospheric pattern with low-pressure center at about $\varphi = 55^0 N$ and $\lambda = 25^0 W$, which is inversely related to the SLP in the rest of the North Atlantic.

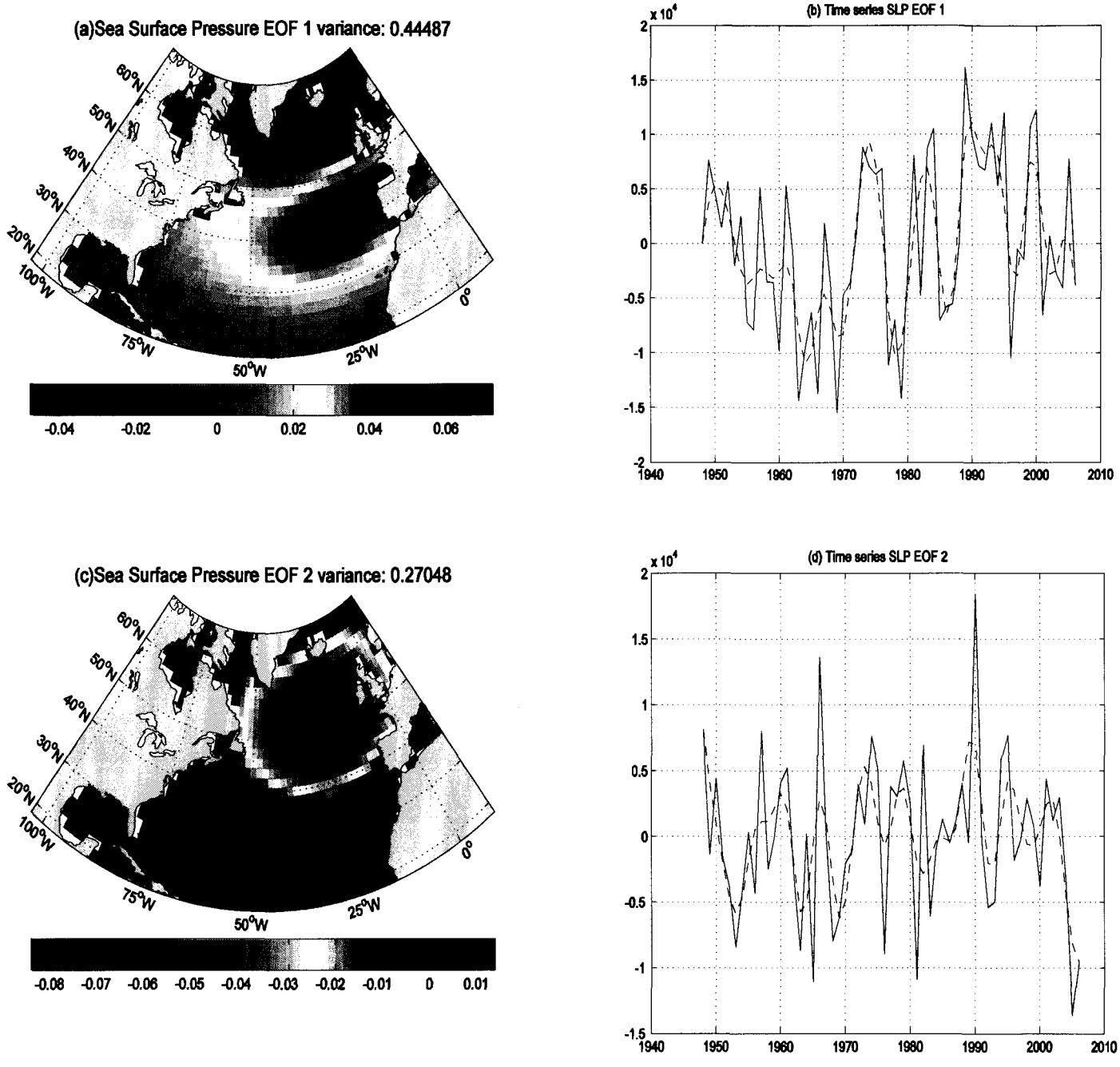

Fig 4.1: *Dominant EOFs of Sea Level Pressure and their time series (red curve is the filtered time series) of North Atlantic.*

4.2 EOF analysis of near surface atmospheric parameters and SST

EOF Decomposition is applied to Air Temperature of North Atlantic (Fig 4.2). The first structure explains 51% of the variance, the second structure 13%, and the third EOF explains 6%. The first EOF has triple structure with positive values of the US coast and opposite negative sign in the Labrador Sea and tropical North Atlantic. The time variability (Fig 4.2b) follows closely the NAO index.

We have compared our results with the results of Deser and Blackmon (1993). The first two EOFs of air temperature are similar with the pattern of SST EOF, just the order of mode is reversed. The second EOF of air temperature, which accounts for 13% of the variance, exhibits maximum amplitude off the Newfoundland, North Labrador Sea and off the coast of east Greenland. The time series of EOF2 is dominated by along warming trend from the 1950s to the 1970s, followed by a cooling trend during 1970s and 2000s.

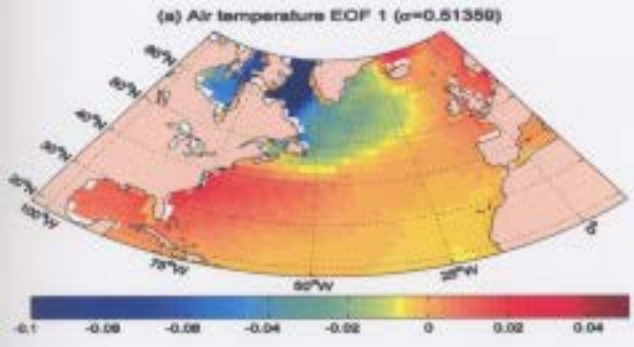

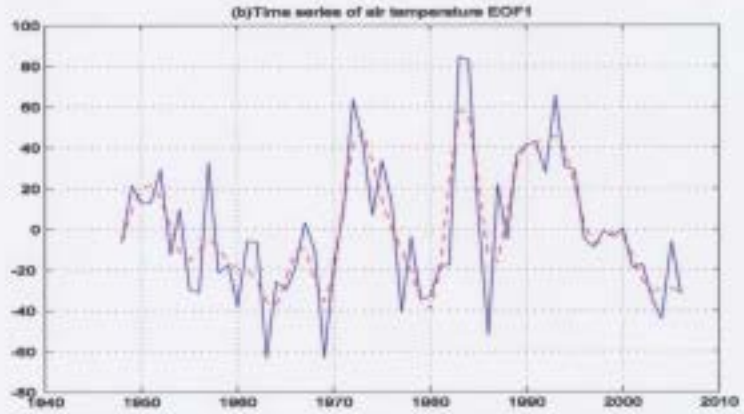

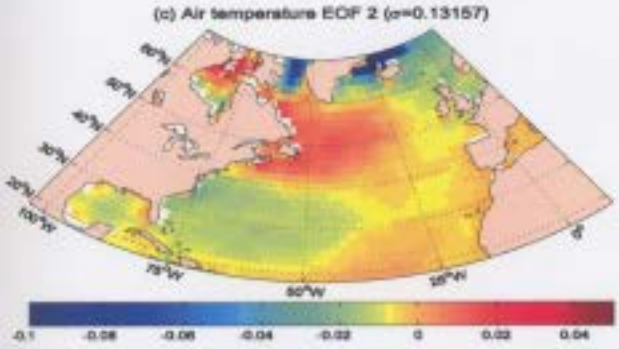

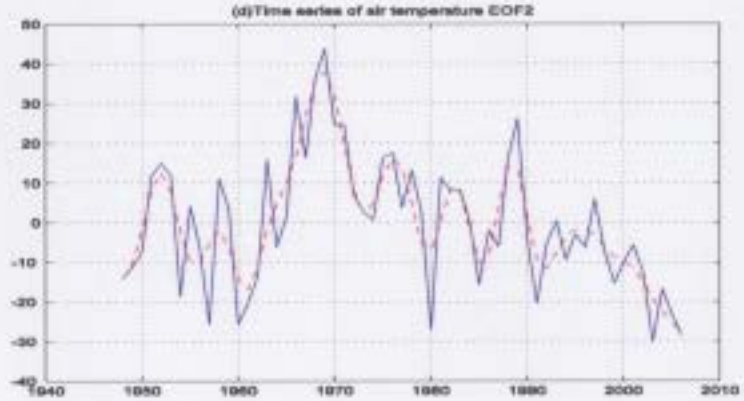

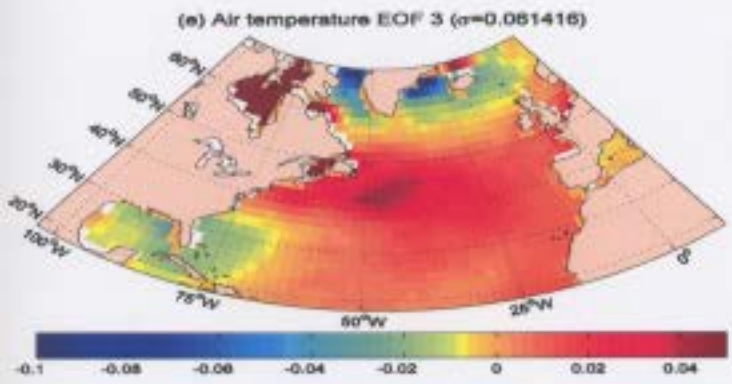

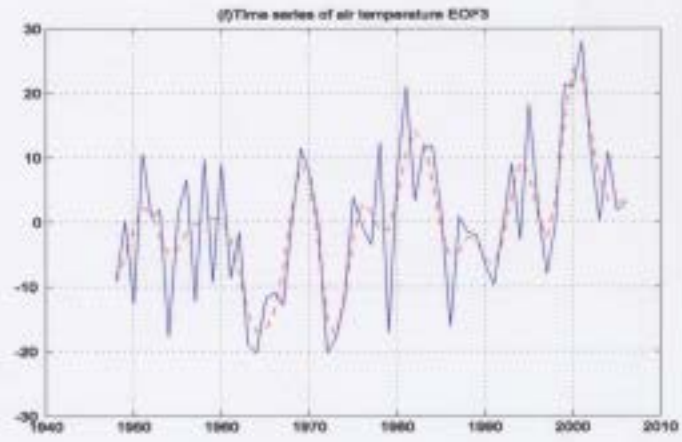

Fig 4.2: *Dominant EOFs of air temperature and their time series (red curve is the filtered time series) of North Atlantic.*

The dominant SST is shown on Fig 4.3. The first normalized eigenvalue is 0.23, the second eigenvalue is 0.18, and the third eigenvalue is 0.14. Recall that normalized eigenvalues represent the fraction of variance explained by the structure associated with that eigenvalue. Therefore, the first EOF structure of North Atlantic Ocean explains 22% of the variance, the second structure 17%, and the third EOF explains 13%.

The SST dominant EOFs define patterns, which are pretty similar to the EOF1 and EOF2 of the heat flux (see below). The EOF1 identifies two areas of opposite variability. The first is southeastern of Newfoundland and Labrador Sea and second is the subtropical North Atlantic and Gulf of Mexico. This structure is very close to the structure of the EOF2 of heat flux. The time variability of EOF1 is different from the EOFs discussed so far. Though it shows some variability at interannual time scale, there is a stronger changes in this EOF at decadal time scale. The coefficient of this EOF is predominantly positive from 1950 to 1970, negative from 1970-1990 and positive in 1990s.

The second EOF defines a triple with two areas in subtropical and subpolar North Atlantic, where SST anomalies due to EOF2 are opposite to those in Gulf Stream Area. This pattern is known (see Cayan, 1992) to be strongly correlated with the NAO. Correspondingly the time variability of the EOF2 coffecient vary in a similar way as the EOF1 of SLP.

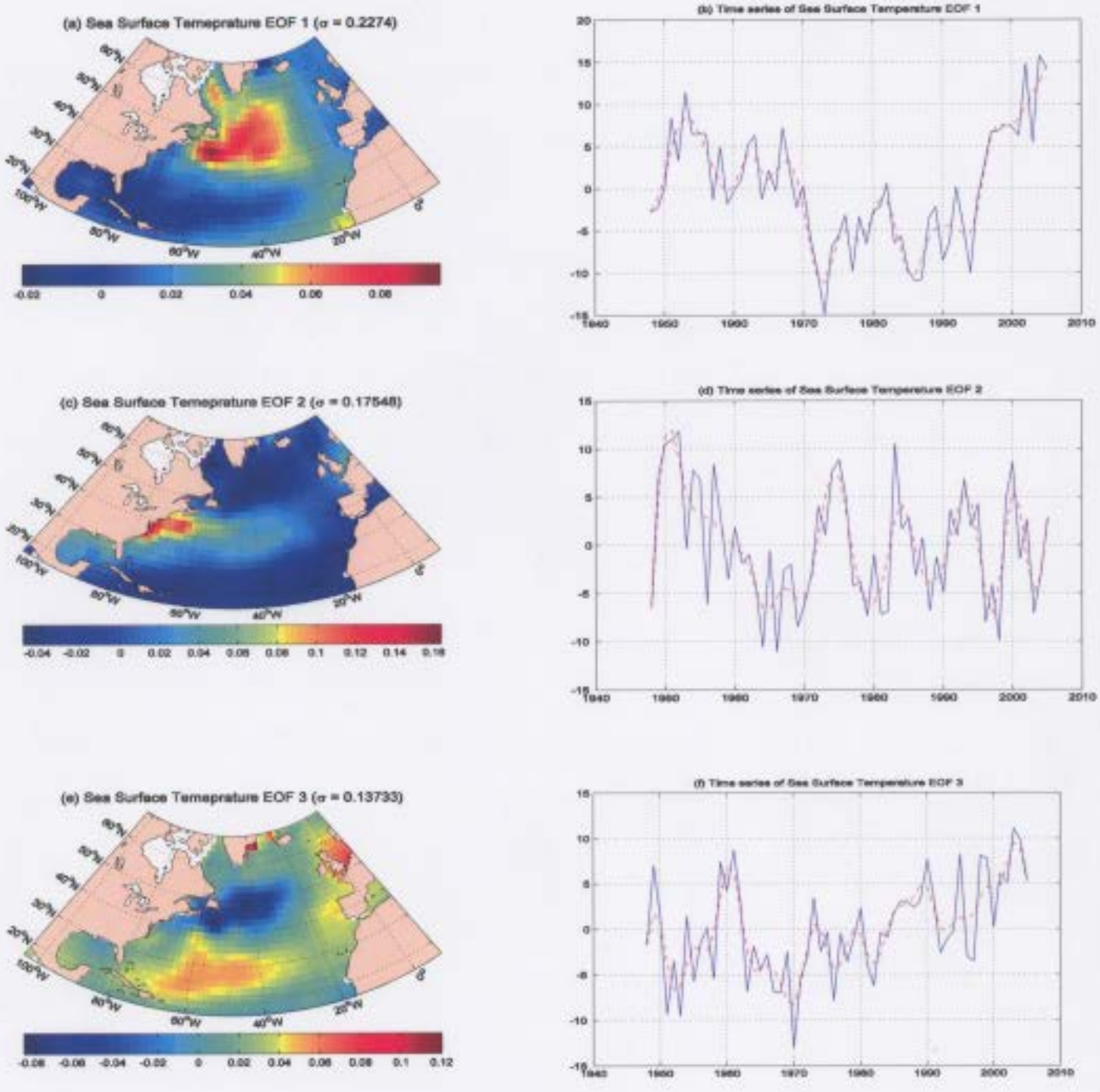

Fig 4.3: Dominant EOFs of SST and their time series (red curve is the filtered time series) of North Atlantic

Deser and Blackmon (1993) have done an EOF analysis of SST in the North Atlantic. They have found the first EOF of SST, which accounts for 45% of the variance, has uniform polarity over the entire basin. The largest loading occurs along the Gulf Stream. The time series of EOF1 SST exhibits a sudden transition from below normal values to above normal values around Second World War. This EOF was not found in the present study and also in the work of Cayan (1992).The technique for measuring SST was not accurate before early 1940s. As also discussed by Deser and Blackmon, the EOF1 is probably related to the change of technique of SST observation.

The second EOF which accounts for 12% of the variance, exhibits a center of action east of Newfoundland at the boundary between the subtropical and subpolar ocean gyres. They have found an opposite polarity located off the southern United States. The time series of EOF 2 exhibits quasi-biennial fluctuation and also quasi-decadal variations. We have also found similar results in our EOF and also the time series is similar after 1948 to onward.

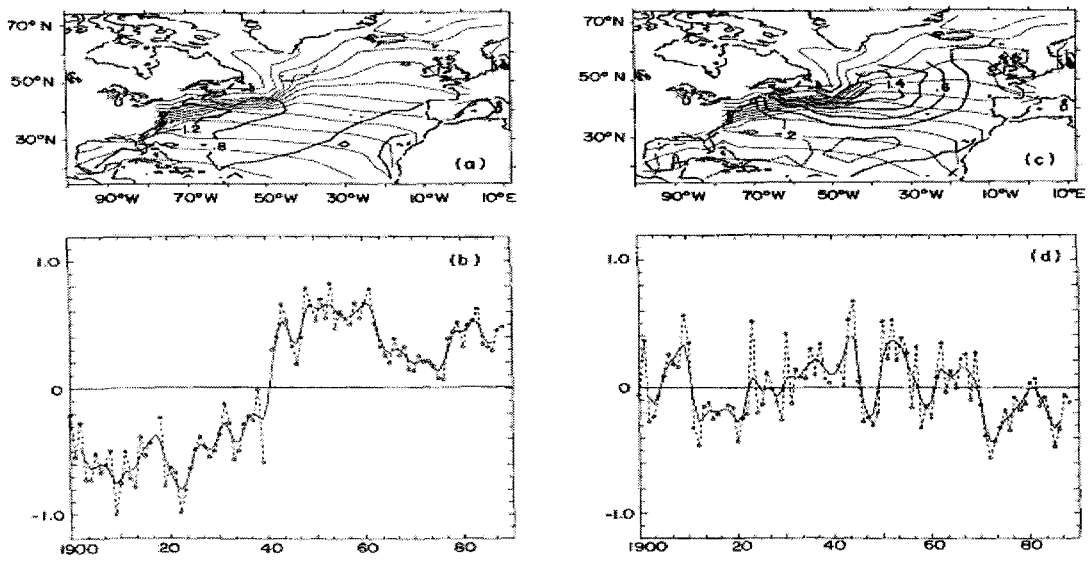

Fig 4.4: *EOF analysis of SST from 1900-1989. (Deser & Blackmon)*

There is also a possibility that interannual and decadal fluctuations in SST are response to ocean and atmospheric variations outside of North Atlantic. Deser and Blanckmon, (1993) have found a link with the sea ice transport in the Davis Strait-Labrador Sea region. Figure 4.5 a) shows the time series winter sea ice concentration anomalies in the Davis Strait-Labrador Sea. The circle denotes the winter anomaly, plotted in the year in which January occurs. The solid curve shows the data smoothed with a three point binomial filter. Decadal variability is evident in the sea ice record, with peaks occurring in the winters of 1957/58, 1971/72, and 1983/84. Figure 4.5 b) shows the sea ice record superimposed upon the time series of the second EOF of winter SST. (Deser & Blackmon, 1993)

It may be seen that the maxima in sea ice concentration precede the minima in SST by 1-2 years. There is a strong lag in correlation between the two time series. This indicate that on the decadal time scale, winters of heavy sea ice in the Labrador Sea precede winters of colder than normal SSTs east of Newfoundland. It is probable that the sea ice anomalies

in the Labrador Sea are advected southwestward, resulting in colder than normal SSTs east of Newfoundland the following year. Thus the quasi-decadal cycle in SSTs east of Newfoundland may result in part low-frequency Arctic sea ice variations.

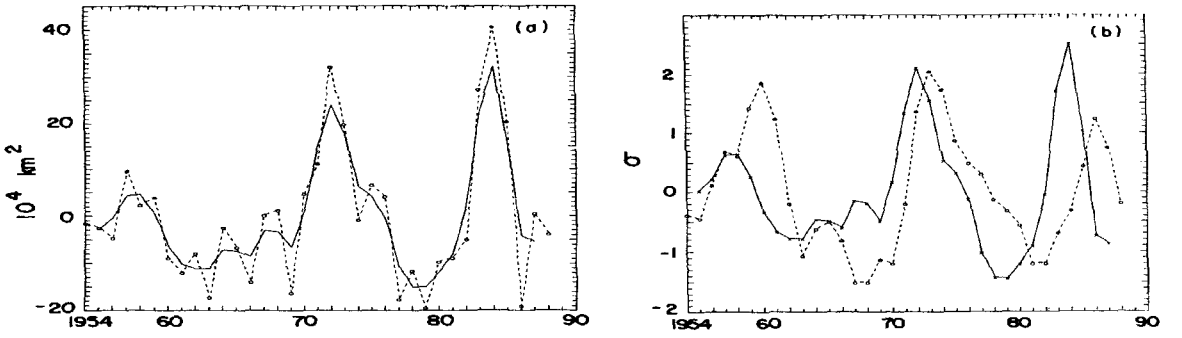

Fig 4.5 *a) Time series of Winter Sea ice area anomalies in the Davis Strait and Labrador Sea region. b) Standardized sea ice anomalies from super imposed upon the standardized time series of EOF2 of North Atlantic winter SST.(after Deser and Blackmon, 1993)*

The dominant EOF mode of wind (Fig 4.6 a) explains 46% of the variance and the second EOF explains 24% of the variance. The dominant EOF defines a pattern which has a dipole structure with opposite variability in the sub-polar and sub-tropical regions. This EOF, which dominates the zonal wind variability, explains in particular the anticorrelation between the winds anomalies southern and northern of 45^0N. The pattern related to the EOF1 constitutes oscillations with opposite phase in these two regions. It's time variability follows closely the NAO index.

The second EOF in the wind defines a triple pattern. The variability related to this EOF in the wind in the mid-latitude area between 30^0N and 55^0N is opposite to that in the subpolar and tropical North Atlantic.

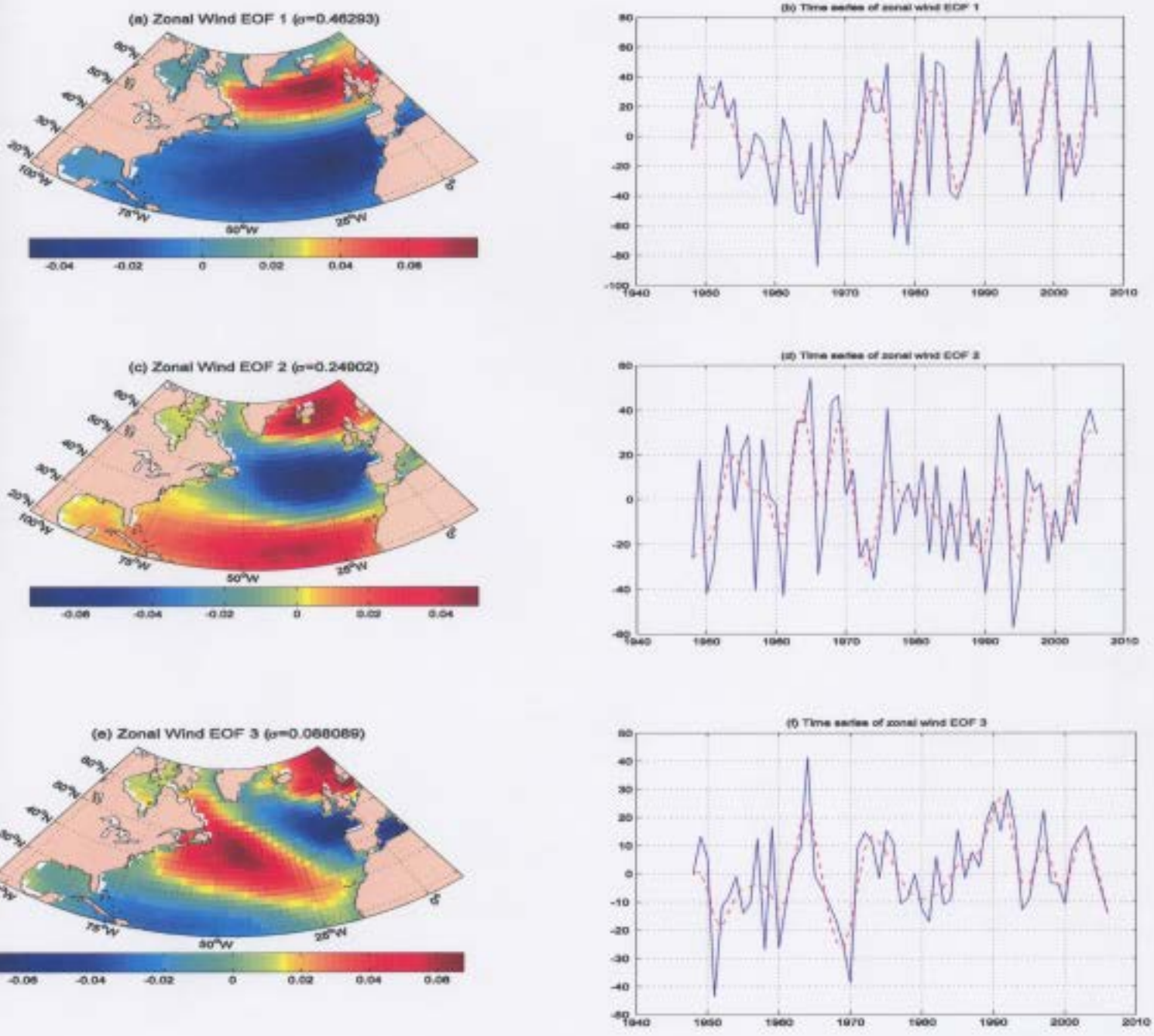

Fig 4.6: *Dominant EOFs of Wind and their time series (red curve is the filtered time seris) of North Atlantic.*

The first EOF of precipitation (Fig 4.7 a) of North Atlantic which explains16% of the variance has highest precipitation rate in the northern coast of Newfoundland and US coast and lowest in the southeastern part of North Atlantic. The second EOF, which explains 14% of variance has highest precipitation rate in Gulf Stream and lowest in central Atlantic. The third EOF of which explains 7% of the variance has highest precipitation all over the Atlantic.

The first three EOFs in total precipitation explain only about 40% of the total variance. The rest of the variance in the precipitation anomalies is due to the higher EOFs. In this way, we need relatively large number of EOFs in order to spawn the precipitation variability. The first EOF coefficient has a time variability, which follows closely the variability of the SLP EOF1 coefficient. This is the pattern closely related to the NAO.

The dominant EOF mode of total heat flux explains 21% of the variance and the second EOF explains 15% of the variance. The third structure explains 8% of the variance. Fig 4.8 shows the dominant EOFs for the surface net turbulent flux. The first EOF (Fig 4.8 a) defines a pattern of alternating anomalies in the areas of subtropical and subpolar ocean gyres. The low-pass filtered time variability of this EOF follows closely the time variability of the first SLP EOF defining the NAO pattern. The second EOF defines a pattern in the heat flux with alternating anomalies in the region southeastern of the Newfoundland and the rest of the North Atlantic.

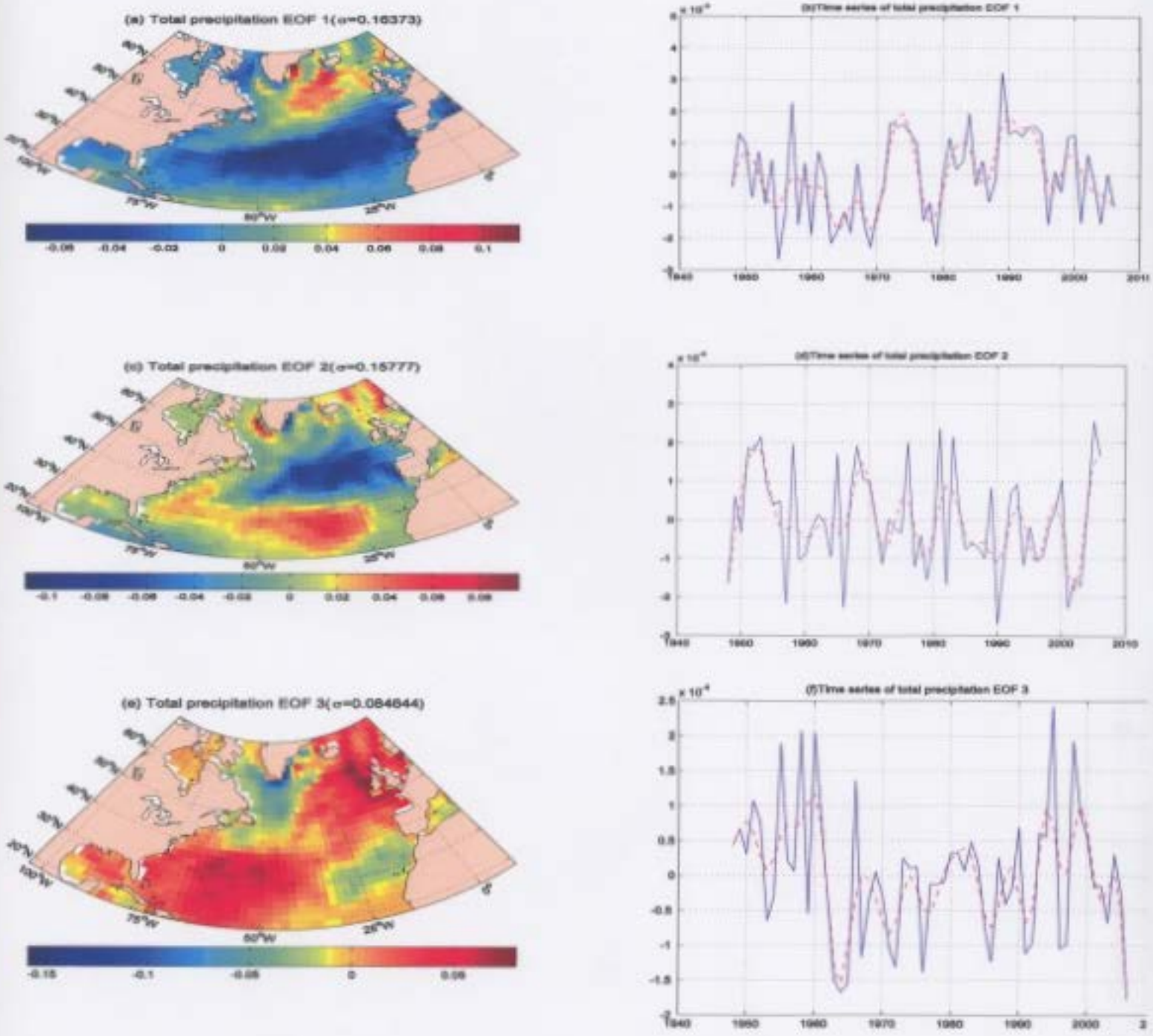

Fig 4.7: *Dominant EOF of Precipitation Rate and their time series(red curve is the filtered time series) of Atlantic.*

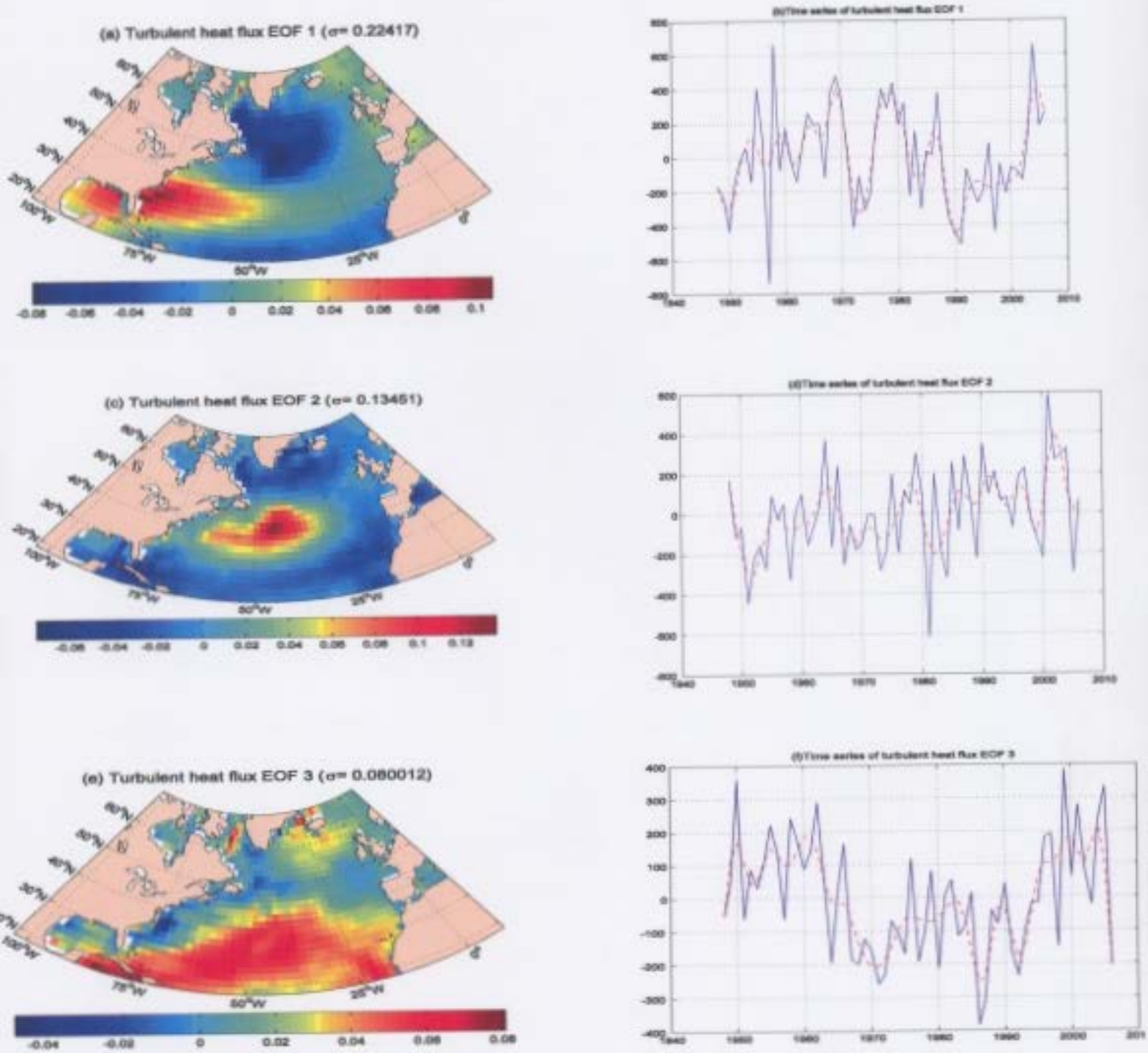

Fig 4.8: *Dominant EOFs of Total Heat Flux and their time series (red curve is the filtered time series) of Atlantic.*

These results correspond to the findings of Cayan (1992). The total heat flux differences associated with positive versus negative extremes of the first two North Atlantic SLP EOFs are shown in Fig 4.9 and corresponding $\Delta SST'/\Delta t$ differences are shown in Fig 4.10, which is the quantity of thermal energy transferred across a unit area of Sea Surface per unit time. SST anomalies fall in regions of positive sea-to-air flux and rise in regions of negative flux. In concurrence with the NAO circulation pattern, the North Atlantic is partitioned into alternating anomalous cells: 1) positive $\Delta SST'/\Delta t$ differences in the northeastern North Atlantic between Great Britain and Scandinavia; 2) negative $\Delta SST'/\Delta t$ differences in the central North Atlantic southeast of Greenland between 50^0N and 60^0N; 3) a broad region of positive $\Delta SST'/\Delta t$ differences extends from the Gulf of Mexico and the eastern seaboard east to the central Atlantic at about 350N,300W; 4) negative $\Delta SST'/\Delta t$ differences occupy the eastern tropical North Atlantic between about 500W and North Africa. The major regions of impact of $\Delta SST'/\Delta t$ are closely harmonized to those of total heat flux, supporting the view that they are linked.

For the North Atlantic SLP EOF2 (EA), the major $\Delta SST'/\Delta t$ features are 1) negative differences in the central North Atlantic east of Newfoundland; 2) positive differences in the Gulf of Mexico and the region just east of Florida and 3) positive differences in the far northeastern Atlantic and the Mediterranean Sea.

There is a difference in the pattern defined by the EOF2 of heat flux (Fig 4.8c) and the corresponding pattern of Cayan (1992). The pattern on (Fig 4.8c) is shifted south-westward and is more extended towards the US coast in the Southern part. This difference may be attributed to the different method used by Cayan (1992), which considers the heat flux distribution during years of extremely high or extremely low

NAO. In this way the patterns of Cayan (1992) represent the structure of most anomalous (in terms of NAO index) years.

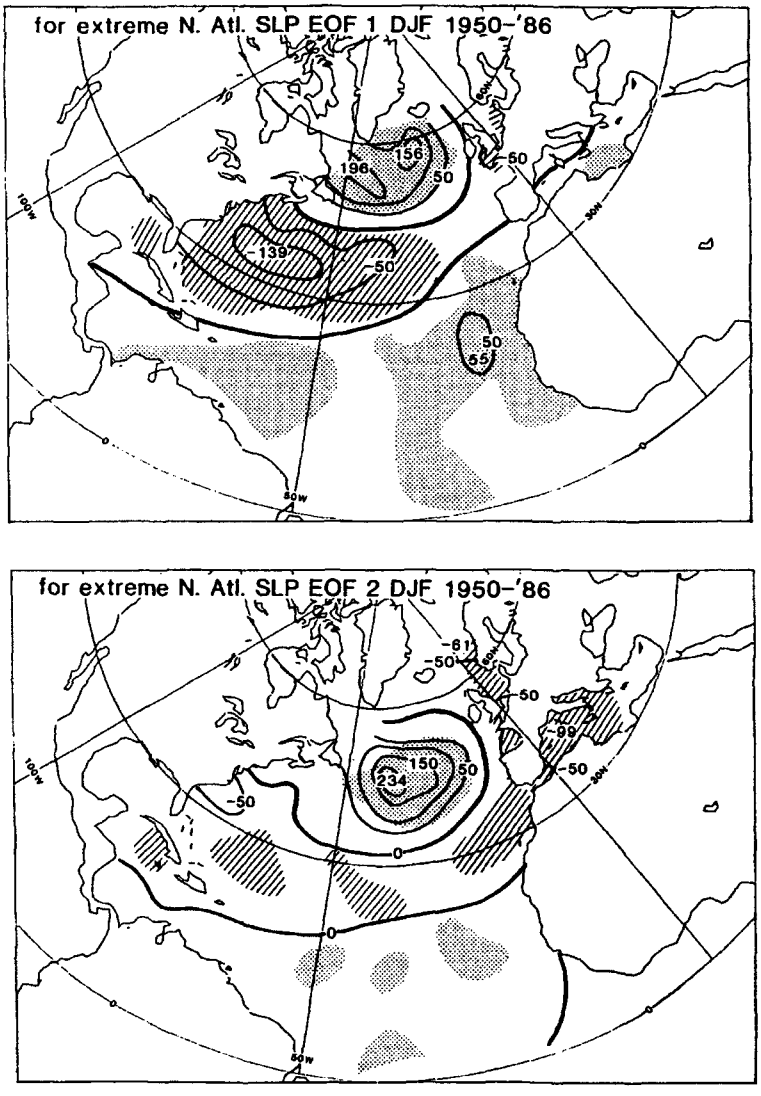

Fig 4.9: *Difference of average total heat flux associated with positive vs negative extreme winter month of North Atlantic SLP EOF1 and 2 of. (Cayan 1992)*

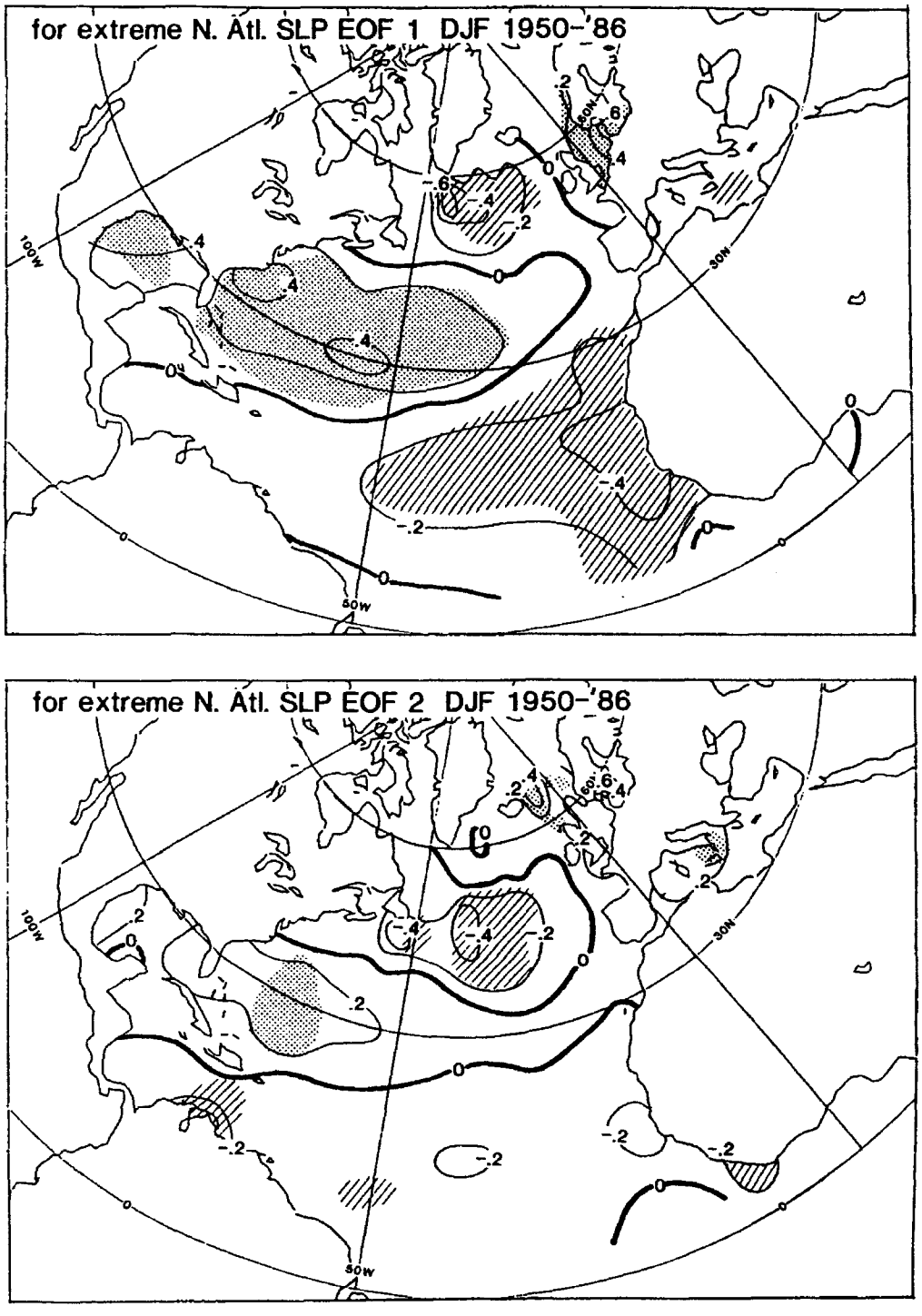

Fig 4.10: *Difference of average $\Delta SST' / \Delta t$ associated with positive vs negative extreme of EOF1 and 2 of North Atlantic SLP. (Cayan 1992)*

The dominant EOFs in the near surface atmospheric characteristics and SST define patterns show close connection to the global atmospheric circulation. The EOF analysis, for the period 1948-2005 in correspondence with previous studies, indicates that the NAO has an impact on the North Atlantic Ocean and atmospheric variability. The EA is another important pattern for the North Atlantic. At the same time it is known that internal ocean variability may also influence the atmosphere and SST. The next chapter studies the connection between the variability in the North Atlantic Ocean and Labrador Sea, and the atmospheric circulation.

Chapter 5

Canonical Correlation Analysis

The anomalies of heat and water exchange between the atmosphere and the Labrador Sea depend on the variability of wind speed, the ocean surface saturation humidity, air humidity and the sea-air temperature difference. These parameters define the intensity of evaporation and the net turbulent heat flux at the ocean-atmosphere interface. Their local values depend on the atmospheric circulation, which defines the intensity of the surface wind speed and the direction of air masses transport. During the winter, the dominant transport is directed from the continent towards the ocean and brings cold and dry air to the ocean surface. The heat and water exchange depends on the intensity of this flow, which is part of the atmospheric circulation

This section presents results from a study of the relation between the atmospheric circulation, and near surface atmospheric variability and SST. The time variability of SLP dominant EOFs discussed in the previous section show some qualitative relation to the EOFs in other atmospheric characteristics (zonal wind, heat flux, atmospheric temperature) and SST. This relation was shortly discussed in previous section. For instance, negative SLP anomalies are related to negative zonal wind anomalies to their north and positive zonal wind anomalies to their south. The analysis of this relation in chapter 4 was just qualitative. Here the method of canonical correlation analysis is used to study the relation between the near surface atmospheric characteristics and SST with the atmospheric circulation variability. Section 5.1 presents results for the North Atlantic.

The relations of the near surface atmospheric characteristics and SST in the Labrador Sea to the atmospheric circulation is discussed in section 5.2.

5.1 Correlation Patterns of Variability in the North Atlantic

Canonical Correlation Analysis (CCA) is used to analyze the relationship between *monthly mean sea level pressure (SLP) or sea surface pressure (SSP)* and *atmospheric temperature, wind, heat flux, SST, precipitation in the North Atlantic.* The data are time series of monthly means of SLP and atmospheric temperature, wind, heat flux, SST, precipitation grided over the North Atlantic north of about 20^0N, for DJF of 1948 to 2005 respectively. Anomalies are obtained at each grid point by subtracting the long term monthly mean from the original values. The CCA yields two pairs of patterns that describe the coherent variations in the two parameters.

The first pattern (Fig 5.1 b) of SLP and SST corresponds to a canonical correlation of 84% that means the areas of strong coupling of SLP with SST indicated by 84%. The coefficient of the second pattern (Fig 5.1d) is 68%. The coefficient of the third pattern (Fig 5.1 f) is 58%. The first pattern (Figs 5.1 a, b) of SLP exhibits the pattern similar to NAO pattern which drives the variability in the SST close to the 2nd EOF and second mode of canonical correlation pattern of SLP describes EA pattern which drives the variability in the SST close to the first SST EOF. These results correspond to the studies of Cayan., (1992) and Deser et al., (2000). These studies in particular relate the second EOF (Fig 4.5), or triple pattern in SST anomaly field with the NAO. The first EOF in SST, defines a pattern that is close to the one derived by Cayan (1992) and driven by Eastern Atlantic pattern in the atmospheric circulation.

The third correlation pattern of SLP and SST (Figs 5.1 e, f) has a SLP structure close to the NAO but with a maximum in the SLP field shifted westward. This canonical correlation pattern in the SST has a dipole structure with opposite variability in the subtropical and subpolar gyres.

The first pair of patterns SLP and atmospheric temperature corresponds to a canonical correlation of 90% of the SLP and air temperature. The correlation coefficient of the second pairs of patterns is 85%. First canonical pattern (Figs 5.2 a) of SLP is North Atlantic Oscillation (NAO) and drives the variability in the air temperature close to the first EOF. The second mode (Fig 5.2 c) of canonical correlation is a combination between NAO and Eastern Atlantic (EA) pattern that drives an air temperature anomaly close to the second EOF. These two patterns show how the variability in atmospheric circulation influences the near surface atmospheric temperatures as discussed in Chapter 1. High NAO index is related to an intensified cyclonic vortex in the Icelandic low. The mean transport in the Labrador Sea favors north-eastern cold winds. The winter storms are passing across the Atlantic Canada and cause low temperature off Newfoundland. The air temperature off the coast of US is warmer than usual.

The shift of the centers of low northward of Iceland and of the high northwestward of Azores Islands in the NAO shifts the areas of high and low temperature in the second canonical correlation patterns northward (Fig 5.2d).

The first pattern of SLP and zonal wind (Fig 5.3 b) corresponds to a canonical correlation of 99.97%. The coefficient of the second pattern (Fig 5.3 d) is 99.90%. The coefficient of the third pattern (Fig 5.3 f) is 99.61%.

The first two dominant SLP-zonal wind patterns (Figs 5.3 a, c) are related with the NAO. In the first pattern the high in Eastern Atlantic is shifted northward of the Azores Island. In this case the zonal wind is intensified in the eastern part of North Atlantic off the coast of England. The zonal transport is weaker than normal in the subtropical North Atlantic Ocean.

The second SLP pattern (Fig 5.3 c) has a structure of the NAO with the low shifted south of Iceland. Correspondingly the area of intensified zonal winds moves southward with respect to the first pattern. The strongest zonal transport related to this pattern is between Newfoundland and Western Europe. The third canonical correlation pattern (Fig 5.3 e) has a structure of the Eastern Atlantic pattern in the SLP. It is known (Barnston and Livezey, 1986) that the low related to EA pattern can move zonaly in the North Atlantic. In canonical correlation pattern three, this center is shifted westward with respect to EOF 2 of SLP. During the positive phase of this pattern, the zonal wind intensify in the tropical North Atlantic and off the west coast of Europe.

The first patterns of SLP and heat flux (Fig 5.4 b) corresponds to a canonical correlation of 99.8%. The coefficient of the second pattern (Fig 5.4 d) is 99.45%. The coefficient of the third pattern (Fig 5.4 f) is 99.09%. The fourth pattern of SLP and heat flux corresponds to a canonical correlation of 98%. First canonical pattern of SLP is NAO which drives the variability in the turbulent heat flux close to the first EOF of the heat flux. The second and third SLP modes (Fig 5.4 c, e) of canonical correlation are similar to the Eastern Atlantic (EA) pattern which drives the turbulent heat flux anomalies close to the second EOF.

The first patterns of SLP (Fig 5.5 b) and precipitation corresponds to a canonical correlation of 95% of the variance of SLP and wind. The coefficient of the second pattern (Fig 5.5 d) is 93% of the variance of SLP and precipitation in the North Atlantic. The coefficient of the third pattern (Fig 5.5 f) is 92% of the variance of SLP and heat flux in the North Atlantic. The fourth pattern of SLP and precipitation corresponds to a canonical correlation of 87% of the variance of SLP and precipitation. First canonical pattern of SLP (Fig 5.5 a) is North Atlantic Oscillation (NAO) which drives the variability in the precipitation close to the first EOF. The second mode (Fig 5.5 c) of canonical correlation is similar to the Eastern Atlantic (EA) pattern, which drives the precipitation anomaly close to the second EOF.

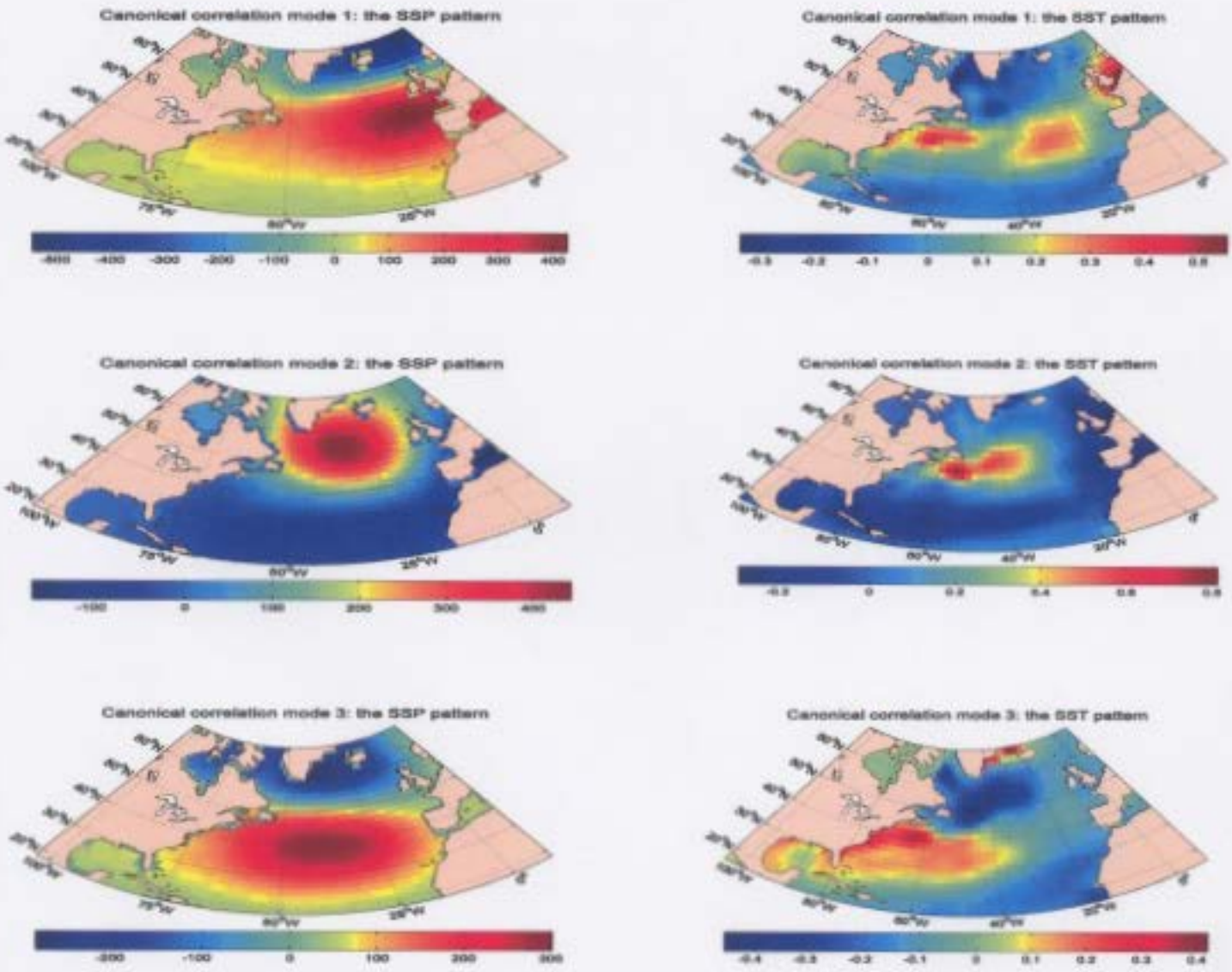

***Fig 5.1**: Upper two panels show the first Canonical correlation pattern for (a) SLP or SSP (b) SST. Middle two panels show the second CC pattern for (c) SLP (d) SST. Lower two panels show the third CC pattern for (e) SLP (d) SST.*

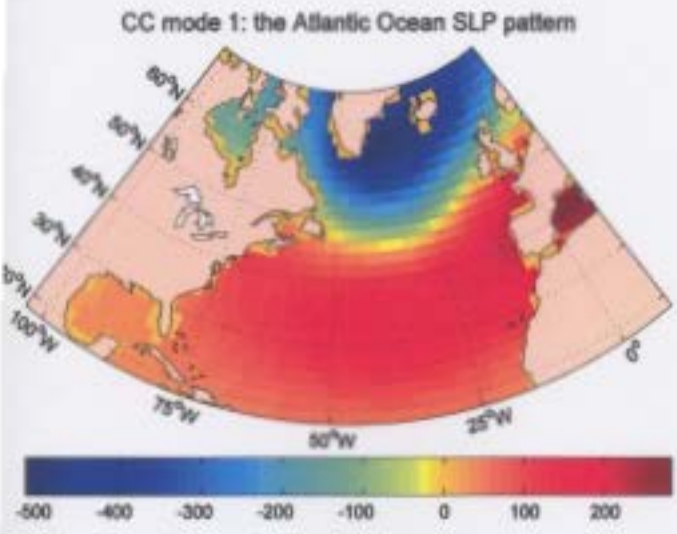

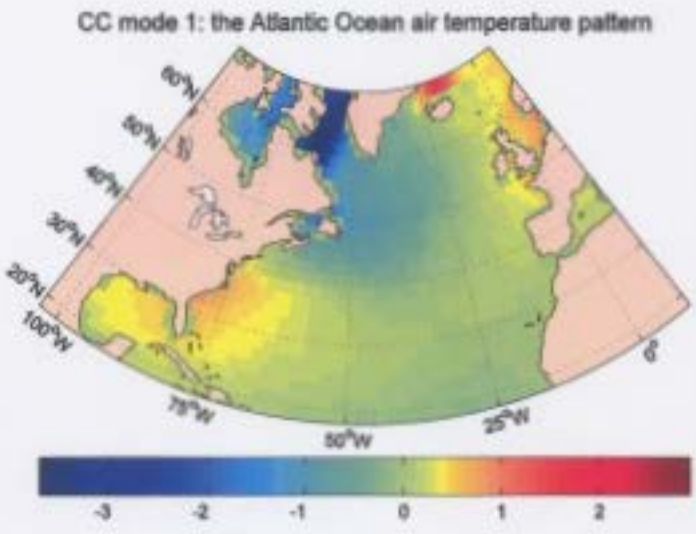

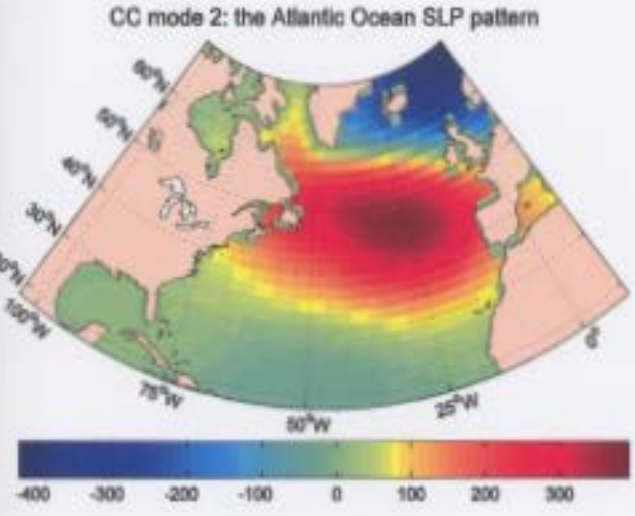

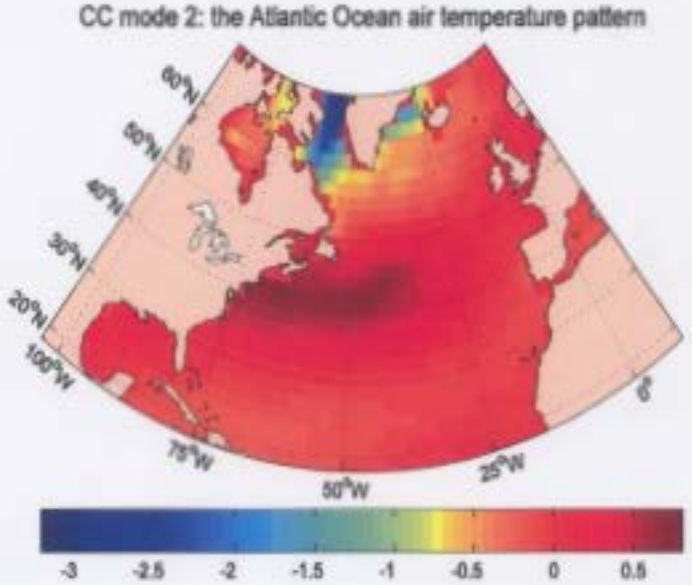

***Fig 5.2**: Upper two panels show the first CC pattern for (a) SLP (b) air temperature.*

Lower two panels show the second CC pattern for (c) SLP (d) air temperature

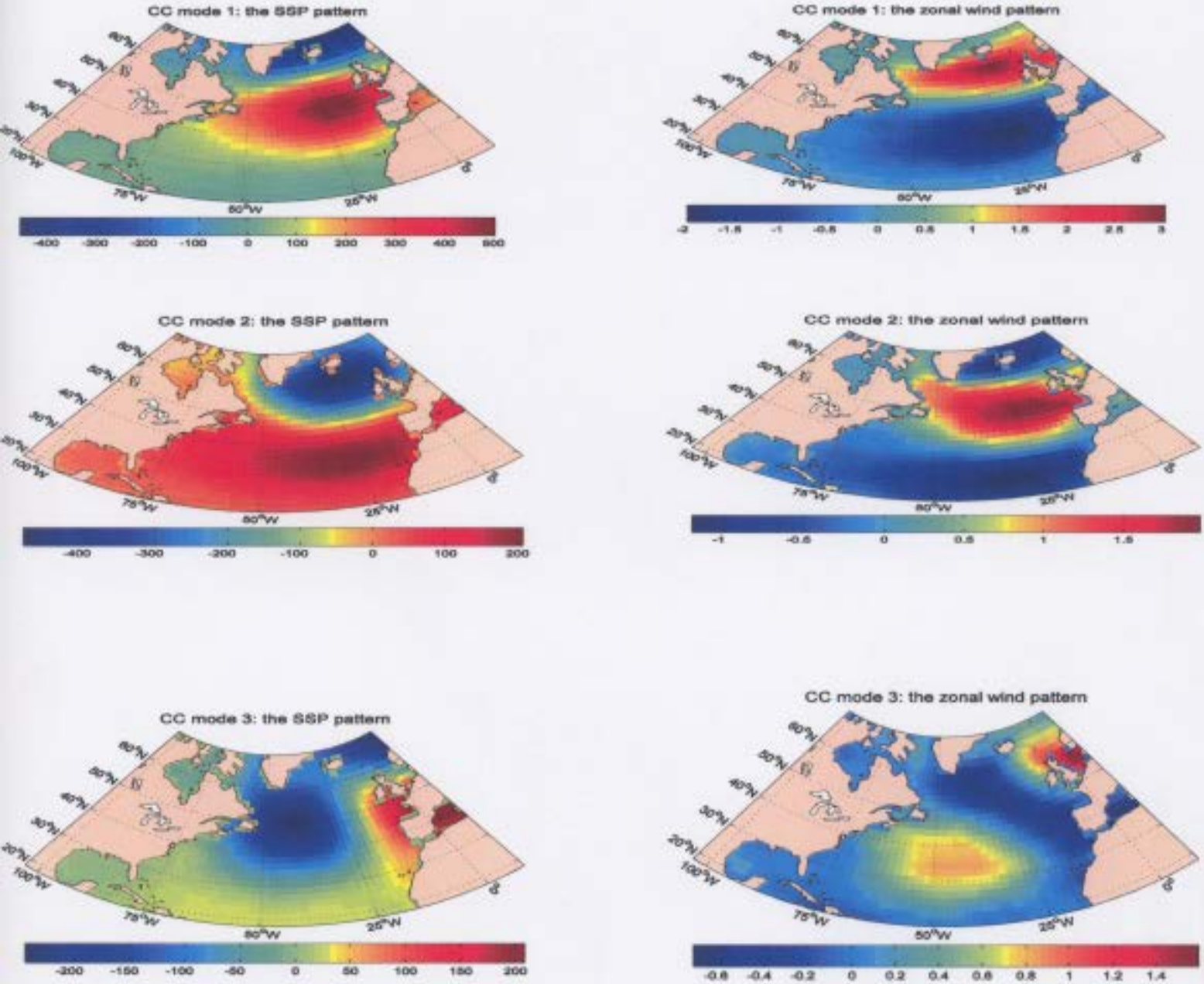

***Fig 5.3**: Upper two panels show the first Canonical correlation pattern for (a) SLP (b) zonal wind. Middle two panels show the second CC pattern for (c) SLP (d) zonal wind. Lower two panels show the third CC pattern for (e) SLP (d) zonal wind.*

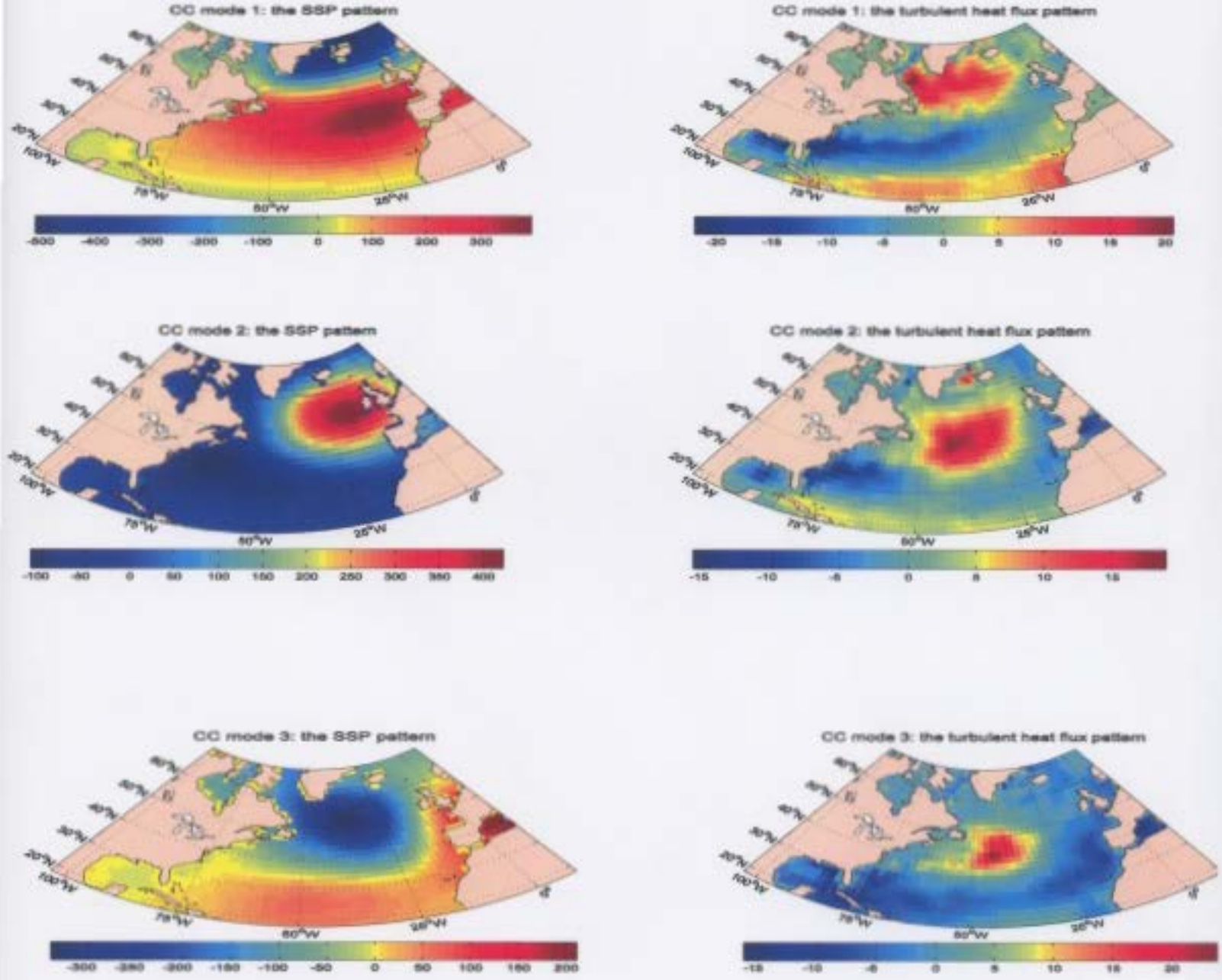

***Fig 5.4**: Upper two panels show the first Canonical correlation pattern for (a) SLP (b) heat flux. Middle two panels show the second CC pattern for (c) SLP (d) heat flux. Lower two panels show the third CC pattern for (e) SLP (d) heatflux.*

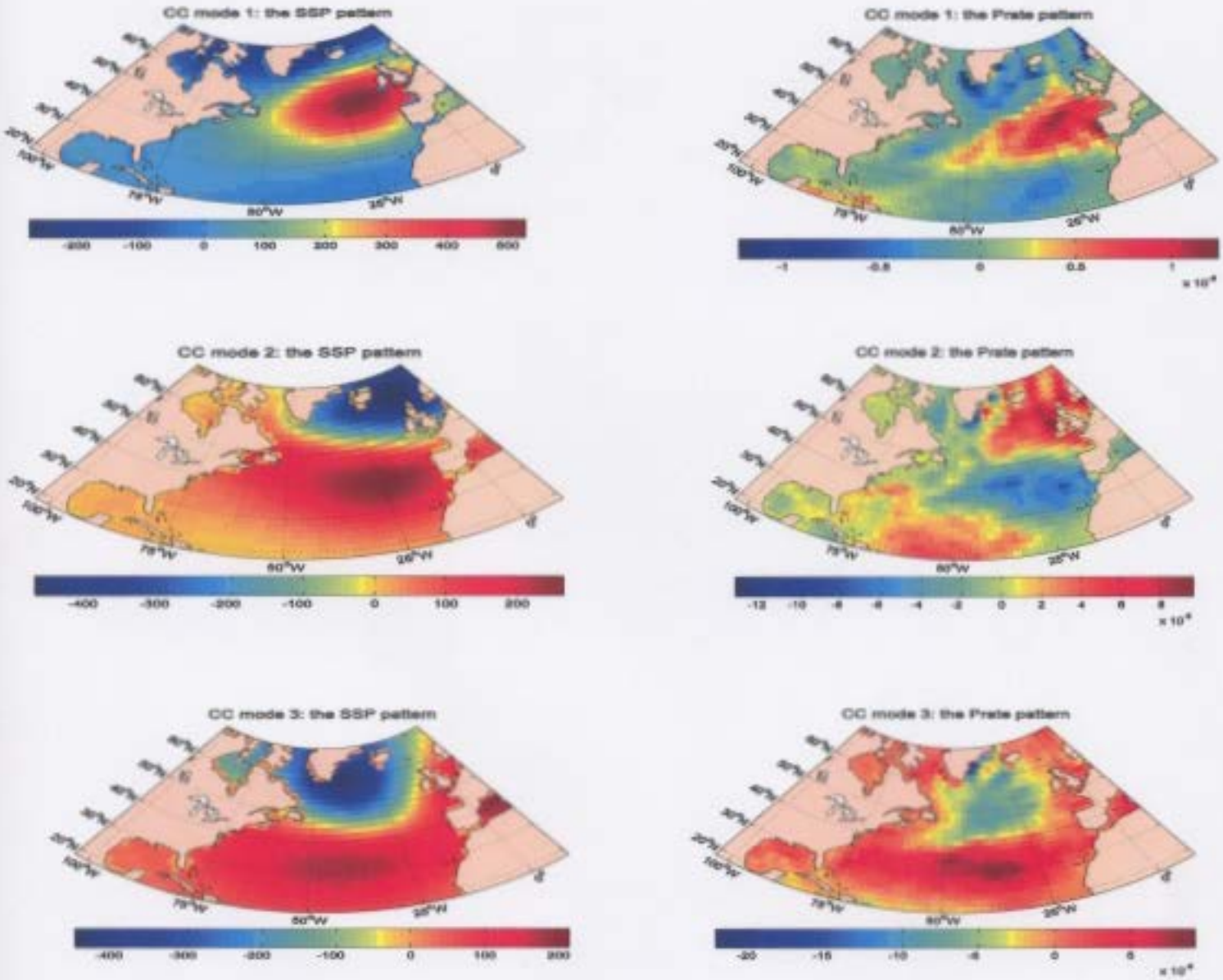

***Fig 5.5**: Upper two panels show the first Canonical correlation pattern for (a) SLP (b) precipitation rate. Middle two panels show the second CC pattern for (c) SLP (d) precipitation rate. Lower two panels show the third CC pattern for (e) SLP (d) Precipitation rate.*

5.2 Correlation Patterns of Variability in the Labrador Sea

In this section CCA is used to study the relationship between *monthly mean sea level pressure (SLP) North Atlantic* and atmospheric *temperature, wind, heat flux, SST, precipitation in the Labrador Sea.* The data are time series of monthly means of SLP and atmospheric temperature, wind, heat flux, SST, precipitation on a grid over the Labrador Sea north of about 50^0N, for DJF of 1948 to 2005 respectively. Anomalies are obtained at each grid point by subtracting the long-term monthly mean from the original values. The CCA yields two pairs of patterns that describe the coherent variations of the atmospheric temperature, wind, heat flux, SST and SLP fields and three patterns that describe precipitation with the SLP fields. These patterns are dominant in describing SLP with other parameters variance in the Labrador Sea.

The first pattern of SLP and SST (Fig 5.6 b) corresponds to a canonical correlation of 85%. The coefficient of the second pattern is (Fig 5.6 d) 72%. First canonical pattern of SLP is North Atlantic Oscillation (NAO) which causes cold temperature in the Labrador Sea with strongest impact in the northern part of the Labrador Sea and some part in the southern area. The second mode of canonical correlation is similar to the Eastern Atlantic (EA) pattern which has strongest impact on the northern part of the Labrador Sea.

The canonical correlation patterns are obtained through linear correlation analysis of SLP and SST fields. The dominant patterns of CCA are well correlated in time and therefore one can use them to predict the values of SST if SLP is known. Prediction of SST is based on using canonical variates for SLP to project variability of SLP into corresponding canonical correlation patterns of SST. The reconstruction of SST by using SLP canonical correlation variates is given by Zorita et al (1992):

$$R_{SST}(t_n) = \sum \rho_i \beta_i^{SLP}(t_n) f_i^{SST} \qquad 5.1$$

This approach is used in statistical weather forecasting methods. Some problems may arise when the CCA is used to reconstruct one parameter (SST) from known values of another (SLP). CCA patterns (Zwiers and von Storm, 1999) can not necessarily explain all the variance of the SST. Following the terminology of Chapter 2, let us consider the two parameters SST = SST_d+SST', SLP = SLP_d + SLP', each consisting of two components – deterministic and stochastic. The canonical correlation analysis is based on the correlation between SLP_d and SST_d represents variabilities in the two parameters which are not correlated. The variance of SLP' and SST' define importance of factors which are not considered by the CCA.

In the case of SST and SLP, the basic assumption of CCA is that atmospheric circulation (SLP) variability influences the surface heat fluxes in the Labrador Sea, which are important for the time changes of temperature in the surface ocean layer. Bjerknes., 1964 suggested this assumption is correct at interannual time scales, i.e. that interannual changes in SST correlate well with the dominant modes of atmospheric circulation. This is not the case, however, for the long term warming trends in the North Atlantic. In chapter 3, it was shown that such trends are present in the North Atlantic in the 1950s and late 1990s. Bjerknes (1964) suggests that the decadal trends of SST are related to the variations of ocean circulation. The figure 5.7 shows water transport between Bermuda and Bravo station. The green curve is NAO index filtered by 12 years and the black curve is water transport and the red curve is SST anomaly. The NAO index (see Fig 5.7) increase from 1980 to 1995. Water transport also increased during this period (Curry & MacCartney, 2001). The SST trend in the 1990s is well correlated with the low pass

filtered NAO index and ocean transport. The major physical process responsible for this long-term correlated trend in the three parameters is the ocean circulation. The transport in the subtropical and subpolar gyre intensified after 1980 due to the NAO which is in positive phase during the most of the time after 1980. The more intensive transport is related to intensified heat transport in the surface ocean layer from the subtropics to the subpolar region. Correspondingly the SST increases as a response to this transport. There are two major properties of the SST, ocean transport and NAO variabilities during the periods of positive SST trends, which are seen on Fig 5.7 and have impact on the quality of the CCA and reconstruction of SST by using SLP:

i. The ocean transport responds with some delay to NAO. Moreover when the meridional heat transport is intensified, during positive phase of NAO the time required by a positive SST anomaly to propagate from the subtropical area to the Labrador Sea is evaluated by Sutton and Allen (1997) as about 7-8 years.

ii. The low-passed filtered variability in the NAO has variance much lower than the variance of NAO at interannual time scale see (blue and red bars on Fig 5.7)

The CCA patterns here do not consider an eventual time lag in the correlations between the intensity of atmospheric circulation and SST. However if such time lag would be considered, CCA will still not capture the correlation in the long term low pass filtered trends between SST and SLP, because the filtered SLP trend has much lower variance than the interannual variability in the nonfiltered SLP data.. Additionally the sea ice variability in the Labrador Sea influences SST, introducing additional changes in SST, which are not directly connected to the SLP variability. Fig 4.7 b shows the ice inflow to

the Labrador Sea through the Davis Strait has a strong impact on the dominant mode of variability with a time lag of 1-2 years.

The CCA SLP-SST does not consider factors like ocean circulation, sea ice transport which are important for the SST variability. Therefore one can expect that the reconstruction of SST by using CCA patterns will not approximate perfectly the real SST field. In order to assess the approximation skills of CCA reconstruction the following parameter is used (Cayan, 1992):

$$\mu = [1 - \sum_k (R_{SST}(t_n) - SST(t_n))^2 / \sum_k (SST(t_n))^2] * 100\% \qquad (5.2)$$

which estimates the variance of SST explained by CCA patterns.

In Figure 5.6 (e) the blue line is the SST anomaly in the Labrador Sea and green line is SST anomaly reconstructed by CCA. In this figure it is clearly shown that the SST is weakly correlated with SLP and only in the cold period from 1970-1980s.

The variance explained by the CCA (Fig 5.6 f) is around 20% in the southern part of the Labrador Sea. In the rest of the basin, the approximation skill is very negative. This result shows that SST in the Labrador Sea is only weakly correlated with SLP patterns and the variability of the atmospheric circulation. Strong impact on the SST in the Labrador Sea have ocean heat and sea ice transport.

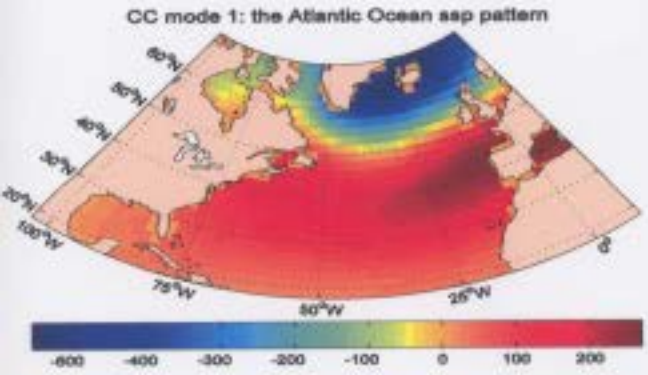

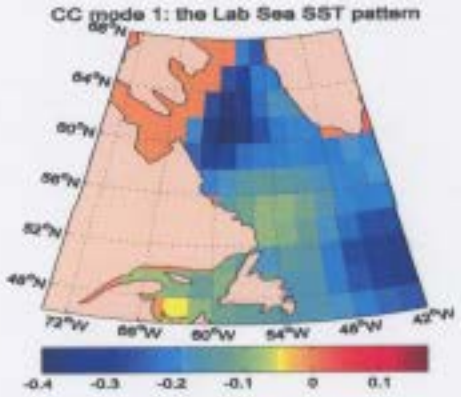

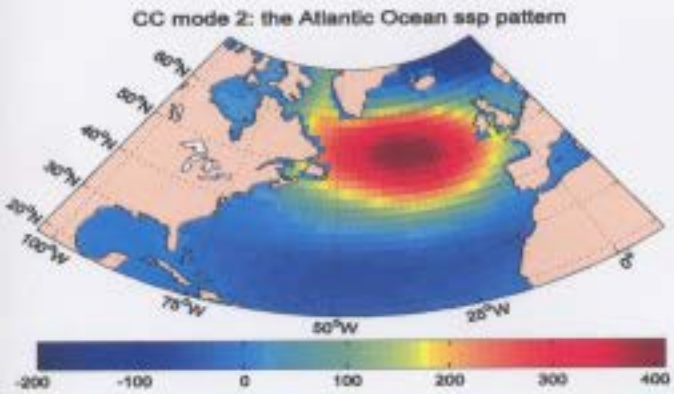

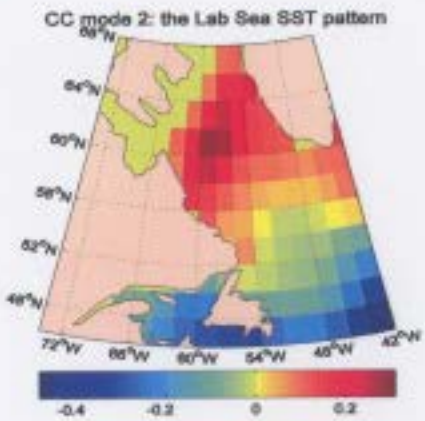

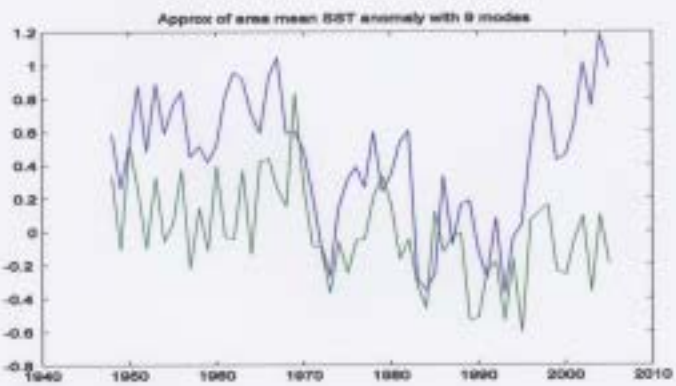

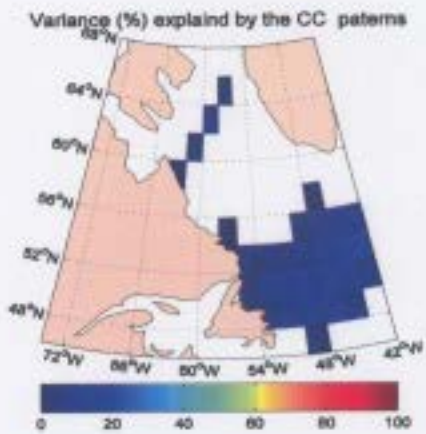

Fig 5.6: *Upper two panels show the first Canonical correlation pattern for (a) SLP (b) SST. Middle two panels show the second CC pattern for (c) SLP (d) SST. e)Lower two panels show SST anomaly (blue curve) and reconstructed SST anomaly (green curve) d)Variance of SST (%) explained by CC reconstruction*

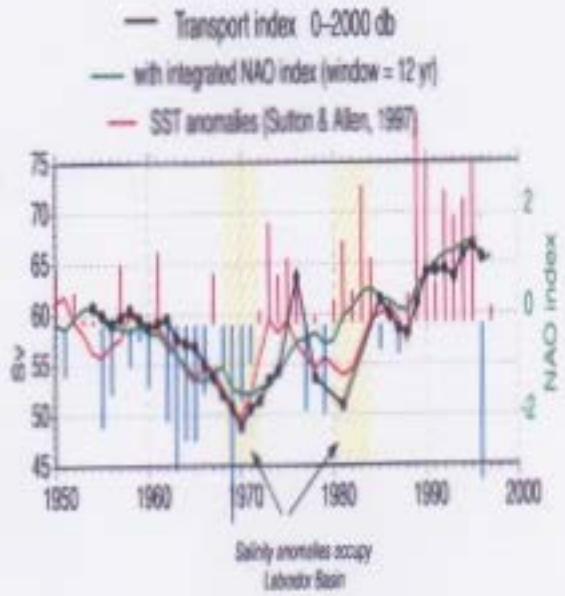

Fig 5.7: *Water transport index, integrated NAO index (Curry and MacCartney, 2001) and SST anomalies (Sutton, Allen 1997).*

The first pairs of patterns of SLP and atmospheric temperature corresponds to a canonical correlation of 98%. The coefficient of the second pairs of patterns is 96%. First canonical pattern of SLP (Fig 5.8 a) which has strongest impact in the northern part of the Labrador Sea is the North Atlantic Oscillation (NAO). The second mode of canonical (Fig 5.8 c) which has strongest impact also in the northern part of the Labrador Sea is similar to the Eastern Atlantic (EA) pattern. The SLP and air temperature in the Labrador Sea are well correlated. The variance explained by the CCA (Fig 5.8 f) is around 60%-80% everywhere except central part of the Labrador Sea where the explained variance is around 40%.

The first patterns of SLP and wind corresponds to a canonical correlation of 99%. The coefficient of the second pattern is 97%. First canonical pattern of SLP (Fig 5.9 a) which has strongest impact in the southern part of the Labrador Sea and near Greenland is North Atlantic Oscillation (NAO). The second mode of canonical correlation (Fig 5.9 c) which has strongest impact near the Greenland coast is similar to the Eastern Atlantic (EA) pattern. The SLP patterns and zonal wind in the Labrador Sea are well correlated. The variance explained by the CCA (Fig 5.9 f) is around 80%-100% everywhere except in the Davis Strait and some costal parts of Newfoundland where no correlation is found.

The first patterns of SLP and turbulent heat flux corresponds to a canonical correlation of 97%. The coefficient of the second pattern is 95%. First canonical pattern of SLP (Fig 5.10 a) which has strongest impact in the southern part of the Labrador Sea and near Greenland is North Atlantic Oscillation (NAO). The second mode of canonical correlation (Fig 5.10 c) which has strongest impact also in the southern part of the Labrador Sea is similar to the Eastern Atlantic (EA) pattern. The SLP and turbulent heat flux pattern patterns in the Labrador Sea are well correlated. The variance explained by the CCA (Fig 5.10 f) is around 60%-80% everywhere except Davis Strait, Hudson strait and coastal part of Newfoundland.

The first patterns of SLP and precipitation corresponds to a canonical correlation of 98%. The coefficient of the second pattern is 97%. The coefficient of the third pattern is 96% of the variance of SLP and heat flux in the Labrador Sea. First canonical pattern of SLP (Fig 5.11 a) which has strongest impact in the northern part of the Labrador Sea and near

Greenland is North Atlantic Oscillation (NAO). The second mode (Fig 5.11 c) of canonical correlation which has strongest impact also in the coastal part of Greenland is similar to the Eastern Atlantic (EA) pattern. The SLP and air temperature in the Labrador Sea are well correlated. The variance explained by the CCA (Fig 5.11 f) is around 60%-80% everywhere except northern part of Labrador Sea and coastal part of Newfoundland.

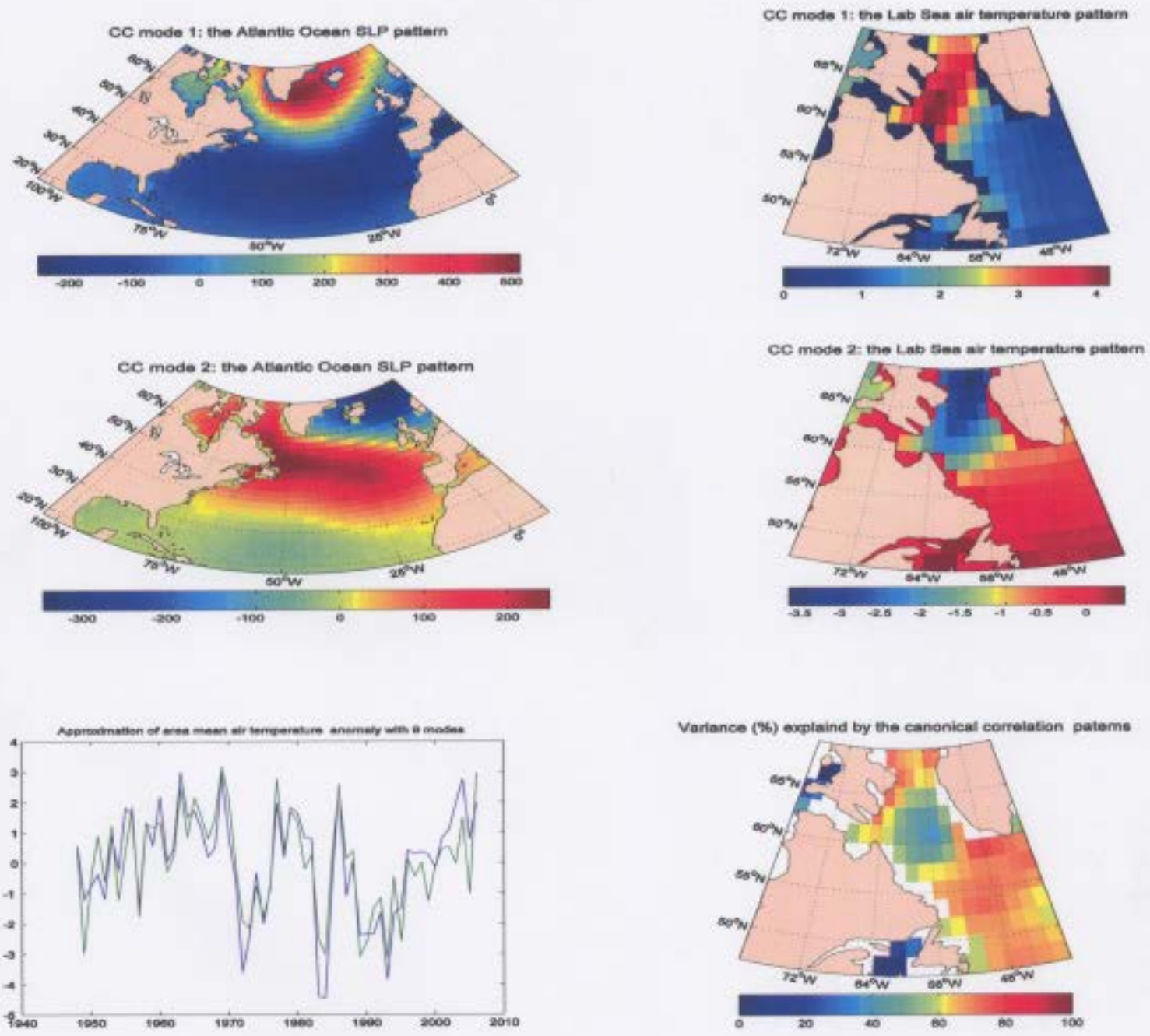

Fig 5.8: *Upper two panels show the first Canonical correlation pattern for (a) SLP (b) air temperature. Middle two panels show the second CC pattern for (c) SLP (d) air temperature. e) Lower two panels show air temperature anomaly (blue curve) and reconstructed air temperature anomaly (green curve) d)Variance of air temperature (%) explained by CC reconstruction*

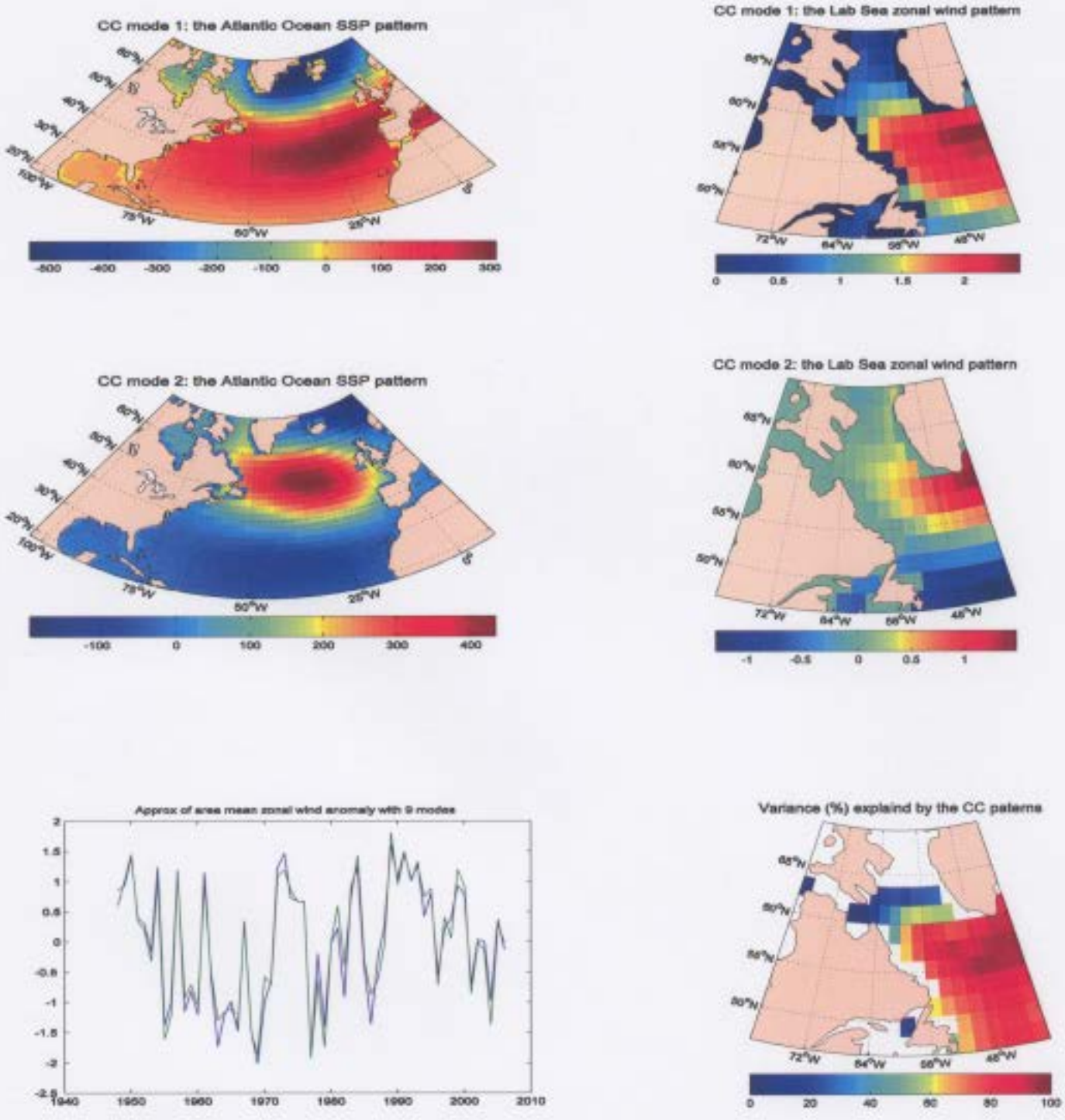

Fig 5.9: *Upper two panels show the first Canonical correlation pattern for (a) SLP (b) zonal wind. Middle two panels show the second CC pattern for (c) SLP (d) zonal wind. e)Lower two panels show zonal wind anomaly (blue curve) and reconstructed zonal wind anomaly (green curve) d)Variance of zonal wind (%) explained by CC reconstruction*

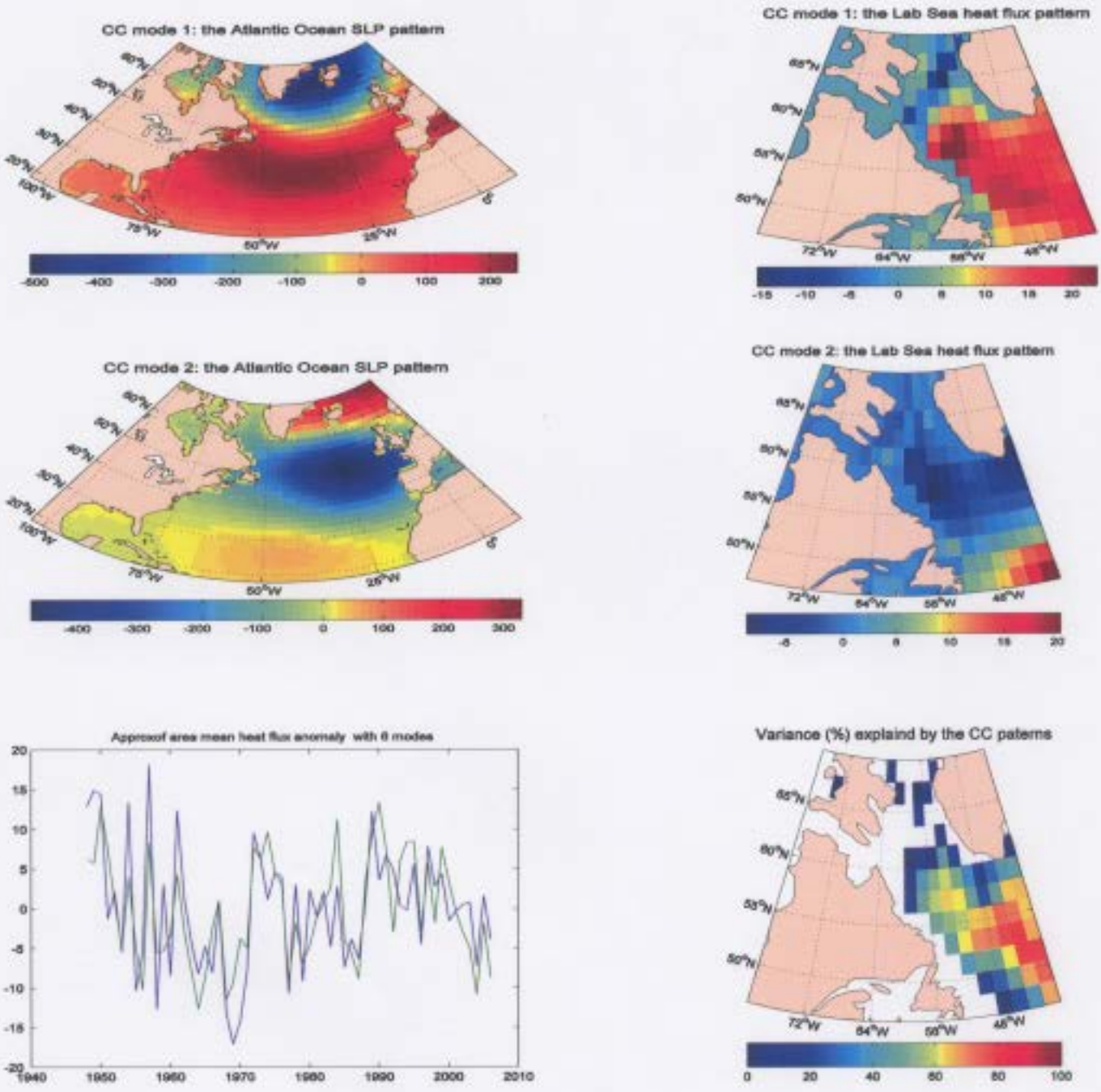

Fig 5.10: *Upper two panels show the first Canonical correlation pattern for (a) SLP (b) heat flux. Middle two panels show the second CC pattern for (c) SLP (d) heat flux. e)Lower two panels show heat flux anomaly (blue curve) and reconstructed heat flux anomaly (green curve) d)Variance of heat flux (%) explained by CC reconstruction*

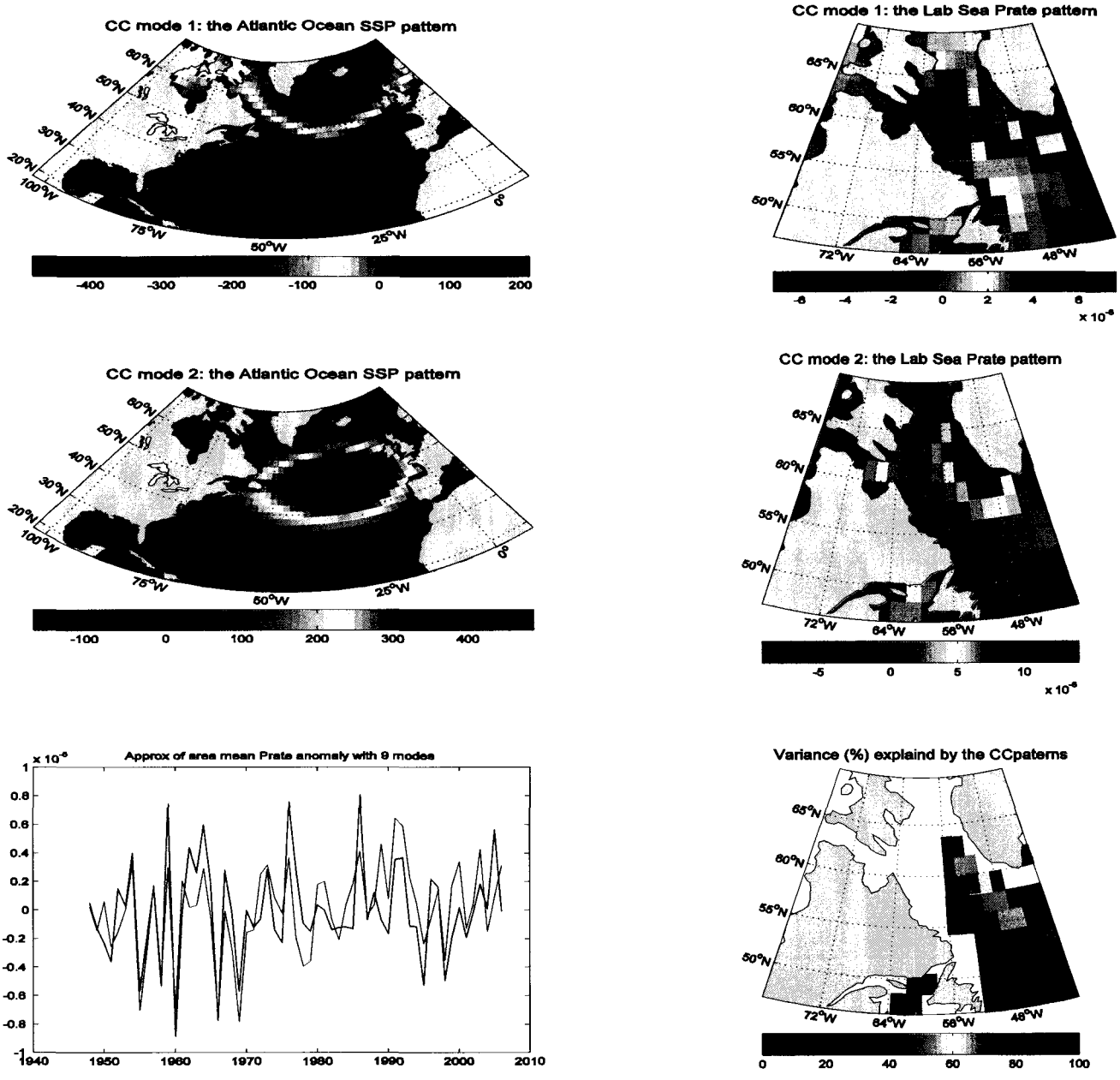

Fig 5.11: *Upper two panels show the first Canonical correlation pattern for (a) SLP (b) prate. Middle two panels show the second CC pattern for (c) SLP (d) prate. e)Lower two panels show precipitation anomaly (blue curve) and reconstructed precipitation anomaly (green curve) d)Variance of precipitation (%) explained by CC reconstruction*

Chapter 6

6. Conclusions and Future Work

EOF and CCA are techniques commonly used in analysis of geophysical data. In this study the application of these two statistical methods are used to study interannual and interdecadal variability of Labrador Sea. The purpose of this study is to find the dominant modes of variability in the North Atlantic SST and near surface atmospheric parameters and to asses the effect of the atmospheric circulation on the SST and the atmospheric parameters in the Labrador Sea and the North Atlantic.

- The SST and near surface atmospheric parameters are studied for the period of time 1950 – 2005.
- The data used in this study is Comprehensive Ocean-Atmospheric Dataset (COADS). The SST data are used from this COADS dataset. And the other parameters are taken from NCEP reanalysis.
- The dominant modes in the North Atlantic interannual variability are found by using EOF analysis
- The dominant modes of interannual variability in the Labrador Sea and their relation to atmospheric circulation are studied by using CCA.
- The approximation skills of canonical correlation patterns of SST, zonal wind, turbulent heat flux, air temperature and precipitations are computed. The CCA SLP-SST does not consider factors like ocean circulation, sea ice transport that

are important for the SST variability. Therefore it can expect that the reconstruction of SST by using CCA patterns will not approximate perfectly the real SST field. In order to assess the approximation skills of CCA reconstruction the following parameter is used (Cayan, 1992):

$$\mu = [1 - \sum_k (R_{SST}(t_n) - SST(t_n))^2 / \sum_k (SST(t_n))^2] * 100\%$$

which estimates the variance of SST explained by CCA patterns.

- The winter SST anomaly in the Labrador Sea especially during warm periods does not show significant correlation with the patterns of atmospheric circulation.
- This result supports Bjerknes (1964) conclusion that decadal variability of SST during warm periods depend mostly on non-local processes of horizontal transport and less on the local heat exchange with the atmosphere. Inter-decadal warming of SST in the North Atlantic is linked to the basin scale interaction. The Gulf Stream and the North Atlantic current respond to the intensifying circulation in the anti-cyclonic gyre.
- The near surface atmospheric parameters show good correlations with SLP.

From the results presented in Chapter 5 it follows that the future analysis of the climate variability in the Labrador Sea should be based on additional data about variability of the Atlantic Ocean. The future work would include the following steps:

- Consideration of the ocean circulation and its long term effect on SST and atmospheric parameters.
- Using of realistic ocean model simulations and observations.
- Application of the EOF and CCA for both atmospheric characteristics and ocean surface and sub-surface parameters.

Abbreviations

- **NAO:** North Atlantic Oscillation. The NAO is the dominant mode of winter climate variability in the North Atlantic region ranging from central North America to Europe and much into Northern Asia. The NAO is a large scale seesaw in atmospheric mass between the subtropical high and the polar low. The corresponding index varies from year to year, but also exhibits a tendency to remain in one phase for intervals lasting several years. The Positive NAO index phase shows a stronger than usual subtropical high pressure center and a deeper than normal Icelandic low. The increased pressure difference results in more and stronger winter storms crossing the Atlantic Ocean on a more northerly track. The negative NAO index phase shows a weak subtropical high and a weak Icelandic low. The reduced pressure gradient results in fewer and weaker winter storms crossing on a more west-east pathway.

- **NCEP:** National Center of Environmental Prediction.

- **COADS:** Comprehensive Ocean-Atmospheric Dataset.

- **EOF:** Empirical Orthogonal Function. The method of empirical orthogonal function (EOF) analysis is a decomposition of a signal or data set in terms of orthogonal basis functions which are determined from the data.

- **CCA:** Canonical Correlation Analysis. A typical use for canonical correlation in the general context is to take a two sets of variables and see what is common amongst the two tests.

- **SST:** Sea Surface Temperature.

- **SSP:** Sea Surface Pressure.

- **LSW:** Labrador Sea Water.

Bibliography

Alexander A. M and Clara Deser (1995). The Reemergence of SST Anomalies in the North Pacific Ocean, *J. Clim*, 2419–2433.

Barnston, A. G., and R. E. Livezey, (1987). Classification, seasonality and persistence of low frequency atmospheric circulation patterns, *Mon. Wea. Rev.*, **115,** 1083–1126.

Battisti D. S, Bhatt U. S, and Alexander M. A (1995). A Modeling Study of the Interannual Variability in the Wintertime North Atlantic Ocean, *J. Clim,* 3067–3083.

Bjerknes, J., (1964) Atlantic air-sea interactions, *Advances in Geophysics*, **10**, 1–82.

Bretherton, C. S., Smith, C., and Wallancw, J.M. (1992). An intercomparison of methods for finding coupled patterns in climate data. *J. Clim*, **5,**541-560.

Cayan, D. R., (1992a). Latent and sensible heat flux anomalies over the northern oceans: Driving the sea surface temperature, *J. Phys. Oceanogr.*, **22**, 859–881.

Cayan, D. R., (1992b) Latent and sensible heat flux anomalies over the northern oceans: The connection to monthly atmospheric circulation, *J. Climate*, **5**, 354–369.

Curry, R. G., and M.S. McCartney, (2001). Ocean gyre circulation changes associated with the North Atlantic Oscillation , *J. Phys. Oceanog.*, **31**, 3374-3400.

Czaja A. and J. Marshall (2001). Observations of Atmosphere - Ocean coupling in the North Atlantic, Quart. *J. of the Roy. Met. Soc.*, **127**, 1893-1916.

Deser, C.,(2000). On the teleconnectivity of the "Arctic Oscillation." *Geophys. Res. Lett.*, **27**, 779-782.

Deser, C., and M. L. Blackmon, (1993). Surface climate variations over the North Atlantic Ocean during winter: 1900-1989. *J. Clim*, **6**, 1743-1753.

Deser C., Walsh JE, Timlin MS .,(2000). Arctic Sea Ice Variability in the Context of Recent Atmospheric Circulation Trends, *J Clim,* 617-633.

Dickson, R. R., J. Lazier, J. Meincke, P. Rhines, and J. Swift, (1996). Long-term-co-ordinated changes in the convective activity of the North Atlantic, *Prog. Oceanogr.*, **38**, 241-295.

Dickson R. R and Namias J. (1976). North American Influences on the Circulation and Climate of the North Atlantic Sector, *Monthly Weather Review,* 1255-1265.

Folland, C. K., and co-authors (2001), Observed climate variability and change, in *Climate Change 2001, The Scientific Basis*, J. T. Houghton, Y. Ding, D. J. Griggs, M. Noguer, P. J. van der Linden and D. Xiaosu, Eds., pp. 99–181, Cambridge Univ. Press.

Frankignoul, C; Hasselmann, K (1977). Application to sea-surface temperature anomalies and thermocline variability. *Stochastic climate models. II.*, **29**, 289-305.

G.R. North, T.L. Bell, R.F. Cahalan, and F.J. Moeng (1982). Sampling errors in the estimation of empirical orthogonal functions, *Mon. Wea. Rev.*, **110**:699-706.

Golub, G. H., and Loan, C. F. V (1996). Matrix Computations (Third Edition), 476p.

Hansen, J., R. Ruedy, M. Sato, and K. Lo (2002), Global warming continues, *Science*, ***295.***

Hasselmann (1976) Stochastic climate models. Part I : Theory, Tellus, 28, 473-485.

Hayden B. P. (1981) Climate change and extratropical storminess in the United States: *J. american water resourse association*. **36**, 1387-1397.

Hurrell, J. W., (1995). Decadal trends in the North Atlantic Oscillation: regional temperatures and precipitation. Science, ***269,*** 676-679.

Hurrell, J. W., and H. van Loon (1997). Decadal variations in climate associated with the North Atlantic Oscillation, *Climatic Change*, ***36,*** 301–326.

Jones, P. D., T. J. Osborn, and K. R. Briffa (2001). The evolution of climate over the last millennium, *Science*, ***292,*** 662–667,.

Kushnir, Y., W. A. Robinson, I. Bladé, N. M. J. Hall, S. Peng, and R. T. Sutton (2002). Atmospheric GCM response to extratropical SST anomalies: Synthesis and evaluation, *J. Climate*, **15**, 2233–2256.

Kushnir, Y., (1994). Interdecadal variations in the North Atlantic Sea surface temperature and associated atmospheric conditions. *J. Climate*, **7**, 141-157.

Lazier, J. R. N., 1980. Oceanographic conditions at Ocean Weather Ship BRAVO, 1964-1974. *Atmos.-Ocean*, **18**, 227-238.

Lazier J.R.N (1995). The salinity decrease in the Labrador Sea over the past thirty years. *Climate on Decade-to-Century Time scales*, National Academy of Sciences Press, 295-302.

Malberg,H, Bokens,G (1997) Winter and summer temperatures in Berlin since 1929 and their relationship with the North Atlantic Oscillation. *Meteorologische Zeitschrift*, Vol.6, No.**5**, pp.230-242.

Mann, M. E., R. S. Bradley, and M. K. Hughes (1999). Northern Hemisphere temperatures during the past millennium: Inferences, uncertainties, and limitations, *Geophys. Res. Lett.*, **26**, 759–762.

Mitchell (1976). An overview of climatic variability and its cause & mechanism. *Quaternary Res*, **6**, 481-493.

Milankovitch M. (1941). History of radiation on the earth and its use for the problem of the ice ages. K. Serb. *Akad. Beogr. Spec. Publ.* **132**. 633 pp.

Portis, D. H., J. E. Walsh, M. El Hamly, and P. J. Lamb (2001). Seasonality of the North Atlantic Oscillation, *J. Climate,* **14**, 2069-2078.

Rogers J. C. (1990). Patterns of low-frequency monthly sea-level pressure variability (1899-1986) and associated wave cyclone frequencies *J. Clim*, **10**, 1635-1647.

Rogers J. C. (1997). North Atlantic Storm track variability and its association to the North Atlantic Oscillation and climate variability of northern Europe, J. Climate, 10, 1635-1647.

Sutton, R. T. Allen, M. R. (1997). Decadal predictability of North Atlantic sea surface temperature and climate. *Nature*, **388**, 563-567.

Talley L.D (1984). Meridional heat transport in the Pacific Ocean, *J. Phys. Oceangr.* **14** 231-241.

Thompson, D. W. J., and J. M. Wallace (2000). Annular modes in the extratropical circulation, Part I: Month-to-month variability, *J. Climate*, **13**, 1000–1016.

Van Loon, H., and J.C. Rogers (1978). The seesaw in winter temperatures between Greenland and Northern Europe. Part I: General description. *Mon. Wea. Rev.*, **106**, 296-310.

Visbeck, M., H. Cullen, G. Krahmann, and N. Naik, (1998). An ocean model's response to North Atlantic Oscillation-like wind forcing. *Geophys. Res. Lett.*, **25**, 4521-4524.

Wallace, J. M., Smith, C., and Bretherton, C. S. (1992). Singular value decomposition of winter time sea surface temperature and 500-mb height anomalies. *J. Clim.*, **5**, 561-576.

Wallace and Gutzler D. S. (1981), Teleconnections in the geopotential height field during the Northern Hemisphere winter, *Mon, Wea, Rev.*, **109**, 784-812.

Woodruff, S.D., R. J. Slutz, R.L. Jenne, and P.M. Steuer, (1987). A compherensive ocean-atmosphere dataset. Bull. *Amer. Metor. Soc*, **68**, 1239-1250.

Zorita. E., Kharinv., and H. von Storch, (1992). The atmospheric circulation and the SST in the North Atlantic area in winter: Their interaction and relevance for Iberian precipitation. *J. Clim.*, **5**, 1097-1108.